Load / deformation / time behaviour of articular cartilage

Jane E. Snaith

LOAD / DEFORMATION / TIME BEHAVIOUR OF ARTICULAR CARTILAGE

by

Jane E. Smith, B.Sc.

Thesis submitted for the degree of Doctor of Philosophy in the Faculty of Science, University of Durham.

October 1976

Abstract

This thesis is concerned with the behaviour of articular cartilage under compressive loading.

An apparatus was built to apply sinusoidal and constant loading to specimens of cartilage. The majority of the tests performed were on specimens of bovine cartilage, although some tests have been conducted on human patella cartilage. Confined tests, with load, deformation and flow confined to an axial direction, were considered most realistic to the conditions in the body, and so the majority of the work was on this type of test. However some tests of an 'unconfined' nature, with axial load but radial flow and deformation, were carried out.

An already established computer model of this behaviour of cartilage was modified and used to reproduce the experimental results. The model is based on fluid flow phenomena only and hence agreement with the experimental work was not entirely satisfactory. However, the model does allow the effect of changes in cartilage properties to be studied. The model yielded its most useful results for sinusoidal loading, where it forecast similar results to the experimental work.

The cartilage is shown to be visco-elastic under conditions of steady load, the creep deformation being achieved by fluid flowing out of the specimen. The creep deformation is shown to be recoverable on removal of load. Under sinusoidal loading, around the frequency of the walking cycle, flow processes are shown to contribute practically nothing to the sinusoidal deformations achieved, the deformations in this case arising almost entirely from the elastic compressibility of the specimens.

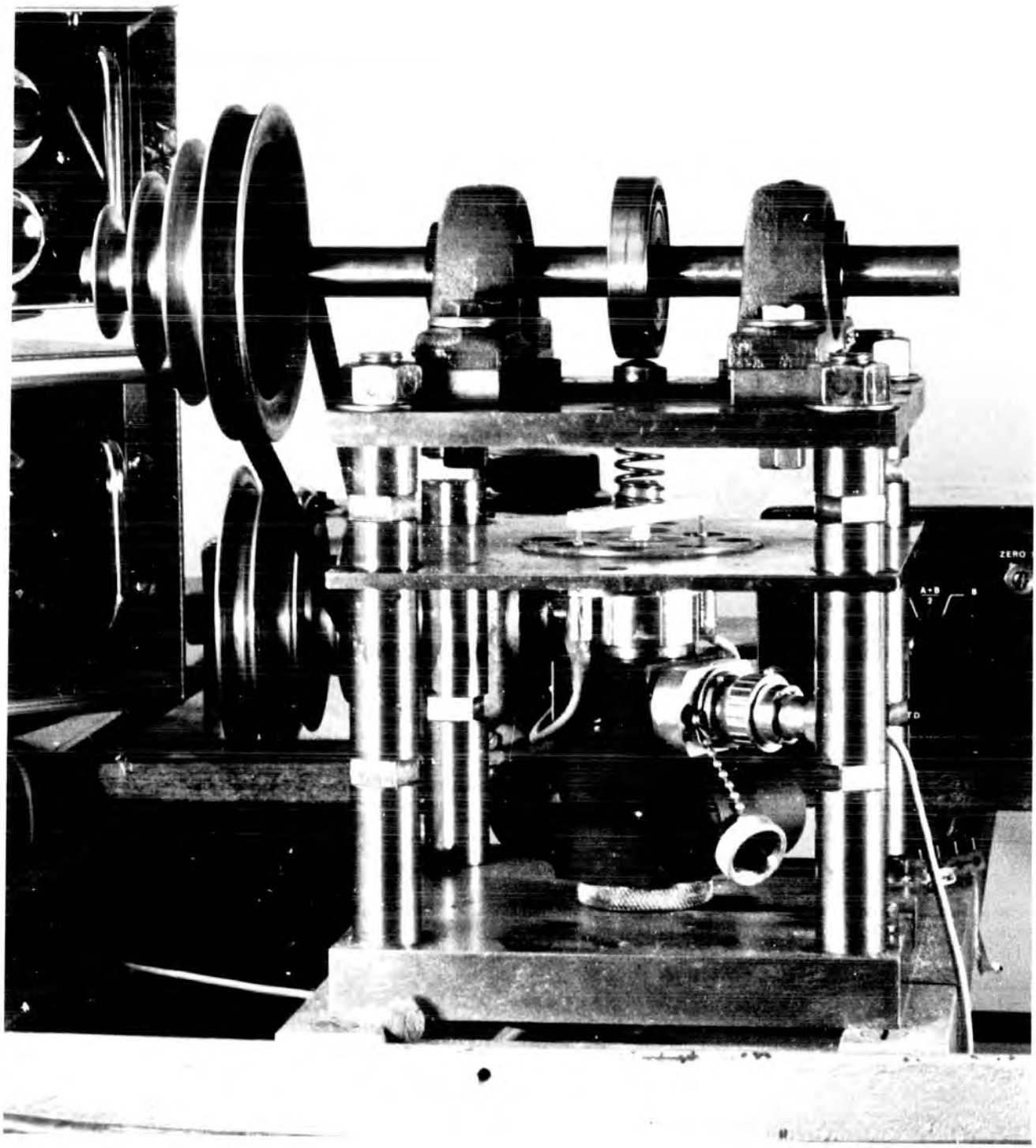
ZERO

Acknowledgements

I would like to express my sincere thanks to Professor G.R. Higginson, under whose direction this research has been carried out, for his active encouragement and invaluable advice.

My thanks are also due to the technicians of the Engineering Science Department, for their willing and valuable help in the experimental work, and to Dr. M.R. Litchfield for allowing me to continue using his original computer model and for permitting its modification.

I am greatly indebted to the Science Research Council for providing me with financial support, and to Mrs. Joy Gill for typing this thesis.

Finally, I wish to thank my husband, Dr. R. Snaith, and my parents, Mr. and Mrs. W.H. Facer, for their support and encouragement over the past three years.

Contents

Notation

A cross-sectional area of specimen

A' area of fluid in a given layer $(=nA)$

a,b constants of force-deflection characteristic

$\delta A, \delta B$ outputs from displacement transducers

δC output from switch selector unit $\left(= \frac{\delta A + \delta B}{2}\right)$

C_a $\left(= \left(r + \frac{\delta r}{2}\right) \delta\theta \, \delta r\right)$

E Young's modulus of elastic material

E^* elastic modulus for confined tests $\left(= \frac{\sigma_z}{\epsilon_z}\right)$

E' elastic modulus based on current length $\left(= E(1-\epsilon)\right)$

F_a applied force

F_s force carried by solid

F_f force carried by fluid

k permeability

k_r radial permeability

k_z axial permeability

$k_{1 \to n}$ permeability of a section within the depth

K_r initial radial permeability

K_o initial axial permeability

K_z overall axial permeability

K bulk modulus

n porosity

p fluid pressure

$p_{1 \to n}$ pressure drop across section within the depth

P_o overall pressure drop

P dimensionless fluid pressure $\left(= \frac{p}{a}\right)$

R external radius

r distance from axis of symmetry

t time

T	dimensionless time (axial case only) $\left(=\frac{K_0 a t}{\eta z_0^2}\right)$
T^*	dimensionless time (radial case only) $\left(=\frac{K_3 a t}{\eta R^2}\right)$
$\Delta T, \Delta T^*$	increments of dimensionless time
u	radial flowrate per unit area
v	initial porosity
V_e	volume of the element
w	axial flowrate per unit area
z	distance along axis of symmetry
δz	size of element in axial direction
z_0	original thickness of specimen
$z_{1 \to n}$	thickness of a section within the depth
z_1	thickness at equilibrium after application of load
δz_0	initial value of δz
Z	dimensionless specimen thickness $\left(=\frac{z}{z_0}\right)$
Z_0	overall thickness of specimen
ΔZ	increment of dimensionless depth
δ	deformation from original thickness
$\dot{\delta}$	rate of deformation from original thickness
δ_0	'instantaneous' response on compression
δ_1	'instantaneous' response after release of load
δ_x	creep deflection
ϵ	strain $\left(=\frac{\delta}{z_0}\right)$
$\epsilon_r, \epsilon_\theta, \epsilon_z$	strains in r , θ , z directions
$\dot{\epsilon}_z$	strain rate in z direction
$\delta\theta$	angle of element
$\sigma_r, \sigma_\theta, \sigma_z$	stresses in r , θ , z directions
σ_s	load per unit area carried by solid
σ_a	applied load per unit area

σ	total applied stress
Σ	dimensionless applied stress $\left(=\frac{\sigma}{a}\right)$
η	dynamic viscosity of fluid
ν	Poisson's ratio
$\phi(\epsilon)$	dimensionless permeability multiplier $\left(=\left(\frac{v-\epsilon}{v}\right)^3\right)$
$\psi(\epsilon)$	dimensionless permeability multiplier $\left(=\frac{(v-\epsilon)^5}{v^5(1-\epsilon)}\right)$

1.0 Introduction

Articular cartilage takes the form of a thin layer attached to the end of each bone in a joint. It is both porous and deformable and is crucial to the normal functioning of synovial joints. It is accepted that its presence enables the transmission of the high loads occurring in joints whilst limiting the contact stresses to an acceptably low level, and that it also, in conjunction with synovial fluid, allows movement of the joint with very low frictional resistance.

The study of the mechanical properties of articular cartilage has continued with increasing fervour for many years. The investigations of its properties have arisen from the interest in the mode(s) of lubrication of joints and the reasons behind joint failure by arthritis or associated diseases.

The work carried out for this thesis has been to investigate the load/time/deformation characteristics of articular cartilage along similar lines to those followed by other workers, but hopefully bringing together some of the most important areas of their individual studies. For example, as will be explained later, the uniaxial tests performed by Edwards (1967) are considered in some ways to be the most realistic tests, but he used only static loading. In the human body, very seldom is there only static loading, so similar tests to Edwards' were performed, but using similar loading to that used by Johnson (1974), a mean constant load with a superimposed oscillating load.

The apparatus was designed to be as universal and to meet as many of the requirements as possible. It was designed to allow a choice of type of test conditions, and loading conditions, with suitable monitoring of each. During the period of this work it became obvious that the situation was more complex than had originally been thought, and rig modifications have been made or been suggested in the later documentation.

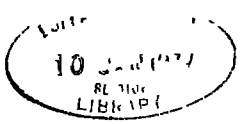

Both bovine trochlea and human patella cartilage have been used. Satisfactory results have been obtained under both static and dynamic loading conditions, and for uniaxial and unconfined tests. With the greater volume of experimental results, it was hoped to use the computer model of articular cartilage formulated by Litchfield (1974) for more comparative studies. However it was found necessary to alter the programme significantly in some aspects, and the programme was also put in dimensionless terms. These comparative studies are reported in this thesis.

A literature review, Chapter 2, has been written, primarily to state some of the present beliefs about articular cartilage and its properties, rather than re-tell its history, which has been done several times by other workers.

Chapter 3 deals with the theory involved in this study, most of which is pertaining to the formulation of the computer model of articular cartilage, but some is included to shed light on the results from the experimental work.

The requirements of the testing apparatus and the way in which the tests were performed is detailed in Chapter 4. This chapter also includes details of the specimens and the way in which they were prepared and handled before the tests.

The results of all the experimental and computational work are presented in Chapter 5, drawing comparison not only with the work performed here, but with the reported results of other researchers in this field.

Discussion of and conclusions about the work are presented finally, with the suggestions for improved techniques and future work being included at relevant positions throughout the thesis and summarised at the end.

Appendix I reports on a short study of the load-deflection properties of subchondral bone, made as a result of the experimental work on cartilage.

2.0 Literature Review of Articular Cartilage

Comprehensive literature reviews of articular cartilage have been written in the last few years by both Johnson (1974) and Litchfield (1974) amongst others. Both of these reviews cover the historical background of research on this topic, and devote sections of the review to specific areas of study e.g. permeability and porosity, mechanical properties, nutrition, cartilage structure, etc.

As a full literature review in this study would essentially be a repeat of the reviews of Johnson and Litchfield, it is proposed here only to touch lightly on the ground that they covered, and to concentrate primarily on presenting the current state of research and beliefs on articular cartilage. Naturally certain areas have been of more importance to the experimental and computational work of this study, for instance the permeability of cartilage, and for this reason these topics will receive fuller coverage.

2.1 Permeability

This seems to have proved one of the most difficult properties of articular cartilage to investigate. Cartilage has a very high porosity but an exceedingly low permeability. Therefore in order to measure permeability many workers have resorted to forcing fluid through a sample under pressure. This is not an ideal situation as any pressure on the cartilage will be transmitted not only to the fluid, hence forcing it through, but also to the matrix. This pressure on the matrix will tend to compress the matrix structure and cause a closing-up of the channels through the matrix, which in turn will lower the value of permeability recorded. Also, due to the physical size of any cartilage samples able to be tested, and the low value of permeability of these, any apparatus used for recording permeability must be perfect. Any leakage, however small, could drastically alter the recorded values.

Munding (1975) performed experiments to determine the permeability of cartilage from the trochlea of a cow, in fact using specimens adjacent to those used for the experimental work recorded in section 5.0 of this thesis. The rig used was based on the idea of squeezing the edges of a cylindrical specimen and passing liquid through the central portion. The liquid was not passed under pressure, the only force driving the liquid through the specimen was the constant head of liquid above the specimen. The permeability in this case is given by:-

$$= \frac{\text{volume flowrate x thickness in m x viscosity}}{\text{head x area of specimen}}$$

The average values obtained were $7.8 \times 10^{-19} m^2$ for tap water and $7.5 \times 10^{-19} m^2$ for Ringer's solution, with the overall range of permeability obtained being from $5.1 - 11.3 \times 10^{-19} m^2$. This is just for normal permeability. Munding did not attempt to measure transverse permeability.

McCutchen (1962) using a disc, 5.3 mm diameter and 0.33 mm thick, trapped between two glass tubes, measured the normal permeability of cartilage from the leg joint of a cow. He applied pressure (1 atm) to the water in the lower tube and recorded the rate of rise of water in the upper column. The value of normal permeability obtained was $5.8 \times 10^{-13} cm^4/dyne\ sec$ ($5.8 \times 10^{-19} m^2$ for water) and because this includes the effect of viscosity the measured permeability would be different for a liquid of different viscosity. McCutchen also measured the tangential permeability by trapping the cartilage between solid plates so constraining fluid flow to a tangential direction. The tangential permeability was obtained from an analysis of the deformation of the cartilage as the liquid 'wrings-out' and gave a value of $5.45 \times 10^{-13} cm^4/dyne\ sec$ ($5.45 \times 10^{-19} m^2$ for water) but due to various factors McCutchen states that this could be too low, possibly by a factor of 2, leaving the possibility that articular cartilage could still have isotropic permeability. McCutchen also investigated the variation of normal permeability with depth from the

surface and quoted values of 7.65×10^{-13} cm^4/dyne sec (7.65×10^{-19} m^2) for the top 0.32 mm disc and 4.3×10^{-13} cm^4/dyne sec (4.3×10^{-19} m^2) for a lower 0.28 mm disc.

Edwards (1967) using similar, but possibly slightly more sophisticated apparatus, measured the normal permeability of articular cartilage from the hip of a dog. He again used pressure, 70 p.s.i.(0.48 MN/m^2) to force the liquid through and so obtained values for the normal permeability of 1.09×10^{-13} cm^4/dyne sec (1.09×10^{-19} m^2) for saline and 3.3×10^{-13} cm^4/dyne sec (3.3×10^{-19} m^2) for Ringer's solution. Edwards does however say that "In practice it is possible that K may change with pressure and this has yet to be determined".

Maroudas (1968) in applying an ion-exchange theory to articular cartilage measured the fixed charge density (F.C.D.) variation with depth. She states that "since fluid flow takes place through the 'pores' of the proteoglycan gel, it is clear that increasing the proteoglycans must lead to decrease in pore size and hence in permeability". Hence as F.C.D. increases, permeability decreases. Besides graphs of F.C.D. with depth, Maroudas produced graphs of permeability coefficient variation with depth. Experimental difficulties were encountered in recording the permeability of the top 0.2 mm of the cartilage from the surface, but below this there appeared to be a near linear relationship between permeability and depth from the surface, the permeability decreasing in the deeper layers. However the difficulties were overcome and the findings from the surface layers were reported in a second paper, Maroudas (1973). An unexpected decrease in permeability at the surface was found in most cases. Two of the typical curves obtained by Maroudas are repeated in Fig. 5.23 . Maroudas suggests that the decrease is due to the fact that the bearing surface of articular cartilage is made up of thickly packed smaller fibres. Maroudas also performed tests which showed that cartilage does have isotropic permeability.

More recently Mansour and Mow (1976) have tried to investigate how some of the external factors affect permeability. They have taken up the point made by Edwards that permeability may change with pressure, and produced graphs of this effect. The permeability versus pressure plots show a non-linear relationship, with the effect of pressure on permeability decreasing as pressure increases. From the graph of permeability versus pressure it can be seen that Edwards' results taken at 70 p.s.i. ($0.48 \times 10^6 N/m^2$) could be about 30% lower than the value they would be at low pressure. Similarly McCutchen's results taken at 1 atm will be also reduced from the value they would have at low pressure.

Litchfield (1974) for his computational work required to know how permeability was affected by strain of the material. For this he used filter tiles of sintered fibres from a polyolefine base, which met his requirements and he arrived at the relationship for axial flow of

$$K_z = K_o \frac{(v-\epsilon)^3}{v^3}$$

Mansour and Mow however investigated the effect of strain on permeability, but were able to use bovine cartilage as the test material. In all the results they quote it would appear that for all driving pressures there is a linear relationship between permeability and strain, the permeability decreasing with increased strain, but this rate of decrease being less at higher pressures.

These findings of Mansour and Mow would have been very important in the computational work of this thesis, but their paper was published only after completion of the computational work and indeed when the writing-up was almost finished. Compression of cartilage causes compaction of the proteoglycan in the tissue, which in turn has been shown by Maroudas and Bullough (1968) to decrease the permeability. Therefore the linear relationship between permeability and strain found from experiments actually performed on cartilage itself would seem to be nearer the truth than

Litchfield's relationship. Fig. 5.22 shows the effect on the computer predicted strain-time characteristics of various relationships between permeability and strain. A large discrepancy can be seen to occur between the linear relationship of (b) and the Litchfield relationship of (d).

Some typical values of permeability quoted by Mansour and Mow are for the lowest driving pressure of 1.4×10^5 N/m^2, $1.4 - 3.4 \times 10^{-15}$ m^4/Ns ($1.4 - 3.4 \times 10^{-18}$ m^2 for water) at zero strain, decreasing to $0.6 - 1.7 \times 10^{-15}$ m^4/Ns ($0.6 - 1.7 \times 10^{-18}$ m^2 for water) at 30% strain. To show the effect of pressure, the quoted figures for permeability are, for zero strain on the specimen, approximately 2.0×10^{-15} m^4/Ns (2.0×10^{-18} m^2 for water) at very low pressure decreasing non-linearly to about 0.3×10^{-15} m^4/Ns (0.3×10^{-18} m^2 for water) at 2.8×10^6 N/m^2 applied pressure.

2.2 Structure

Investigations of the structure of articular cartilage have spanned many centuries and produced many schools of thought. Originally Hunter (1743) said the fibres ran radially, but this was questioned by Hassell (1849) and Schäfer (1920) who thought, after light microscope studies, that cartilage was a completely homogeneous structure. After this, came discoveries of fibre orientation at the surface, and that cartilage was made up of collagen and ground substance. This was followed by conclusions of a 3D network of fibres made up of fibrils grouped together. The orientation of this 3D network has alone caused controversy with some workers favouring the idea of arcades of fibres, some believing in an oblique orientation between bone and surface and more recently McCall (1969) that there were 3 distinct zones through the depth. These are the superficial, intermediate and deep zones, each with their own orientation of fibres. The idea of these, see Fig. (2.1) three zones seems generally accepted today. The deep zone is composed of a tight mesh of the thickest fibres arranged to run in a direction perpendicular to the bearing surface. The intermediate zone, which is much the largest

region is made up of S shaped coiled fibres randomly orientated and enclosing larger spaces. The superficial zone, or bearing surface, is made up of parallel bundles of fibres running in directions parallel to the surface.

The surface of the cartilage itself could be the most important of all the areas of study into cartilage structure. Maroudas (1973a) stressed its importance in the permeability of cartilage, and it is exceedingly important when studying the lubrication mechanisms of joints. The surface alone has been investigated by Balazs et al (1966) who studied bovine cartilage between 7 months of embryonic life and 12 years old.

In the very young specimen they found a random distribution of collagen fibres at the surface with chondrocytes very close to the surface. However, a fibrous material, thinner than the dominant collagen fibres was visible, especially close to the surface, but no distinct layer of such material was evident. In the older specimens the collagen fibres have a random structure and are denser than in young adults. The chondrocytes are always remote from the surface. However by adult life fine filaments 60 - 90 Å thick, intermingled with some amorphous material, appear to be accumulating on the surface. With increased age this felt-like filamentous-amorphous surface layer became denser and thicker. This eventually produces a distinct layer on the surface of the collagen fibres which could be what is sometimes referred to as the lamina-splendens, which in no way resembles the basement membrane. The authors put forward suggestions as to what this surface layer is and to its function, but whatever it is made up of, it could certainly be the cause of the unexpected permeability drop at the surface and could enhance or dispel certain beliefs about lubrication mechanisms in joints.

Very recently studies have been performed and reported, Minns and Stevens (1976), on the collagen fibril organisation of human articular cartilage. Using a newly devised technique for selectively depolymerising the proteoglycan, which strongly adheres to collagen, they removed the

proteoglycan and examined the pure collagen in the scanning electron microscope. They agreed that in the deep zone the collagen fibres ran radially, then upwards in an arcaded manner to the upper zone, where the fibres ran, in an unorganised fashion, parallel to the surface. They reported the absence of any layer that could be termed the lamina splendens, a fact they expected as the enzyme digestion technique used in preparation would have removed such a layer.

2.3 Mechanical Properties of Articular Cartilage

Investigations of the mechanical properties have been in progress for over a century, and workers have employed many techniques for studying them. Throughout there have been three main types of test performed:

1) Indentation; this has the advantage of being very simple to perform and does not require the cartilage to be disturbed before testing.

2) Unconfined tests where a plug of cartilage or cartilage and bone is removed and compressed in a manner allowing strains in all directions, and

3) Confined tests or uniaxial tests which are similar to the unconfined tests but restrict strains and flow to one direction only, the direction of load application.

Methods of interpretation of the results obtained have also varied, some studying long term responses and some instantaneous responses or the responses to oscillating loads.

It is intended in this review to present in chronological order the work already reported, although only brief comment will be made on some of the papers where they are not especially relevant to the work in this thesis.

Leidy (1849) despite little instrumentation studied the compression of cartilage and noted its capability of imbibing synovial fluid and returning to its original dimensions after drying. He noted that the imbibing of synovial fluid still took place when the dried cartilages were loaded with about 10 lbs/in^2 (69 x 10^{3}N/m^2), showing the power with which this process takes place. He claimed that the properties of cartilage would enable it to

diminish the violence of blows or shocks, and that it was possible for cartilage to wear, but afterwards it would lay down new surface layers, as these appeared to him to look newer than the deeper layers.

A long time interval then elapsed before Hirsch (1944) took up the investigation with indentation tests on in situ human cartilage. He noted instantaneous then creep deformations with recovery following the same pattern, but he did not find that complete recovery took place, probably due to his tests being conducted in air. He noted that longer than 30 mins. was required to reach equilibrium on loading, and the longer the loading the greater the permanent deformation when unloaded. Hirsch agreed that indentation tests were not true to life conditions and said they more closely represented a faulty joint with restricted contact area.

McCutchen (1962), besides studying porosity and permeability, studied the stiffness of articular cartilage from the leg joint of a cow. He compressed discs (5.45 mm diameter and 0.825 mm thick) between porous plates, and produced deformation/time graphs for increasing loads. From these he calculated values of Young's Modulus for the first 0.28 mm deflection of $5.8 \times 10^5 N/m^2$ for water and $3.2 \times 10^5 N/m^2$ for saline. The instantaneous modulus of $1.1 \times 10^7 N/m^2$, being greater than the others, was attributed to "not very mobile water."

Camosso and Marotti (1962) performed compression tests on cubes of bone and cartilage together and on bone alone. From their rather confusing paper their conclusions seem to be that the rate of deformation $\dot{\delta}$ decreases for increased load for the bone and cartilage combination, but that $\dot{\delta}$ increases with increased load for the bone alone.

Elmore et al (1963) took up the investigations of Hirsch. They used a low friction apparatus for studying the compression and recovery. They validated the findings of Hirsch, but made the very important discovery that the recovery is only complete when the specimen is immersed in a fluid.

This they termed the "Imperfect Elasticity" of cartilage. They also discovered the geometry of the indenter used for the tests had an effect on the deflections recorded. They had not at this stage found a successful method of measuring the cartilage thickness.

Linn and Sokoloff (1965) found the recovery rate was similar to the rate of uptake of water in cartilage on release of load. Although they state the immediate "instantaneous" linear deformation is too large to be accounted for solely by lateral fluid flow in an axial test, they attribute this to a rubber-like displacement.

Sokoloff (1966) studied the elastic properties of patella cartilage using a conical indenter. He states that the creep of articular cartilage resembles the visco-elastic flow of a polymer, but that it is due to the extrusion of fluid rather than rearrangement of molecules. A penetrating depth gauge and a dissecting microscope were used to determine the cartilage thickness. He studied the continuous long term compression under dead load and the instantaneous indentation at various stress levels. His findings from instantaneous tests indicated that the hardness of cartilage is comparable with rubber, and after short periods of loading the recovery displayed variable but considerable hysteresis. From the long term tests he found no change, due to age, in the deformation or recovery, but the indentations varied with the site on the patella, also the indentations were influenced by the subchondral bone when the cartilage was less than 2 mm thick. He quotes an instantaneous elastic modulus of 230 g/mm^2 (2.25 MN/m^2) and a modulus of 70 g/mm^2 (0.69 MN/m^2) after 1 hour of loading for human cartilage, and for bovine cartilage an instantaneous modulus of 1,229 g/mm^2 (12.0 MN/m^2) and a delayed modulus (after 5 mins) of 59 g/mm^2 (0.58 MN/m^2) in distilled water and 33 g/mm^2 (0.32 MN/m^2) in saline.

Edwards (1967) appears to be the first to perform confined tests. His apparatus was a porous piston and cylinder type with the specimen being a circular disc enclosed on all sides. Flow of liquid out of the specimen

when loaded was possible through the porous piston. He presented graphs of equilibrium thickness against pressure, and percentage liquid exchange against time. The time to reach equilibrium was the same for all specimens (6.6 mm diameter and 0.48 mm thick) and the water content of the specimens remained constant after equilibrium. The recovery curves were similar in shape to the compression curves. All of Edwards' results were based on the fluid flow in and out of the specimen, which was determined by weighing the specimen at intervals during the test. Therefore, none of the dramatic instantaneous response recorded by other workers was evident, as this is not attributed to fluid flow, but to the elastic response of the specimen, and naturally this response is also greatest when the specimen is unconfined. Edwards concluded that at equilibrium the applied load is carried partly by elastic stresses in the fibrous network and partly by osmotic forces generated mainly in the ground substances.

Kempson et al (1970, 1971, 1971a) used indentation tests to give them the relationships between compressive stiffness and various chemical constituents of human femoral head cartilage. These tests enabled them also to produce maps of cartilage stiffness areas which show a considerable range over the femoral head. They calculated a value of Poissons' Ratio for cartilage of 0.48 and quote values of the 2 second creep modulus in the range 4 - 10 MN/m^2.

Linn (1967) designed an Arthrotripsometer to study the friction and deflections in canine ankles. From the deflections recorded he had to subtract the rig deflection, which as will be seen in section (5.2) was also done in the experimental work of this thesis. For static loading Linn observed the normal initial and creep deformations which he claimed continued at a decreasing rate for up to 24 hours. However with oscillations in loading the deformation became constant at a steady value within 5-6 mins, showing some recovery is taking place between cycles. He noted recovery was also

speeded up if oscillation was allowed after load removal.

Simon (1971) studied the differences in intrinsic elasticity demonstrated by variations in indentations produced on similarly thick specimens for the same stresses. The differences between species corresponded roughly to the variation in water content of these species. He found the instantaneous recovery on removal of load to be always less than the instantaneous compression on application of load. Most of the deformation on indentation was observed to occur in the upper 50% of the specimen, which was discovered by successive removal of layers. He also performed oscillatory tests at a frequency of 1Hz and found the final deformation was less than with constant loading, a similar finding to that of Linn (1967). Frequency of loading was investigated, and as loading periods were increased so did the final deformations, until for periods of loading of 60 seconds or more the final deformations were the same as for static loading.

Radin et al (1970) investigated the dynamic force transmitting properties of subchondral bone and articular cartilage from the metatarso- and metacarpophalangeal joints of cows. The tests were between porous plates, but not confined; however they state that the dimensions of the specimens were such as to count the effect of barrelling as negligible. The compliance of cartilage decreased with increased strain rate and the transmitted peak force increased as impact load rate increased. The values of elastic modulus for cartilage quoted increase from 5 - 10 MN/m^2 at zero strain to around 50 MN/m^2 between 15 and 25% strain depending on the surrounding liquid and strain rate. They concluded that synovial fluid in a joint has no significant force attenuating qualities, but cancellous bone is equal or better than articular cartilage in its attenuation of dynamic peak forces, although it is about ten times stiffer because there is physically much more bone than there is cartilage.

In another paper on the subject, however, Radin and Paul (1970) state that only bone and the periarticular soft tissue of the joint have force

attenuating properties and that articular cartilage like synovial fluid plays no part in this attenuation. These findings were from work on intact joints by successively removing each of the components under investigation.

Maroudas (1973) summarises the response of articular cartilage to static (long-term) loading and to cyclic loading. She maintains the same viewpoint as Linn (1967) that at each load application in the cyclic cases some fluid will be lost which is not fully imbibed in the unloaded half of the cycle, a process which continues until steady state is reached when the cyclic load imposes an elastically recoverable 'instantaneous' deformation on the steady state deformation. This viewpoint is not shared by Yannas (1970) who maintains that fluid transfer in loading and unloading of cartilage is a linear relaxation process, and at normal walking frequencies no residual permanent deformation occurs, the recovery curve being an exact inverted image of the creep curve. Yannas draws close correlation to the work of Edwards (1967) and claims good agreement with the work of Linn and Sokoloff (1965).

Freeman et al (1975) studied the stress-lowering function of articular cartilage. The work was similar to that of Radin et al (1970) but Freeman et al used intact joints. They studied the response to cyclic loading of the intact joint, the cartilage alone, and the bone alone, after removal of the cartilage. Their findings showed that for healthy joints even up to 2000 cycles there was no recorded permanent deformation, but after removal of the cartilage the same loads caused fractures in the bone and permanent deformation. Therefore cartilage prevents the maximum stresses exceeding the fatigue fracture level.

The findings of other workers that for short loading periods flow processes do not play a dominant role in the deformation of articular cartilage were again upheld by Hayes and Mockros (1971). They performed uniaxial

(confined) compression tests and torsion tests from which they obtained values of bulk modulus, elastic modulus and Poissons' Ratio. The cartilage deformed similarly in the initial stages with or without a free draining boundary, leaving them to conclude that fluid flow was negligible at this stage. They quote values of Young's Modulus as $1.2 \times 10^7 N/m^2$ for short term responses and $7.1 \times 10^6 N/m^2$ for long term responses.

2.4 The Lubrication of Synovial Joints

The desirability of low friction in human joints is now widely accepted but the methods by which this is achieved are still in question. Many workers feel that not only would an effective lubricating film reduce friction, but also minimise wear and surface damage of the joint. There have been several proposed mechanisms, hydrodynamic, boundary, weeping, elasto-hydrodynamic and various combinations of these.

Originally hydrodynamic lubrication was favoured, MacConaill (1932), but Charnley (1959) disputed this, putting forward arguments in favour of boundary lubrication. However he questioned the origin of the fluid film between the articular surfaces; did it originate from the free cavity of the joint or from the deeper layers of the cartilage?

Around the same time McCutchen (1959) first posed his idea of a 'weeping bearing' and followed this (1966, 1967) with the idea of a possible 'osmotic lubrication'. 'Weeping lubrication' implied a special form of self acting hydrostatic bearing composed of a soft, elastic, porous layer of articular cartilage, lining a more rigid impervious backing. The important features of the layer were that the modulus of elasticity was low and that the pores were closed distally from the articulation by the impervious bone substrate. The effects of this combination, according to McCutchen, were to allow the elastic matrix to deform while the applied load was carried by the incompressible fluid within the matrix. Thus fluid film lubrication could be

affected by allowing fluid to 'weep' from the cartilage matrix. The 'osmotic' explanation of the boundary lubrication involves the constituents within the synovial fluid. The large molecules within the fluid are laid down on the cartilage surface, forming a carpet-like gel. As the fluid is pressurised under load the watery base fluid disperses and the volume of the gel decreases, hence increasing the osmotic pressure, and the gel volume tries to expand. McCutchen says this osmotic pressure would help to take the load.

Tanner (1966) introduced another possible lubrication regime, elastohydrodynamic (e.h.l.). He suggests that e.h.l. is the principal load carrying mechanism, but in the small areas of cartilage contact, which produce the friction, there must be boundary lubrication. This boundary lubrication, he states, would be provided by the long-chain hyaluronic acid molecules in the synovial fluid.

Fein (1967) proposed that synovial joints were probably squeeze film lubricated, with the film being replenished by hydrodynamic action when sliding or rolling occured. Dowson (1967) in summarising the previous thoughts on lubrication problems, concluded that classical hydrodynamic analysis was inadequate but e.h.l. films may be formed during normal movement. Squeeze film action might preserve the lubricant after motion stops at the end of each walking cycle, but he felt that the e.h.l. films would be unlikely to persist under severe conditions of little or no sliding. Therefore the synovial fluid must act as a boundary lubricant to encourage low starting friction. The major lubrication mechanism then seemed to be a combination of e.h.l., squeeze film and boundary, depending on the circumstances at the particular time.

Walker et al (1968) and Dowson et al (1970) proposed yet another possible mechanism, that of 'boosted' lubrication. They came to this conclusion after a study of the geometry of the surfaces involved. They found the cartilage

surface to be rough compared to most engineering surfaces, and considering the size of the molecules in synovial fluid and possible film thicknesses, these molecules must play an important role in lubrication. Using the earlier work of Maroudas et al (1968) they postulated that under pressure, a gel of concentrated synovial fluid formed as the hyaluronic acid molecules were too large to pass into the cartilage along with the base fluid. This gel became trapped in pools between the asperities. 'Boosted' lubrication was therefore based on the formation and entrapment of these pools of concentrated (and therefore more viscous) synovial fluid.

Higginson and Norman (1974) in a theoretical and experimental study of possible lubrication mechanisms, concluded that the permeability of cartilage was too low to be a significant factor in lubricating joints except perhaps under conditions of extremely thin films when boundary lubrication regimes will be dominant. This work suggested that lubrication regimes involving short term flow into or out of the cartilage would be ineffective during normal movement. Such mechanisms are 'weeping' lubrication and 'boosted' lubrication, which was analogous to the first enrichment mechanism investigated by Higginson and Norman. The second enrichment mechanism (filtration) and entrapment process seemed to be most likely. These are not exclusive systems, entrapment being an e.h.l. phenomenon during thick films and filtration taking over as the film closes. Finally they conclude "that the mere presence of the soft impermeable layer has a greater effect than do either of the complicated mechanisms of 'weeping' or enrichment".

These latter findings of Higginson and Norman were based on simulated cartilage materials; however the work reported in chapter 5 of this thesis, both experimental and computed, supports their findings. Fluid flow into or out of the cartilage is shown to be insignificant under cyclic loading having

a frequency similar to that encountered in walking. So it seems unlikely that this mechanism has a significant role in the lubrication mechanism of human joints.

More recently Mansour and Mow (1976, 1976a) have published their findings on the lubrication mechanism present in synovial joints. These findings are based on a three-layer computer model of articular cartilage. They modelled both healthy and degenerate cartilage and produced the flow fields in each under load. The calculated flow field for healthy cartilage (i.e. that with an intact surface of low permeability) shows that the tissue creates a naturally lubricated surface. The interstitial fluid is exuded in front of and near the leading half of the moving surface load, and imbibed behind or near the trailing half of the load. However in degenerate cartilage (i.e. that with a high surface permeability) the flow is out of the loaded region and therefore cannot aid the load carriage and formation of a lubricating film. They claim that neither 'weeping' nor 'boosted' lubrication fully describes the predicted process of joint lubrication.

Their findings however are in contrast to the findings of Higginson and Norman (1974) and those in this thesis, both of which support the view that for the short loading periods in a normal walking cycle, with the permeability of cartilage being so low, flow processes play little part in the short dynamic deformations and therefore lubrication of the joint.

3 Theory

3.1.0 Mechanical Model of Articular Cartilage

An initial formulation of a programme to model cartilage was produced and documented by Litchfield (1974). Further development work has since been done and a modified programme produced.

The model is designed to reproduce the load/deformation/time characteristics of a porous solid. Then by choosing distinct boundary conditions and data the model can be used to reproduce approximately these characteristics for articular cartilage.

The main restriction made on the theory when applying it to cartilage is that deformation is uniaxial and there is no lateral strain. Some justification for neglecting lateral strains is found by considering the geometry of a highly conforming joint such as the human hip joint. The thickness of cartilage in such joints is only about 2.0 mm whereas the load is applied over an area of several cm^2. In such a case axial strains will predominate. Further, the main aim of this investigation is to secure an understanding of the mechanical behaviour of cartilage, and much of the experimental information available has been obtained under conditions of axial symmetry, sometimes with zero radial strain.

The deformation of articular cartilage can be separated conceptually into an 'elastic' component which would exist alone if all the fluid in the matrix were unable to move, and a 'fluid' component arising from the flow of fluid into and out of the solid matrix. In evaluating the second, the matrix and the fluid will be treated as incompressible.

The computer model is a fluid flow model and all volume change within the specimen is brought about by fluid flow into and out of the matrix.

The basic assumptions for this are:-

1) The deformation is uniaxial

2) The fluid is incompressible

3) The solid matrix is incompressible

The model therefore deals with only one of the two responses to load of a porous solid. Because lateral strains are excluded, the magnitude of any 'elastic' component of deformation would be restricted to the order of the bulk modulus effect and be very small compared to deformations caused by fluid flow.

The load/deformation/time model must allow large strains and incorporate the resulting changes in the relevant property values. The three fundamental considerations that must be satisfied are:-

1) Equilibrium

2) Continuity of flow

3) The law governing fluid flow in a porous solid

The law governing fluid flow in a porous solid, Darcy's Law, incorporates a term p, the fluid pressure. When relating this law to articular cartilage the value of p used in the programme is taken as the value of the fluid pressure relative to the equilibrium osmotic pressure. The osmotic pressure arises from the physico-chemical effects of the solutes in the fluid, and hence complicates any assessment of the contribution of the fluid pressure to load carriage in cartilage. This can be obviated by using as the 'base' behaviour the experimentally determined static load/displacement characteristics of articular cartilage, taken as the equilibrium displacements for a series of incremental loads. This then inherently builds into the programme the effect of osmotic pressure and any calculated value of p can be considered relative to this.

3.1.1 Continuity

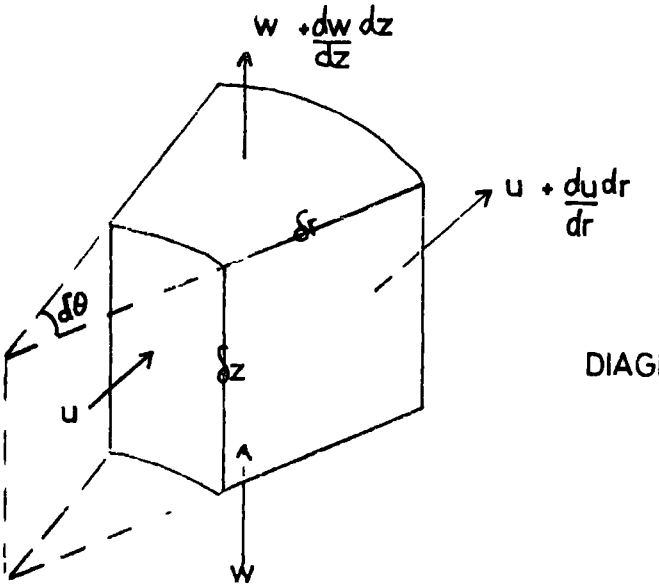

DIAGRAM 1

Consider the element in diagram(1) with cylindrical coordinates $\delta r, \delta\theta, \delta z$

The continuity equation gives:-

flow in = flow out + rate of volume change

If u is the flowrate in the radial direction, w is the flowrate in the axial direction, and because of axial symmetry $\delta\theta$ remains constant, and δr also remains constant as only uniaxial strains are considered, then the continuity equation becomes:-

$$u(r\delta\theta\delta z) + w(r+\frac{\delta r}{2})\delta\theta\,\delta r = (u+\frac{du}{dr}\delta r)(r+\delta r)\delta\theta\,\delta z + (w+\frac{\delta w}{\delta z}\delta z)(r+\frac{\delta r}{2})\delta\theta\delta r + \dot{V}_e \qquad (1)$$

where V_e is the volume $(r+\frac{\delta r}{2})\delta\theta\delta r\,\delta z = C_a dz$

where C_a is a constant and with $\delta\theta$ and δr being constant

$$\dot{V}_e = C_a \frac{d(\delta z)}{dt}$$

Now

$$dz = dz_0(1-\epsilon_z)$$

$$\epsilon_z = -\left(\frac{dz - dz_0}{dz_0}\right)$$

and

$$\frac{dz}{dt} = -dz_0\dot{\epsilon}_z$$

where dz_0 is the initial value of dz and ϵ_z is the axial 'engineering' strain. With the convention taken such that compression is positive

Therefore
$$\dot{V}_e = - C_a \, dz_0 \, \dot{\epsilon}_z$$
$$= - C_a \frac{dz}{1-\epsilon_z} \dot{\epsilon}_z$$
$$\dot{V}_e = - \left(r + \frac{dr}{2}\right) dr \, d\theta \, dz \, \frac{\dot{\epsilon}_z}{1-\epsilon_z} \qquad (2)$$

Substituting equation (2) into equation (1), cancelling equal and very small terms leaves the continuity equation in the form:-

$$\frac{u}{r} + \frac{du}{dr} + \frac{dw}{dz} - \frac{\dot{\epsilon}_z}{1-\epsilon_z} = 0 \qquad (3)$$

3.1.2 Fluid Flow

The modern extension of Darcy's Law will be used to relate the flow rates to the pressure gradients. Although flow is assumed axially symmetric, radial and axial permeabilities could be expected to differ.

Darcy's Law gives
$$u = - \frac{K_r}{\eta} \frac{dp}{dr}$$
$$w = - \frac{K_z}{\eta} \frac{dp}{dz}$$

K_r and K_z are radial and axial permeabilities η is the dynamic viscosity

$$\frac{du}{dr} = - \frac{K_r}{\eta} \frac{d^2p}{dr^2} - \frac{1}{\eta} \frac{dK_r}{dr} \frac{dp}{dr}$$
$$\frac{dw}{dz} = - \frac{K_z}{\eta} \frac{d^2p}{dz^2} - \frac{1}{\eta} \frac{dK_z}{dz} \frac{dp}{dz}$$

Substituting these into the continuity equation gives

$$\frac{K_r}{r} \frac{dp}{dr} + K_r \frac{d^2p}{dr^2} + \frac{dK_r}{dr} \frac{dp}{dr} + K_z \frac{d^2p}{dz^2} + \frac{dK_z}{dz} \frac{dp}{dz} + \frac{\eta \, \dot{\epsilon}_z}{1-\epsilon_z} = 0 \qquad (4)$$

where p is the value of fluid pressure, relative to the equilibrium osmotic pressure.

3.1.3 Equilibrium and the load carrying mechanism

In order to use the value of p calculated from equation 4 consideration must be paid to the roles played by the fluid and the solid matrix in supporting the applied load.

It can be assumed that at any time and in any layer of the porous solid the applied load will be supported by the sum of these two components.

$$F_a = F_s + F_f \qquad (5)$$

F_a = applied force

F_s = component carried by the solid matrix

F_f = component carried by the fluid in the form of hydrostatic pressure

Equation 5 can be rewritten as

$$\sigma_a \delta A = \sigma_s \delta A + p \delta A \qquad (6)$$

where σ_s is the load per unit area carried by the solid matrix

σ_a is the applied load per unit area

Litchfield (1974) considered the fluid pressure to act solely on an area $\delta A'$ the area of the fluid is a given layer. This is now believed to be an erroneous assumption as, although the area of fluid is less than the total area by the factor of porosity, $\delta A' = n \delta A$ where n is the porosity, the effect of hydrostatic pressure will be transmitted throughout the whole solid as hydrostatic stress

Equation 6 could be rewritten as

$$\sigma_a \delta A = \sigma_s \delta A + p(1-n)\delta A + pn\delta A \qquad (7)$$

where the terms ($\sigma_s \delta A + p(1-n)\delta A$) are in fact the total load carriage capability of the solid matrix and $pn\delta A$ is the load carriage capability of the fluid in the layer.

The value of p therefore in equation 4 incorporates the last two terms of equation 7.

Equation 6 can be used to work out the equilibrium strain, by knowing the value of σ_s at this point

$$\sigma_s = f_n(\epsilon_z)$$

This function can be calculated from the variation of σ_a with ϵ_z when p is zero, as at this point equation 6 becomes $\sigma_a = \sigma_s$

When p is zero the fluid pressure throughout the porous material is zero and hence there is no fluid flow. Zero in this case referring to zero gauge pressure, the external fluid pressure. If there is no flow, there is no increase in ϵ_z and the material has reached equilibrium.

From experimental work the equilibrium $\sigma_a - \epsilon_z$ characteristics have been obtained, and although non linear they are reversible and repeatable. A good empirical fit to these characteristics is

$$\sigma_a = \sigma_s = \frac{a\epsilon_z}{1 - b\epsilon_z} \qquad (8)$$

where a and b are constants and ϵ_z the compressive strain. When loads are applied producing strains very close to the initial porosity of the material the pores at the surface close, allowing no flow, and any increase of load after this point is compressing solid only. This can be seen from the asymptotic nature of the $\sigma_a - \epsilon_z$ curves at strains near the value of porosity.

In equation 8, a can be regarded as the static or slow strain modulus at small strains and b the non-linear effect at large strains.

3.1.4 Permeability and Porosity Variation

A final consideration to be taken into account in the formulation of the computer model is the way both permeability and porosity vary in a porous solid, as that solid is strained

i.e. $n = f_1(\epsilon_z)$

$K_r = f_2(\epsilon_z)$

$K_z = f_3(\epsilon_z)$

From Litchfield (1974) it is shown that

$$n = \left(\frac{v - \epsilon_z}{1 - \epsilon_z}\right) \qquad (9)$$

where n is the porosity at a given strain ϵ_z

and v is the unstrained porosity of the porous solid

Litchfield (1974) also investigated the functions f_{m_2}, f_{m_3} as there was no documentation of the effect of strain on permeability. This was done with a polymeric filter material of porosity 0.4 and the results showed that

$$K_r \propto \frac{(v - \epsilon_z)^5}{1 - \epsilon_z} \qquad (10)$$

$$K_z \propto (v - \epsilon_z)^3 \qquad (11)$$

Equations 9, 10, 11 are used in the computer model

3.2 Axial Flow

3.2.1 Theory related to the special case of axial flow only

Already assumed through axial symmetry is the fact that $\frac{d}{d\theta} = 0$ now in the axial flow case variations of pressure and permeability in the radial direction are zero $\frac{d}{dr} = 0$

Flow cannot take place radially, nor can strains vary radially, and the effect of an applied load is to produce only axial flow and axial strains. The problem is therefore reduced to one dimension.

Equation 4 becomes

$$K_z \frac{d^2p}{dz^2} + \frac{dK_z}{dz}\frac{dp}{dz} + \frac{\eta \dot{\epsilon}_z}{1 - \epsilon_z} = 0 \qquad (12)$$

The permeability variation with strain in equation 11 was shown by Litchfield (1974) to be reasonably approximated by

$$K_z = K_0 \frac{(v - \epsilon_z)^3}{v^3} \qquad (13)$$

Again the assumption leading to equation 5 and the experimentally determined $\sigma_a - \epsilon_z$ relationship of equation 8 must be used.

In future, when considering axial flow only, all z suffixes can be dropped.

3.2.2 Dimensional Analysis for Axial Flow

Calculations and presentation are made more compact by the use of dimensionless groups.

The relation between displacement and time for a given mode of loading is obtained from the solution to equations 6, 8, 12, 13 for the axial flow case.

The independent variables in a study of articular cartilage behaviour or any porous solid are:-

δ	deflection	Dimensions	L
z_o	initial thickness		L
σ_a	applied stress		$\frac{M}{L T^2}$
t	time		T
v	initial porosity		—
K_o	initial permeability		L^2
η	viscosity		$\frac{M}{LT}$
a	constant } from equation 8		$\frac{M}{L T^2}$
b	constant }		—

Using these variables the system could be described by 6 dimensionless groups, however on studying the governing equations, it can be seen that K_o and η appear only as a ratio, so one variable can be omitted and hence

$$\delta = f_n (z_o , \sigma_a , t , v , \frac{K_o}{\eta} , a , b)$$

This compacts the system to 5 dimensionless groups.

Using the Buckingham Π Theorem these groups appear as:-

$$\frac{\delta}{z_o} , \frac{\sigma_a}{a} , \frac{K_o a t}{\eta z_o^2} , b , v$$

hence

$$\frac{\delta}{z_o} = f_n \left(\frac{\sigma_a}{a} , \frac{K_o a t}{\eta z_o^2} , b , v \right)$$

The fluid pressure p, which cannot be counted as an independent variable in the problem, can however be represented in a dimensionless manner, by making it an extra group in the form of $\frac{p}{a}$

Equation 12 must now be represented in terms of these groups (N.B. dropping suffix z)

Write $K = K_0\frac{(v-\epsilon)^3}{v^3}$ as $K_0\,\phi(\epsilon)$ (14)

On substituting for K and dividing by K_0 throughout equation 12 becomes

$$\phi(\epsilon)\frac{d^2p}{dz^2} + \frac{d\phi(\epsilon)}{dz}\frac{dp}{dz} + \frac{\eta}{K_0}\cdot\frac{\frac{d\epsilon}{dt}}{1-\epsilon} = 0 \qquad (15)$$

Writing

$$T = \frac{K_0 a t}{\eta z_0^2} \quad , \quad P = \frac{p}{a} \quad , \quad Z = \frac{z}{z_0}$$

on substituting for t , equation 15 becomes:-

$$\phi(\epsilon)\frac{d^2p}{dz^2} + \frac{d\phi(e)}{dz}\frac{dp}{dz} + \frac{\eta}{K_0}\frac{aK_0}{\eta z_0^2}\frac{\frac{d\epsilon}{dT}}{1-\epsilon} = 0$$

substituting for p

$$\phi(\epsilon)a\frac{d^2P}{dz^2} + \frac{d\phi(\epsilon)}{dz}a\frac{dP}{dz} + \frac{a}{z_0^2}\frac{\frac{d\epsilon}{dT}}{1-\epsilon} = 0$$

substituting for z

$$\phi(e)\frac{a}{z_0^2}\frac{d^2P}{dZ^2} + \frac{d\phi(\epsilon)}{dZ}\frac{a}{z_0^2}\frac{dP}{dZ} + \frac{a}{z_0^2}\frac{\frac{d\epsilon}{dT}}{1-\epsilon} = 0$$

The final dimensionless representation of equation 12 is

$$\phi(\epsilon)\frac{d^2P}{dZ^2} + \frac{d\phi(e)}{dZ}\frac{dP}{dZ} + \frac{\frac{d\epsilon}{dT}}{1-\epsilon} = 0 \qquad (16)$$

3.2.3 Numerical Method for Computing

The solution to the governing equations, giving variation of deformation with time under specific loading is obtained by a relaxation method and finite difference formulae.

A finite difference formulation of equation 16 must be used to give an expression for the fluid pressures in terms of local strains and permeabilities in the material. As all loading was through flat plates it was assumed that strains in any horizontal plane were equal and hence fluid pressures in any one layer could be integrated to total fluid force in that plane.

Initially at time $T = 0$ the total thickness is divided into equal increments of depth ΔZ and hence finite difference representation of equation 16 would be relatively straight forward. Using a technique of equal increments of depth, after each interval of time the new total thickness would need to be redivided into equal increments, which would have no relationship to the points within the solid during the previous time interval. Therefore in order to keep to the same sections of solid for each time increment, so as to enable comparison of the effects of time on certain cross-sections of the solid throughout the loading period, finite difference equations are required that allow for variations of ΔZ that are not constant with time or with distance from the surface.

The method of obtaining such finite difference equations for varying step lengths of ΔZ follows

Refer to figure 3.1a

An imaginary point $(P_{I+1})'$ is obtained, which is at an equal increment above P_I as P_{I-1} is below it. The gradient of the straight line joining these points is then assumed to be the same as the gradient at point P_I

i.e. $$\left(\frac{dP}{dZ}\right)_I = \frac{P_I - P_{I-1} + \frac{\Delta Z_{I-1}}{\Delta Z_I}\left(P_{I+1} - P_I\right)}{2\,\Delta Z_{I-1}} \qquad (17)$$

Similarly

$$\left(\frac{d\phi}{dZ}\right)_I = \frac{\phi_I - \phi_{I-1} + \frac{\Delta Z_{I-1}}{\Delta Z_I}\left(\phi_{I+1} - \phi_I\right)}{2\,\Delta Z_{I-1}} \qquad (18)$$

A similar method is used to obtain $\left(\frac{d^2P}{dZ^2}\right)_I$. Here two imaginary points must be utilized. See figure 3.1b.

The first evaluation of $\left(\frac{d^2P}{dZ^2}\right)_I$ is obtained from using the change in the gradients at points $P_{I-\frac{1}{2}}$ and $\left(P_{I+\frac{1}{2}}\right)'$, a point halfway to $\left(P_{I+1}\right)'$

This gives $$\left(\frac{d^2P}{dZ^2}\right)_I = \frac{P_{I-1} - P_I + \frac{\Delta Z_{I-1}}{\Delta Z_I}\left(P_{I+1} - P_I\right)}{(\Delta Z_{I-1})^2}$$

The second evaluation of $\left(\frac{d^2P}{dZ^2}\right)_I$ is obtained from points $\left(P_{I-\frac{1}{2}}\right)'$, a point halfway to point $\left(P_{I-1}\right)'$, and point $P_{I+\frac{1}{2}}$

This gives $$\left(\frac{d^2P}{dZ^2}\right)_I = \frac{P_{I+1} - P_I - \frac{\Delta Z_I}{\Delta Z_{I-1}}\left(P_I - P_{I-1}\right)}{\Delta Z_I^2}$$

As both of these evaluations are only an approximation of the truth, and are on either side of it, an average of both was taken arriving at the final presentation:-

$$\left(\frac{d^2P}{dZ^2}\right)_I = \frac{\Delta Z_I + \Delta Z_{I-1}}{2\Delta Z_I \Delta Z_{I-1}}\left[\frac{P_{I-1}}{\Delta Z_{I-1}} + \frac{P_{I+1}}{\Delta Z_I} - P_I\left(\frac{1}{\Delta Z_{I-1}} + \frac{1}{\Delta Z_I}\right)\right] \qquad (19)$$

Equations 17, 18 and 19 are put into equation 16 to give

$$P_I = f_n\left(P_{I+1}, P_{I-1}, \phi_I, \phi_{I+1}, \phi_{I-1}\right)$$

Finite difference presentation of P_I where $I = 1$ will not be possible as P_0 is non-existent in the programme.

Therefore to find P_1 a technique is used which fits a polynomial to points P_2 and P_3 and from this curve fit polynomial point P_1 can be estimated. This polynomial turns out to be

$$P_1 = \frac{(\Delta Z_1 + \Delta Z_2)^2 P_2 - \Delta Z_1^2 P_3}{2\Delta Z_1 \Delta Z_2 + \Delta Z_2^2}$$

3.2.4 Computation

A flow diagram of the computer model is shown in figure (3.2). The solution to the dimensionless equations giving variation of deformation with time under specific loading is obtained using a relaxation method and the finite difference formulae.

The programme uses increments of dimensionless time ΔT and of depth ΔZ

Initially a guess is made of the strain in each element of depth, from this values of $\phi(\epsilon)$ and then P are calculated for each depth. A summation of these 'pressures' at any cross-section gives the contribution of fluid pressure to the 'load' at that section and hence by difference from the total applied 'load' the share of 'load' carried by the matrix. Once the matrix 'stress' is calculated the strain can be obtained. This strain is then compared with the initially guessed strain, and iteration continues until convergence is achieved for one time interval. The programme will then print out the strain and the dimensionless time. Time is then increased by ΔT and the procedure repeated until no increase in strain is achieved by increasing time, at which point the equilibrium has been reached.

3.3 Radial Flow

3.3.1 Theory related to the special case of radial flow only

Again, already assumed through axial symmetry is the fact that $\frac{d}{d\theta} = 0$, now in the case of radial flow only, changes of permeability and porosity in the z direction are also zero, $\frac{d}{dz} = 0$ and K_r is a function only of time

Equation 4 becomes

$$\frac{K_r}{r}\frac{dp}{dr} + K_r\frac{d^2p}{dr^2} + \frac{\eta\dot{\epsilon}_z}{1-\epsilon_z} = 0 \qquad (20)$$

Integration and calculation of constants gives

$$p = \frac{\eta\dot{\epsilon}_z}{4K_r(1-\epsilon_z)}(R^2 - r^2) \qquad (21)$$

To calculate the fluid force at a level in the specimen equation 21 is integrated from 0 - R over an area of $2\pi r\delta r$

$$F_f = \int_0^R \frac{\eta \dot{\epsilon}_z}{4 K_r (1-\epsilon_z)} (R^2 - r^2) 2\pi r \delta r$$

$$F_f = \frac{\eta \dot{\epsilon}_z \pi R^4}{8 K_r (1-\epsilon_z)} \qquad (22)$$

The permeability variation with strain in equation 10 was shown by Litchfield (1974) to be reasonably approximated by

$$K_r = \frac{K_1 (v - \epsilon_z)^5}{v^5 (1 - \epsilon_z)} \qquad (23)$$

Then equation 22 becomes

$$F_f = \frac{\eta \dot{\epsilon}_z \pi R^4 v^5}{8 K_1 (v - \epsilon_z)^5} \qquad (24)$$

Here again the assumptions leading to equation 5 and the experimentally determined $\sigma_a - \epsilon_z$ relationship of equation 8 must be used.

In future when considering radial flow the suffixes z may be dropped.

The final representation of equation 5 in the radial flow case becomes:-

$$\sigma_a \pi R^2 = \frac{a \epsilon_z \pi R^2}{1 - b\epsilon_z} + \frac{\eta \dot{\epsilon}_z \pi R^4}{8 K_r (1-\epsilon_z)} \qquad (25)$$

3.3.2 <u>Dimensional Analysis for Radial Flow</u>

Again dimensional analysis was used to rationalise the computation of the radial flow case.

The relationship between ϵ and time for a given mode of loading is obtained from the solutions to equations 5, 8, 20, 23, which are combined in equation 25.

Because the specimen is uniform through the thickness, $\frac{z}{z_0} = \epsilon$

is uniform through the thickness also, and ϵ varies only with time.

The independant variables become

ϵ	strain	Dimensions	—
σ_a	applied stress		$\frac{M}{LT^2}$
t	time		T
R	Radius		L
K_1	Initial permeability		L^2
a	constant } from equation 8		$\frac{M}{LT^2}$
b	constant }		—
v	initial porosity		—
η	viscosity		$\frac{M}{LT}$

Again, K_1 & η as with K_0 & η in the axial flow case, can be combined as a ratio since they only appear together and hence:-

$$\epsilon = f_n\left(\sigma_a, t, R, a, \frac{K_1}{\eta}, b, v\right)$$

Using the Buckingham Π theorem again, the 5 dimensionless groups appear as:-

$$\epsilon = f_n\left(\frac{\sigma_a}{a}, \frac{K_1 a t}{\eta R^2}, b, v\right)$$

Equation 25 must now be rewritten in terms of these groups

Firstly write

$$K_r = \frac{K_1(v-\epsilon)^5}{v^5(1-\epsilon)} \quad \text{as} \quad K_r = K_1\psi(\epsilon) \tag{26}$$

Substituting for K_r and dividing by $\pi R^2 a$ equation 25 becomes

$$\frac{\sigma_a}{a} = \frac{\epsilon}{1-b\epsilon} + \frac{\eta\dot{\epsilon}R^2}{8aK_1\psi(\epsilon)(1-\epsilon)}$$

Writing $T^* = \frac{K_1 a t}{\eta R^2}$, $\Sigma = \frac{\sigma_a}{a}$ and $dT^* = \frac{K_1 a\, dt}{\eta R^2}$

Substituting Σ equation becomes

$$\Sigma = \frac{\epsilon}{1-b\epsilon} + \frac{\eta R^2 \frac{d\epsilon}{dt}}{8aK_1\psi(\epsilon)(1-\epsilon)}$$

Substituting for δt

$$\sum = \frac{\epsilon}{1-b\epsilon} + \frac{1}{8\psi(\epsilon)(1-\epsilon)} \frac{d\epsilon}{dT^*}$$

Rearranging gives

$$-\frac{d\epsilon}{dT^*} = \left(\sum - \frac{\epsilon}{1-b\epsilon}\right) 8\psi(\epsilon)(1-\epsilon) \qquad (27)$$

Equation 27 is the final dimensionless form of equation 25 required for the computation.

3.3.3 Computation - Radial Flow

A Flow diagram of the computer model is shown in figure (3.3).

The solution to equation 27 throughout the time of loading is brought about by an iterative method.

Initially a guess is made at the strain rate in the present increment of T^*. Using this value of $\frac{d\epsilon}{dT^*}$ a value for ϵ is calculated and used in equation 27. This then produces another value of $\frac{d\epsilon}{dT^*}$ which is compared with the initial one. The iteration continues until the guessed and calculated values are equal. At which time the ϵ is written out. The time is then increased by ΔT^*, a new guessed strain is chosen and the iterations begin again for the new increment of T^*.

If required the programme can be halted when the final strain is reached or the programme will continue at this time to remove the loading on the specimen and calculate values of strain in the recovery phase.

3.4 Determination of overall permeability from the distribution of permeability through the depth

The computer model as explained in the earlier sections of this chapter requires an overall value for permeability of the slice of cartilage being considered. This assumes that initially every point throughout the

depth of the slice has the same permeability, and then, as time of loading increases this value is modified by the term $\left(\frac{v-\epsilon}{v}\right)^3$ (Equation 13). It is possible in the computation to vary the parameters making up the dimensionless groups and so define their effect on the strain/time characteristics. However Maroudas (1973a) presented graphs showing that throughout the depth of the cartilage the permeability was not constant. It was decided therefore to build into the programme, not only the facility for changing the overall permeability of a slice, but a distribution of permeability through the slice. As Maroudas herself said "There does not seem to be a correlation with age, either in magnitude of the permeability coefficient or in the shape of the permeability versus depth curve".

The following analysis was devised to obtain a value for the overall permeability of a slice if the permeability at discrete points within it are known.

Assume therefore a slice of cartilage as in diagram (A), below, divided into n sections. The overall pressure drop, thickness and permeability are given by P_D , Z_O and K_Z . For each of the slices these properties are given by p_{1-n} , z_{1-n} , k_{1-n} .

DIAGRAM A

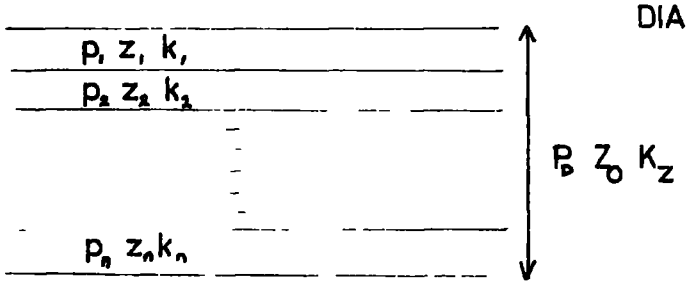

Now Darcy's Law states

$$w = -\frac{K}{\eta}\frac{dP}{dz}$$

or Total pressure drop, $P_D = -\frac{\eta}{K_Z}$ x Volume Flow x Total Thickness

$$P_D = -\frac{\eta\, w Z_O}{K_Z}$$

This law can be applied to each section giving

$$P_1 = -\frac{\eta w z_1}{k_1}, \qquad P_n = -\frac{\eta w z_n}{k_n}$$

Since

$$\Sigma_P = P_1 + P_2 + \quad + P_n = P_p$$

$$-\frac{\eta w z_1}{k_1} - \cdots - \frac{\eta w z_n}{k_n} = -\frac{\eta w Z_0}{K_z}$$

Since the flow through each slice must be the same, with no radial flow, and this must equal the total flow out, therefore:-

$$\frac{z_1}{k_1} + \frac{z_2}{k_2} + \quad + \frac{z_n}{k_n} = \frac{Z_0}{K_z}$$

If you now consider all sections to be of equal thickness this gives

$$z_1\left[\frac{1}{k_1} + \frac{1}{k_2} + \quad + \frac{1}{k_n}\right] = \frac{Z_0}{K_z}$$

Since $Z_0 = nz_1$

This is easily expressed as

$$\frac{1}{n}\Sigma\left(\frac{1}{k}\right) = \frac{1}{K_z} \qquad (28)$$

and gives a method for calculating the overall permeability of a slice from a known distribution of permeability throughout the slice.

3.5 The Elastic Modulus Calculated from Confined Tests

Considering now an ideal Hookean solid in the confined situation with strains restricted to the axial, z, direction only, the elastic modulus $E^* = \frac{\sigma_z}{\epsilon_z}$ is not simply either the Young's Modulus, E, or the Bulk Modulus, K, of the material. The following analysis of the situation produces a term for this modulus in terms of the Bulk Modulus and Poissons' Ratio of the material.

For the confined test, $\epsilon_r = 0$ and $\epsilon_\theta = 0$

However when applying σ_z, σ_r and σ_θ are not zero.

From Hooke's Law

$$E\epsilon_z = \sigma_z - \nu(\sigma_\theta - \sigma_r) \qquad (29)$$

$$E\epsilon_r = \sigma_r - \nu(\sigma_z - \sigma_\theta) \qquad (30)$$

$$E e_\theta = \bar{\sigma}_\theta - \nu(\sigma_z - \bar{\sigma}_r) \qquad (31)$$

Substituting and rearranging gives

$$E^* = \frac{\sigma_z}{\epsilon_z} = \frac{E}{(1-2\nu)} - \left(\frac{\sigma_r}{\epsilon_z} + \frac{\sigma_\theta}{\epsilon_z}\right) \qquad (32)$$

Substituting again for σ_r and σ_θ produces

$$E^* = \frac{\sigma_z}{\epsilon_z} = \frac{E(1-\nu)}{(1-2\nu)(1+\nu)} \qquad (33)$$

Since

$$K = \frac{E}{3(1-2\nu)}$$

$$E^* = 3K\frac{(1-\nu)}{(1+\nu)} \qquad (34)$$

This shows that for the conditions of a confined test the modulus, E^*, calculated from the oscillating load experiments, is:-

$$\frac{\text{Magnitude of axial stress}}{\text{Magnitude of axial strain}}$$

From equation 34 it can be seen that as

$$\nu \longrightarrow \frac{1}{2} \quad , \quad E^* \longrightarrow K \longrightarrow \infty$$

and in general, for $\nu < \frac{1}{2}$

$$E^* > K$$

4. The Experiments and Design of the Test Rig

4.1 Proposed Tests

The aim of this work as laid out in the introduction has been to investigate the load/displacement/time behaviour of articular cartilage under compressive stresses such as are present in the lower limbs.

As shown in the literature other workers have done compression tests on articular cartilage and published results. Most of their tests are of the indentation type, which are easy to perform but less easy to interpret. Other tests have been mainly of the conventional unconfined compression type; very few of the confined compression type have been reported. See figure 4.1 .

Indentation tests are useful in providing comparative studies of variation of properties across an intact bone end. They are usually performed by applying load through a blunt ended indenter at right angles to the cartilage surface. Removal of the cartilage from the bone is not required and therefore no errors arise from damage to the cartilage on removal. These tests are probably the least realistic in relation to the actual loading of a joint.

The unconfined tests as carried out by several workers in the field are not as simple to perform, but the results obtained are relatively easy to interpret. Load is applied to the specimen through impervious pads above and below the specimen. These tests have the disadvantage of requiring a specimen to be removed from the bone end before testing. This naturally introduces the possibility of errors arising from damage to the cartilage around the cut surface, and moreso if the cartilage is also removed from its underlying bone for testing.

For a confined compression test also a specimen must be removed from the joint, and it is tested either on the bone, or as a small disc of cartilage alone. The test is performed in a cylinder and piston arrangement, with the cylinder walls and base impervious and the piston made of a rigid

porous material. This arrangement applies load axially to the specimen and allows axial strain and flow. Radial strains and flow are prevented.

In indentation and unconfined compression tests all recorded results show an 'instantaneous' deflection on the application of load, followed by a creep component, with a similar sequence being followed on removal of load. The work by Elmore et al (1963) has shown that given time and an appropriate surrounding fluid articular cartilage will recover from compressive strains of up to 50% or more.

The action of cartilage under load can be divided conceptually into two parts, being an 'elastic' response which would exist alone if the fluid in the matrix were unable to move and a 'fluid' response arising from fluid flow in the matrix. The magnitude of the 'elastic' response will be dependent on the constraints on the specimen, especially in a material with a much higher volumetric stiffness than sheer stiffness. Higginson et al (1976).

In unconfined and indentation tests the 'elastic' component of deformation will be substantial as there are few constraints on the specimens. This probably accounts for the major part of the instantaneous deflections recorded.

In an actual joint, however, where cartilage is in the region of 2 mm thick and the load is distributed over a contact area of several square centimetres, the strains will be predominantly in the direction of loading. In this case the 'elastic' component will be restricted to the order of the bulk modulus effect.

For this reason it was decided that the majority of tests to be performed should be of the confined nature, as described earlier, as this most closely parallels the conditions of cartilage in a load-bearing joint.

4.2 Modes of Testing and requirements from the Rig

The work aimed at investigating the creep response of articular cartilage to applied loads indicating fluid flow in an axial direction. These could be termed as static tests or long term tests.

Investigation was also required into the dynamic response or short term response of cartilage to applied loads. To do this it is convenient to apply a sinusoidal load and study the periodic response of the cartilage. The load and response can be monitored to give hysteresis loops, from which details of moduli and phase angles can be taken. However any applied sinusoidal load will have a mean value over a cycle and this will act as a static component of load with the sinusoidal component superimposed upon it. The response will therefore be that of a typical creep test with an applied load of the magnitude of this mean value with a rippling response due to the sinusoidal load.

Therefore the two major requirements of the rig were to enable both static loading and dynamic loading of the specimens.

The rig had to include facility for confining the specimen, preferably with as little friction on the cylindrical surface as possible. The loads applied to the specimen must be axial, and there must be facility for recording them. The deformation of the cartilage must be monitored against time. For tests involving the recovery of cartilage from a state of loading the cartilage must have an ample supply of fluid.

The requirements of the test rig were therefore:-

a) To hold the specimen in a low-friction confined manner, allowing liquid exchange through one end surface only.

b) To keep an ample supply of immersion fluid available to the cartilage

c) To apply axial load to the cartilage

d) To have facility for making this load either static or sinusoidal

e) To have facility for recording this load.

f) To have facility for recording the displacements of the cartilage

4.3 Design of the Rig

4.3.1 Specimen holder

The specimen was of cylindrical form with parallel ends and therefore the holder was designed as a thick walled brass cylinder with a permanent P.T.F.E. lining. See figure (4.2).

The specimen was introduced into this tube between the impermeable plain end of the plunger and a fine sintered bronze disc, with the bone end, or cut surface of the cartilage, against the impermeable plunger. This then as closely as possible allowed no flow radially or upwards, and only flow downwards through the sintered bronze disc from the 'free' surface of the cartilage. This bronze disc had a reasonably smooth surface in contact with the cartilage to avoid extrusion of cartilage under load into the passages of the disc, but had much greater permeability (about 108 times bigger) than the cartilage and hence did not inhibit fluid flow out of or into the cartilage.

This disc rested on a spigot in the centre of the stainless steel fluid retaining dish. The spigot was perforated with small interlaced holes, again to allow fluid flow.

The level of the fluid, Mammalian Ringer's Solution, in the dish was maintained above the level of the cartilage in the inner tube. This was to cause a slight positive pressure gradient, as in the recovery tests the design of the rig required fluid to flow upwards into the cartilage as it is swelling.

The dish was located centrally on top of the load recording device. The perforated spigot in the centre of the base of the dish and perpendicular to it, ensured the faces of the sintered bronze disc, the cartilage and the plunger were parallel to the base of the dish.

The permanent P.T.F.E. lining to the tube surrounding the specimen caused considerable problems at first. The P.T.F.E., being unstable and very dependent on external conditions, was difficult to machine to the exact

dimensions required. These dimensions were such that the specimen O/D should be as close as possible to the P.T.F.E. I/D to eliminate radial strains. After a few tests with this lining the specimen holder was removed from the rig and studied. This showed a permanent deformation of the P.T.F.E. in the region of the specimen. The pressures in the specimen during tests had so deformed a local area of the lining as to invalidate the tests as being confined. Although the two ends to the tube had dimensions required for confined tests the I/D at the point where the specimen was housed during tests had been greatly increased. This problem naturally had to be overcome and it was decided to remove the permanent P.T.F.E. lining.

It was felt, however, that a lining was necessary to minimise friction inside the tube, but anything regarded as permanent was discounted as constant monitoring of its I/D would be laborious. A thin walled P.T.F.E. sleeve readily available on the market and with an I/D very close to that required was used in all future tests as the tube lining surrounding the specimen. It had the disadvantage of requiring a new cutter to be made for obtaining specimens of its exact I/D, but had the advantage that for each new test it was a simple procedure to replace the sleeving.

The plunger which can be counted as part of the specimen holder had to ensure that the load was applied axially. To do this the lower face was flat and in contact with the specimen and the upper end was hemispherical. The load was then applied to this hemispherical surface through a coned member, allowing self-centring of the components and axial loading.

The effectiveness of this system to apply axial loads and reduce friction was tested by inserting firstly solid steel specimens in place of the cartilage and then samples of rubber, both of similar dimensions to the cartilage specimens. By applying known loads above the plunger and recording load at the base of the dish, the load transmitted through the specimen and

the amount of load lost due to friction could be measured.

Over a series of tests conducted the average loss to friction was 2% of the applied load. This is reasonably small and in fact does not need to be accounted for in the calculations of the results as the load used in these calculations has always been the load recorded by the load cell, not the applied load. This is done as it can be guaranteed that load received by the load cell is actually transmitted through the cartilage, whereas applied load, as shown, can be lost before application to the cartilage.

4.3.2 Load recording

The rig where possible was to be designed around already available instrumentation or instrumentation easily made up. This was done both from a cost point of view and for speed of manufacture of the test rig.

Some analysis was performed on the design of a suitable sized load sensing device, using strain gauges, and this could have been acceptable. However, already available in the laboratory was a D90/250 Sangamo Controls Proof Ring Load Transducer and a Sangamo Direct Reading Transducer Meter type C52. Therefore for speed of manufacture of the rig it was decided to use these as the load recording devices. The Load cell has a basic accuracy of 0.1% full scale deflection and when used with this meter will give accuracy of 1% of the selected range. Although this meter has a maximum rated load of 1112N its smallest selected range is 0-44.5N with the accuracy of 1%.

This load transducer was used on its lowest two ranges 0-44.5N and 0-111.2N, and proved perfectly satisfactory, both statically and dynamically.

4.3.3 Load Application

As stated, the load must be applied either statically or sinusoidally, and in sinusoidal tests it should be possible to apply a constant load plus a superimposed oscillating component.

The static loading caused little problem as a yoke could be employed to rest above the plunger and have weights added at a point beneath the specimen. By having the weights centrally placed and the upper member of the yolk coned at the point of contact with the domed top of the plunger, the system ensured axial loading. The yolk was lowered by hand onto the plunger head, using a forked lever arrangement.

For the sinusoidal loading a more elaborate mechanism was required. The easiest and cheapest way of applying such a load was thought to be an eccentric on a rotating shaft, acting upon a soft spring to keep loading about constant as specimen strains. However a single eccentricity would not allow the application of various magnitudes of oscillating load, and a solid cam rotating across the top of a spring would induce sideways movements in the spring and jeopardise the axial loading. A system was therefore devised to a) provide a variety of eccentricities b) to apply a point load to the centre of the spring, this point also being stationary c) to provide guides for the spring to avoid sideways movement, and d) to allow alteration of the constant load.

The spring rests on a lightweight carrier above the plunger. This carrier is again coned to allow self centring on the plunger and has a small spigot for locating the spring centrally. At the upper end of the spring is another spigotted member located in a P.T.F.E. bush allowing vertical movement only. Above this are a series of smaller interlocking spacers. These can be added to or removed to allow an alteration of the permanent deflection required from the spring, giving the facility of choice of static loading for the test. The top spacer has a well defined domed surface, giving only central contact.

The variation in eccentricity on the shaft is obtained by a combination of a ball race with an eccentric bush and an eccentric on the shaft See figure 4.3. The outer race remains stationary, in contact with the

upper domed spacer, therefore avoiding sideways forces. The eccentric bush and the eccentric on the shaft can be rotated with respect to each other and located by a small bolt to give any of 10 eccentricities.

The central shaft is rotated by a belt drive from a variable speed motor and gear box.

4.3.4 Displacement Recording

The instrument for recording displacement had to be capable not only of recording the D.C. Creep deflections, which it was considered could be up to around 1 mm, but also of detecting and measuring any superimposed oscillatory deflection at all points during the creep phase.

It was decided to use linear variable differential transformer (L.V.D.T.) type transducers for the purpose of recording the displacement. These are rugged, accurate and stable devices for detecting static and dynamic displacements with infinite resolution, and with no wearing parts. The type chosen was R.D.P. Electronics Ltd., D5/100 with a linear range of ±2.54 mm and linearity on calibration of 0.5%. A disadvantage of these is that the body and armature must be mounted separately, and due to the layout of the rig, recording displacement in the load line was impossible.

The inability to record displacement in the load line, led to the use of two transducers positioned symmetrically about the centre line. The signals from each of these δA and δB can then be fed to a Sangamo Switch Selector Unit type C35 with outputs of δA, δB and δC where $\delta C = \frac{\delta A + \delta B}{2}$. δC is therefore the displacement along the centre line of load application.

The displacement of the specimen should also be the displacement between the dish and the top of the plunger. This fact was used in deciding on the mounting positions of the transducers. The body components were threaded into a lip around the dish. The armatures were threaded into the spring support plate, in contact with the plunger head. See figure 4.2.

Relative motion of the armature and body sections is the deflection of the cartilage.

The output of the transducers is again suitable to be fed to a Sangamo direct reading transducer meter type C52/1

4.4 Instrumentation

As stated the outputs from the load transducer and the displacement transducers are fed to transducer meters type C52/1. These give direct readings but no permanent record. To obtain a permanent record the filtered output from these meters must be fed to a second recording system. Initially a U.V. recorder was used, this appeared to work satisfactorily; however there was too great a possibility of human error in interpreting the traces. The U.V. record was in the form of two traces, one monitoring load and one monitoring displacement, both the creep and sinusoidal displacements superimposed. Therefore to obtain hysteresis loops for values of modulus these had to be transferred by hand to a suitable graphical form, introducing interpretation errors.

This method of obtaining a permanent record was discontinued and superseded by an Advance oscilloscope type OS250 with X - Y facility. This was fitted with a Polaroid Land camera for permanent records of the traces.

The load gave the y-trace and displacement the x-trace. Some difficulty was encountered with the displacement trace as the creep component of the displacement caused considerable drift of the trace especially at the beginning of the test where this was most prominent. Also there was mains hum on both traces.

This was overcome by filtering the output from the C52/1 meters. Filters were made up to remove mains frequencies and above, and also cut out any D.C. or very low frequency components of the signal, thereby removing the creep component of the displacement signal. Although this D.C. Filter was not

required for the load, two matched filters were used, one for each signal, to obviate any phase change brought about by unmatched filters.

This system produces very acceptable hysteresis loop photographs of load/deflection characteristics of the specimen over the required frequency range.

4.5 Calibration

Before any testing all the recording and measuring systems were calibrated, and again several times over the period of the work.

The major problem that arose with the recording was with the D90/250 proof ring load transducer. After several months of efficient recording it developed a serious drift with time to all readings. This transducer was replaced with a new D91/250, nominally the same.

The calibration of the displacement transducers, and the estimation of their errors proved very important when taking oscillating readings. These errors are negligible for the static loading cases but not for the oscillating signals. A summary of these errors is in section 5.2.

4.6 Preparation of the Specimens

Due to the availability of suitable test material most of the tests have been performed on bovine specimens taken from the distal end of the femur See figure 4.4. The joint was acquired with the synovial sack intact from the slaughter house. All specimens were from 2-3 year old cows. Once opened the joint was stripped of tissue and kept submerged in Ringer's solution to avoid drying of the cartilage.

The specimens taken from the medial trochlea (see figure 4.5) of the femur were only removed from the joint as required. The joint was stored unfrozen in a refrigerator for the duration of testing, up to 3 days. This method of storage avoided the joint ever being frozen and thawed, and removal of specimens immediately prior to testing obviated the swelling effects of

storing individual specimens in Ringers.

The trochlea was the chosen section of the joint as this had the largest 'flat' area in the loaded region. The trochlea was studied with the naked eye and specimens taken from the most 'normal' region for testing. This was done following the guidelines for determining macroscopically normal cartilage as laid down by Meachim and Stockwell (1973). A simple Indian Ink preparation was then used to verify that the areas chosen did not show overt fibrillation. The trochlea was bathed in Indian ink and then rinsed. Areas of fibrillation showed up as residual staining of the cartilage. The areas of least or no staining were taken as the most normal and specimens removed from these areas.

The bovine specimens obtained showed very minimal signs of fibrillation, with the majority of the area required being entirely free of visible abnormality.

Trephines were used for removing the specimen. Commercially available trephines, as used by Johnson (1974) were tried, but did not work satisfactorily due to the hardness of the underlying bone. Therefore our own trephines were made up to the size determined by the P.T.F.E. liner as described in section 3.1.

Considerable practice was required to achieve specimens with flat surfaces of cartilage perpendicular to the cut surfaces, and with a good length of subchondral bone intact. The trephines were placed perpendicular to the cartilage surface and used to trepan a specimen from the bone end. The cutter was driven through to a considerable depth and then a sharp sideways movement broke the underlying bone. The greatest care must be taken when trepanning through the cartilage so as not to tear the surface. Once the bone is broken the whole specimen can be removed within the trephine. To eject the specimen, the trephine had been fitted with a central plunger.

At this stage specimens without a flat cartilage surface perpendicular to the cylindrical sides of the specimen were rejected. Attempts were made to

out off the subchondral bone, parallel to the cartilage, with a scalpel, but the bone was too hard. Therefore the specimen was put in a collet up to a back stop so as to give a consistent length of specimen, and the bone end was carefully machined off in a watchmakers' lathe. Radin et al (1970) also used a lathe when preparing specimens from the metatarsophalangeal and metacarpophalangeal joints of freshly slaughtered cows.

Throughout the stages of preparation of the specimens the cartilage surface was not allowed to dry out.

For tests involving cartilage alone, without a backing of subchondral bone, the collet was again used. This time the bone end was introduced into the collet until only the cartilage protruded. This cartilage layer was then sliced off with a straight scalpel blade.

Later in the research it became possible to obtain human specimens for testing. The most easily obtainable area of load bearing cartilage was that on the patella. Patellae were obtained from post mortem specimens of various ages. An initial naked-eye examination of the cartilage showed it to be in a less perfect condition than the bovine cartilage.Indian ink staining was therefore used again to determine the most normal areas for removing the specimens. Typical results of this staining technique are shown in figure 4.6. Once the specimen site had been determined removal and handling of the specimen proceeded along similar lines to the bovine specimens.

4.7 Test Procedure

The test procedure was as follows:-

1. Have C52 meters warmed up
2. Check calibration levels on C52's.
3. Prepare specimen
4. Record total thickness of specimen a) cartilage alone
   or b) cartilage + bone
5. Test - recording displacement, load and time
   taking oscilloscope photographs during oscillatory tests.

6. Remove specimen
7. Record specimen thickness to give independent reading of deflection.
8. Take cartilage off bone
9. Record bone thickness - this gives original cartilage thickness
10. Where applicable take oscilloscope photographs of the bone and rig characteristics over the same load range
11. Plot results correcting readings for zero error and rig and bone deflections.
12. Calculate moduli.

5.0 Results

5.0 Introduction

The experimental work carried out began as a follow up to Litchfield's (1974) work on a computer model of articular cartilage. Good agreement had been reached between the predicted load/time/deformation characteristics of the model and the experimental results of Edwards (1967).

Edwards' tests were of the confined type using articular cartilage from the femeral head of a dog in normal Saline at 20°C. Curves were presented of

a) Specimen thickness at equilibrium as a function of applied pressure

b) Percentage liquid exchange as a function of time for four different loads

c) Percentage liquid exchange as a function of applied pressure.

Comparison of the above graphs a) and c) show the relationship between change in specimen thickness and liquid exchange is approximately constant, showing that deformation could be accounted for solely by fluid flow out of the matrix. Using this fact the graphs presented were transposed to read as strain as a function of time for the given loads. This new graph was then used by Litchfield in his comparisons with the fluid flow computer model.

As stated in section 3.1 the theory behind the computer model has been altered in several ways since Litchfield's thesis was written and for all comparison purposes the improved model has been used.

No attempt has been made in this study to investigate the load/time/deformation characteristics of articular cartilage by the indentation technique used by other workers (see literature review). However the initial programme of work aimed at reproducing Edwards' results for the computer model comparison was extended to investigations of the static load response and dynamic load

response in both confined and unconfined tests, both on Bovine and Human articular cartilage.

A small study was also undertaken on the response of the underlying bone to these loadings. In studying dynamic load responses of the cartilage the effect of frequency was investigated.

5.1 Experimental Results - static loading

Figures 5.1 and 5.2 show typical strain v. time curves obtained in static loading of bovine and human cartilage in a confined test. This is allowing axial strains and flow only, as in Edwards (1967) tests on dog cartilage. The graphs show loading and recovery periods and it is immediately apparent that recovery takes considerably longer. Figure 5.1 shows that virtually complete recovery was obtained even after strains of 0.5, but the greater the strain achieved on loading the longer the recovery period. In comparing figures 5.1 and 5.2 it can be seen that on loading the bovine cartilage reached 'ring-out' after about 60 mins whereas the human patella cartilage had perhaps not even fully "rung-out" after 240 mins. This seems a vast discrepancy, however the dimensionless analysis of section 3 shows that the time involved is proportional to the term $\frac{1}{z_o^2}$ where z_o is the initial thickness. This result of the analysis is verified by figures 5.1 and 5.2 as the bovine specimens were of the order of 1.0 mm thick and the patella specimens around 2.0 mm thick. Therefore being twice as thick the patella specimens took four times as long to "ring-out". Edwards' tests on dog cartilage are also in line with this result as his tests reached "ring-out" after about 20 mins and his specimens were 0.48 mm thick.

The recovery, like the loading times, can be seen to take much longer again in figure 5.2 than figure 5.1. Here again the fact of the patella specimens being twice as thick would cause this increase. However it is felt

that the thickness played an extra role here in lengthening the recovery time, because there was much more contact area with the confining sleeve and hence more friction. This effect would not be so noticeable during the loading cycle as the applied load would tend to overcome friction, especially in the oscillatory tests, however when the load is removed there is only the swelling of the specimen itself to overcome friction.

In both figures 5.1 and 5.2 no, or very little instantaneous deflection is apparent at either the moment of applying or removing the load. Edwards' results from confined tests show a similar lack of instantaneous deflections as his tests were recording fluid flow only, and such instantaneous deflections as noted by other workers in indentation and unconfined tests are attributed to elastic deformations or barelling of the cartilage matrix and fluid. In a confined test with no radial strains permitted such elastic deformation is reduced to the order of the bulk modulus compressibility which is very small compared with long-term strains due to fluid flow.

Figures 5.3 and 5.4 show the same as figure 5.1 but these are for unconfined tests on bovine specimens. Here, both axial and radial strains and radial flow are permitted. The curves have the same overall appearance of a creep deflection with time, but with two distinguishing features compared with confined tests.

Firstly an instantaneous deflection is apparent in figures 5.3 and 5.4. This deflection at application is considerably bigger than at removal of load. An analysis by Litchfield (1974) shows that

$$\frac{\delta_0}{\delta_1} = \frac{\delta_x}{z_1} + 1$$

where δ_0 = 'instantaneous' response on compression

δ_1 = 'instantaneous' response on removal of load

z_1 = cartilage thickness at equilibrium before removal of load.

δ_x = the creep deflection

Hence the ratio of $\frac{\delta_0}{\delta_1}$ can never be less than 1 and figure 5.3 is in agreement with this. For example in figure 5.3 with load of $0.68 \times 10^6 N/m^2$

$$\delta_0 \simeq 01$$

$$z_1 \simeq 0.58$$

$$\delta_x \simeq 0.48$$

These yield the value of .055 for δ_1 the instantaneous deflection on removal of load which is approximately correct.

The second obvious difference between the confined and unconfined results is the rate of recovery. In the unconfined tests figure 5.3 it can be seen that after the initial instantaneous recovery, the recovery rate is far slower and for a large portion of the period is almost linear with time.

Figures 5.1 and 5.4 were based on specimens of nominally the same size, 5.6 mm in diameter and 1.0 mm thick, however it appears that the time to "ring-out" in the unconfined cases is marginally longer.

The equilibrium strains at "ring-out" were used to plot the static load stress-strain curves of figures 5.5 - 5.8 for bovine cartilage.

Figures 5.5 and 5.6 are results from confined tests, figure 5.6 showing the majority of results obtained in this study and figure 5.5 showing the results from just two series of tests. It is the tests performed to produce figure 5.5 that were used for comparison purposes with the computer model for confined static loading. As stated in section 3.1.3 the model requires the values of a and b from the equation of the stress-strain curve at equilibrium. Figure 5.5 gives these values at $a = 0.28 \times 10^6 N/m^2$ and $b = 1.47$.

The asymptote of this curve is the line where the final strain reaches the porosity of the material, given by $\frac{1}{b}$. Hence it can be estimated that these bovine specimens had a porosity in the region of 0.68.

Figures 5.7 and 5.8 show the same as 5.5 and 5.6 but for unconfined tests. Also shown on figure 5.7 are results obtained by McCutchen (1962) when

testing cartilage from the leg joint of a cow in water. Agreement between our results and those of McCutchen is felt to be very good, and the discrepancy shown could easily be accounted for by variation in the condition of the test material or the sites from which they were taken. McCutchen only states his specimens were from the leg joint of a cow, which may not have been the medial trochlea of the femur from where our specimens were taken.

If comparison is made between these stress-strain curves for confined and unconfined tests it is noted that they are quantitatively very similar. The process by which the final strains are reached is quite different as borne out by figures 5.1, 5.3 and 5.4, but the end results show that for a given load virtually the same strains will be reached in both confined and unconfined tests.

This phenomenon was demonstrated by a simple test -

Small circular discs of cartilage were removed from the trochlea of a cow. The unstrained dimensions of these discs were recorded. The discs were then held in a micrometer and a known strain applied. Immediately the strain was applied the diameter increased. Whilst strained the cartilage was kept submerged in Ringers solution. At intervals during the test the diameter was measured. It was found that with time, as liquid was expelled from the cartilage the diameter decreased. After about one hour the diameter had returned to its value before the strain was applied. See figure 5.9. This seems to show that after the state of equilibrium was reached the specimen had the same dimensions as if it had been part of a confined test, the process by which it achieved these final dimensions being the different factor.

Figure 5.10 shows the stress-strain curve at equilibrium for the human patella specimens. The curve of the form $\sigma = \frac{a\epsilon}{1 - b\epsilon}$ fitted to these points for computing purposes has the values of $a = 0.455 \times 10^6 N/m^2$ and $b = 1.5$.

Comparison of these experimentally obtained curves is made in figure 5.11 for confined tests. Edwards (1967) results indicate that dog tibia cartilage is much stiffer than either human patella or bovine femur cartilage, with the bovine cartilage appearing to be softest. From the curves fitted to the experimental points the values of porosity, that is $\frac{1}{b}$; are

Dog	0.55
Human	0.67
Bovine	0.68

Edwards does not quote directly the initial porosity of the dog cartilage he used, but figures are given which allow porosity to be calculated and yield a figure of 0.71. This figure is closer to those obtained above for human or bovine, but is in variance to the figure calculated for dog cartilage. However an explanation of this possibly lies in the fact that the stress-strain curves would yield a figure for $\frac{1}{b}$, or porosity, which is for freely moveable fluid within the specimen, whereas the figure of 0.71 arrived at from Edwards data is obtained from the fully swollen and dry masses of the specimen, and hence includes liquid entrapped in the matrix and not free to be forced out under normal loading. However this effect of altering porosity will be seen in section 5.3 to have only a slight effect on the load/deformation/time characteristics of cartilage.

5.2 Experimental results - Dynamic Loading

The dynamic load tests were carried out using the rig in the configuration of section 4.3.3 with the load applied to the spring by an eccentric cam.

In these tests there was a constant load produced by an initial set deflection of the spring, with the oscillating load superimposed upon it. The constant load produced the characteristic creep deflections of section 5.1 and

the oscillating load produced an additional small rippling deflection. The magnitude of this ripple was small compared with the creep deflections, even in cases where the amplitude of the oscillating load was about equal to the constant load. Because of the very small deflections being measured the whole of the test apparatus and procedure came under scrutiny, as any additional deflections recorded, extraneous to the deflection of the cartilage alone, would greatly alter the values of strain and modulus calculated.

Firstly the rig was investigated and did show a load dependent deflection characteristic, see figure 5.12. This rig deflection was substantial compared with the specimen deflections and rather surprisingly non-linear. The rig deflection was checked at several intervals during the period of the work. The explanation of the non-linearity lies presumably in the contact between the spherical end of the plunger and its conical seating in the spring support plate, and also perhaps in the porous bronze disc. The rig deflection characteristics were also found correct, not just for static load deflections but for oscillating loads. Oscilloscope photographs were taken of the rig deflections alone under varying magnitudes of oscillating loads. The recorded deflections matched the deflections read off the graph for the corresponding load levels and were in phase with the load, e.g. an oscillating load between 10 and 20N caused an in phase oscillating deflection in the rig of 0.0102 - 0.0064 mm, i.e. 0.0038 mm.

These rig deflections were repeatable and although largely inexplicable it was considered acceptable to treat them as a figure to be subtracted from the total. They are a large part of the deflections recorded in oscillatory tests, but are negligible in the static loading cases.

In tests on cartilage alone the rig deflection was subtracted directly as stated above to give the net deflection of the cartilage. However in all the unconfined tests, and some of the confined tests, where the cartilage was

tested without removing it from the underlying subchondral bone, an additional test was carried out. Here the cartilage was removed from the bone after the test and the bone and rig alone were then subjected to the same loading conditions.

Consideration of the bone deflections led to a small study of the bone characteristics themselves, see Appendix 1. The deflections recorded from the bone can be seen to be insignificant in considering static load characteristics of cartilage but again had to be taken into consideration in the dynamic tests. They were treated with the rig deflections as a figure to be subtracted from the overall deflections.

The accuracy of the displacement transducers and the B.P.A. recording meter was investigated at these small displacements. The L.V.D.T. transducers as supplied have infinite resolution, a linearity on calibration of 0.5% and were of grade A1 which gives an accuracy of 0.1% of full scale deflection over the lower 20% of range and 0.5% of the actual value over the upper 80% of range. The B.P.A. meter is quoted as having an accuracy of ±1% of full scale deflection. Therefore using the B.P.A. on its most sensitive scale with these transducers, i.e. a full scale deflection of 0.1 mm, it should be accurate to ±0.001 mm. At no time was it attempted to take values of the oscillating deflections directly off the B.P.A. except to obtain a very rough guide to the size of deflection. All readings of these small deflections were taken from the oscilloscope photographs. The accuracy of the combination of the transducers, the switch selector unit type C35, the B.P.A. meter and the oscilloscope was studied using a Hilger and Watts vertical Microptic measuring machine to apply known small deflections to the transducers. This Microptic has a stated accuracy of ±0.0008 mm for the range of 0 - 25 mm.

The outcome of this investigation was that for deflections of 0.012 mm or above the accuracy of the combined system was around ±2.5% of the reading;

this being taken as the error between the trace measured from the oscilloscope and the known travel of the microptic. However for displacements less than 0.012 mm the error increased as the displacement decreased. Considering the largest errors recorded, the % error on readings appeared to increase linearly as displacements decreased until at a displacement of 0.001 mm the error could be in the region of ±50 - 60% and were quite randomly positive and negative. However at such small deflections the error recorded is of the same order as the error stated for the Microptic itself, and may not be error in the transducers.

In calculating the actual deflection of the cartilage, as stated above, the rig deflection is subtracted from the recorded deflection. Therefore in the worst cases where both recorded and rig deflections are very small the addition of these errors could produce errors in the cartilage deflection of around ±100%.

This implies that the displacement recording instrumentation is grossly inadequate for these purposes. However, as will be shown later, the results obtained followed a definite pattern and produced fairly repeatable graphs. The errors found above were not all positive or negative and therefore should produce random alterations to the final values. Therefore if it is accepted that the characteristics of cartilage can change from one specimen to the next, be they either from different joints or even different sites on the same bone end, as referenced in the literature review, the scatter in the results could be put down to the different specimens. As, for any one specimen, the figures seem consistent, then it could be assumed that these estimated errors are rather too severe and perhaps are underestimating the accuracy of the instrumentation.

Confined Tests

Figure 5.13 shows the hysteresis loops produced by dynamic loading of confined specimens. Although scales on these photographs are different the

phase angles in each case can be compared. From figure 5.13 it can be seen that the phase angles are

a) Bovine 5^{o} and 9^{o}

b) Human 0^{o} and 7^{o}

c) Rubber 15^{o}

These photographs presented here are typical of all the tests. As can be seen the traces are not perfectly smooth. There is noise on the load (vertical) axis. This noise at first was thought to be due to friction in the confining sleeve around the specimens, but as can be seen from figure 5.16 the same noise is present on the hysteresis loops for unconfined tests. Investigations took place, but the cause of the noise was not discovered until very late in the period of this work. Modifications are planned to eliminate the noise, but will be too late for inclusion in this thesis. This noise must be within the frequency range of 0 - 50Hz as filters in the electrical circuits cut out any signals outside this range. The noise has been traced to vibration. Whereas the needle on the B.P.A. meter is damped and showed very smooth oscillating loads, the oscilloscope is more sensitive and is undamped. When there was only static loading there was no noise on the trace. However when the motor is on and rotating the shaft carrying the eccentric which applies the load to the spring, the noise is present on the trace. This presumably could be corrected by mounting the rig and the motor plus gearbox on separate frame-works or by isolating mountings

For a typical trace the maximum noise was in the region of 2 mm to a signal trace of 53 mm. This was equivalent to 2.6 mV noise on a signal of 70 mV. Hence the noise to signal ratio is 0.037 or approximately 4%.

The phase angles recorded in the tests did not seem to change significantly with any other variable. The variables that could possibly have had some effect are:

1) The D.C. creep strain of the specimen, as this is altering the specimen to one with less fluid component and more matrix to its volume.

2) The frequency of the dynamic loading

3) The ratio of the amplitude of the dynamic load to the constant mean load during the test.

As no trend between any of these variables and phase angle was obvious the mean phase angle for all tests was calculated. This mean was 7° for bovine, which will tend to be slightly on the low side as in many tests where the hysteresis loop was very close to being in-phase, calculation of the phase angle was impossible and these tests were given the phase angle of 0°.

The mean value of the phase angles for the combined tests on rubber was 13°, and for the human specimens 12.6°.

These phase angles being similar for cartilage and rubber tested under the same conditions, indicates that the compression of the cartilage under the dynamic loading is essentially an elastic compression and not a fluid flow phenomenon.

From these hysteresis loops the 'moduli' can be calculated. Knowing the scale factors involved and having the oscilloscope calibrated the amplitudes in the X and Y directions as read off the photographs give the deflection and load amplitudes respectively. The deflection can then be converted to a strain amplitude and the load to a stress amplitude. The dynamic modulus is then calculated as $\frac{\text{stress amplitude}}{\text{strain amplitude}}$

As stated previously this method of testing allows no radial strains. Here then under dynamic conditions it has been shown that fluid flow is playing practically no part in the process, and that the behaviour is essentially linear. This dynamic modulus therefore resembles the E^* for a Hookean solid discussed at the end of section 3.5.

Figures 5.14 and 5.15 show the variation of this calculated modulus against the corresponding creep strain of the specimens for bovine and human specimens under confined compression. The graphs show a wide scatter of results which for the most part could be due to the varying conditions of the test specimens. However the wider scatter at the larger values of creep strain is probably attributable to the greater innaccuracy of the deflection measuring system in this region as here the amplitude of the deflection is much smaller. From both the graphs however it is obvious that as creep strain increases so does the modulus.

For bovine specimens, figure 5.14, this increase is from 0.8 x $10^8 N/m^2$ at a creep strain of 0.05 to around 10 x $10^8 N/m^2$ at a creep strain of 0.6. The bovine specimens were all from young beasts and none appeared, on naked eye examination, to have any degenerate areas. Therefore the bovine specimens could be considered as virtually the same.

However from figure 5.15 for human patellae specimens it can be seen that each specimen shows its own relationship between modulus and creep strain.

Patella A (81 year old male) has a characteristic very close to that shown in figure 5.14 with the modulus increasing from 0.6 x $10^8 N/m^2$ at 0.05 strain to 6.0 x $10^8 N/m^2$ at 0.35 strain. Patella B (78 year old male) however shows much less increase with strain, varying only from 0.5 x $10^8 N/m^2$ at 0.05 strain to 1.65 x $10^8 N/m^2$ at 0.4 strain. Patella C (17 year old male) again has a characteristic much closer to Patella A and that shown in figure 5.14 with the modulus increasing from 0.8 x $10^8 N/m^2$ at 0.05 strain to 2.6 x $10^8 N/m^2$ at 0.3 strain. The specimens in each case were taken from the most normal areas of the patellae.

Unconfined Tests

Figures 5.16 and 5.17 show the same as figure 5.13 and 5.14 but for unconfined tests on bovine specimens. For the unconfined tests the phase

angles in figure 5.16 were

Bovine 6° and 21°

Rubber 17°

As with the confined tests, no trend was apparent between phase angle and any other variable so again the average value of phase angle was calculated. These were 16° for bovine specimens and 17° for rubber.

Figure 5.17 shows the variation of modulus with creep strain for unconfined tests on bovine specimens. The modulus again increases with creep strain from $0.5 \times 10^{8} N/m^{2}$ at 0.05 strain to $10 \times 10^{8} N/m^{2}$ at 0.525 strain.

Johnson (1974) performed similar oscillating load tests on unconfined specimens of human articular cartilage. He applied a sinusoidal load, superimposed upon a static preload and monitored the strain amplitude and creep strain with time. His results were qualitatively similar to those of figure 5.17. However the moduli quoted for the human tissue are only about 25 - 50% of the moduli achieved in bovine tissue. The hysteresis loops presented by Johnson are very similar to those of figure 5.16. Both sets have a very small area within the loop, giving low phase angles, and both sets are slightly non-linear.

Effect of frequency on Modulus

The tests to study the effect of frequency of loading on the A.C. Modulus were carried out on several specimens, and produced the same results in each case. All these tests were performed in the confined configuration. The test on each specimen was carried out at a frequency of 1 Hz . At prescribed intervals during the test the frequency was altered to 0.2 Hz and then 5 Hz without stopping the test, or unloading the specimen. A short interval of time, approximately one minute, was allowed between changing frequency and taking the results, to enable the whole system to settle and also for checking the new frequency.

Figure 5.18 shows the effect of frequency on modulus as recorded against creep strain in three of the tests on bovine specimens.

Plotting against creep strain, as opposed to time is preferred as, during the first part of the test, the change in creep strain with time is very pronounced, and during the minute's delay between readings the creep strain varied.

Figure 5.19 shows for the frequencies selected which were about normal walking speed, and five times faster and slower than that, there is very little change in the modulus. A slight tendency could be seen towards a higher modulus at a higher frequency, but this is not a significant trend. The apparent possible change in modulus with frequency at higher levels of creep strain could be attributed to the higher degree of inaccuracy in the displacement transducer readings as pointed out previously in this section.

Figure 5.19 shows these results plotted together, and accentuates the scatter in the results obtained. This scatter is attributable to the conditions of each specimen used, as, for each specimen alone the points fall very close to a single line as seen in figure 5.18.

These results would tend to suggest that viscous effects were unimportant in determining the stiffness of cartilage in these experiments. Within the range tested 0.2 Hz to 5 Hz the compression as previously indicated by the hysteresis loops is due purely to a bulk modulus effect and fluid flow is negligible.

5.3 Theoretical Results - Constant Loading

As stated in section 5.0 the experimental work was initially a follow up to Litchfield's (1974) work on a computer model of articular cartilage. The computer model was mainly used to reproduce the results of Edwards (1967). Litchfield (section 5.4) explains how the results of Edwards yield the data for the computer model. This data is

Applied stress levels	1.02, 2.04, 3.10, 6.895 x $10^6 N/m^2$
Permeability	1.09 x $10^{-19} m^2$
Porosity	71%
Specimen thickness	0.48 mm

The graph of deformation against applied pressure as given by Edwards yields the values of the material property constants a and b from the curve fit of the form $\sigma = \frac{a\epsilon}{1-b\epsilon}$ as explained in section 1.1.3. These values are $a = 1.655 \times 10^6 N/m^2$ and $b = 1.825$.

Chapter 3 describes the ways in which the theory behind Litchfield's original programme has been altered. Figure 5.20 shows the effect of these alterations on the strain-time characteristics, for just two of the Edwards loading conditions.

At low loads the new programme lags the experimental curve whereas the original programme always led, but agreement between the new programme and the experimental results is still good. However at higher loads the agreement between the new programme and the experimental results is improved, especially during loading.

Litchfield's original programme, at higher loads had a tendency to give a strain-time characteristic which became more and more linear, crossed over the experimental results and then flattened off sharply to the final strain. A similar type of response also occurred after the release of load. The new programme produces a much smoother curve, always remaining to one side (lagging) the experimental results.

Apart from this comparison all the following computing has been done using the new modified programme, mainly in its dimensionless form. To show the effect of varying different parameters on the computed strain-time characteristics, the case of Edwards lowest applied load, 1.02 x $10^6 N/m^2$ has been used throughout.

The dimensionless analysis gave the dimensionless groups as

$$\frac{\delta}{z_0}(\epsilon) \cdot \frac{\sigma}{a} \cdot \frac{Kat}{\eta z_0^2} \cdot b \cdot \nu$$

The values of a and b are set by the experimental results being modelled, $\frac{\sigma}{a}$ is set by the applied loading conditions, and the dimensionless programme produces the relationship between $\frac{\delta}{z_0}$ and $\frac{Kat}{\eta z_0^2}$. Therefore the first parameter to be investigated was the initial porosity of the specimens.

Figure 5.21 shows the effect of the porosity on the computed strain. It can be seen that porosity does have some effect on the strain, which increases as the value of porosity becomes closer to the value of the final strain. This can be extrapolated to the case where the initial porosity equals the final strain; in this situation as soon as the load is applied, the pores at the surface will be closed up and no fluid will be able to escape. If this situation actually occurred then, no, or very little, strain would result.

The effect of altering permeability is now built into the dimensionless time group $T = \frac{Kat}{\eta z_0^2}$ from which can be seen the relationship that Litchfield came upon by a different route. That is at any value of strain there is a certain value of T, and if the value of K incorporated in T is doubled then the value of t, real time, to reach that strain is halved, and vice versa.

The next relationship to be investigated was that between permeability and strain, Litchfield had shown that for axial flow the permeability K varied as $K = K_0 \left(\frac{\nu - \epsilon}{\nu}\right)^3$. Figure 5.22 shows what effect there would be if this relationship obeyed a different power law. An increase in the power delays the reaction, and decreasing the power speeds up the reaction. The extreme of this is where the permeability remains constant with strain, and as seen in figure 5.22 the cartilage in this case would deform almost linearly with time to a value near its final strain and then quite suddenly level out to its final strain.

The permeability does not only however vary with strain. Maroudas (1973) showed that throughout the depth of a slice of cartilage the permeability varies. Figure 5.23 shows this variation for just two of the cases Maroudas quoted. From the theory of section 3.4, equation 28, the mean permeabilities were calculated as:-

for 35 year old $4.48 \times 10^{-19} m^2$

27 year old $3.313 \times 10^{-19} m^2$

Using the same data, except permeability, as for Edwards lowest load, figure 5.24 shows the effect of this permeability distribution. The permeability is still governed in these cases by $K = K_0\left(\frac{v-\epsilon}{v}\right)^3$ but for the case of variation of permeability through the depth the value of K_0 used is in fact a curve fit to the graphs of figure 5.23. It appears that, just as Maroudas said there seems to be no correlation between age and permeability distribution, so too, each of these distributions has its own effect on strain. The only consistent fact emerging from these two distributions is that both produce a faster reaction than in the constant initial permeability case.

Extending this distribution of permeability with depth to the arbitrary curve of figure 5.25 led to the computed curves of figure 5.26. This simple quadratic distribution of permeability through the depth was used, as there is a belief by some workers (see literature review) that cartilage has a very thin surface layer, the lamina splendens, which has very low permeability. The curve of figure 5.25 $K = (C + 20x - 20x^2) \times 10^{-19}$ where x is the distance from the surface allows values of C to be chosen giving very low surface permeability. Most of the curves of Maroudas (1973) showed the permeability increasing from the surface and then decreasing towards the deeper zones, as does the curve of figure 5.25. The computation was done with $C = 0.1, 0.2, 0.5, 1.0$.

For the case of $C = 0.2$ the overall mean permeability was calculated from equation 28 to be $2.94 \times 10^{-19} m^2$ and the effect of altering C

is compared with this constant permeability curve. (It is accepted that altering C would also slightly alter the overall mean permeability but not by a very large amount for the range of C used) From figure 5.26 it can be seen that for very low values of C , i.e. when the surface permeability is very small the reaction of the cartilage is slowed down, this will be due to the low surface permeability hampering the passage of the fluid from the deeper layers out through the surface.

In all the computing so far it has been assumed that the fluid is flowing out into a region of zero gauge pressure. Figure 5.27 shows the effect of altering this surface fluid pressure. Again for the conditions of Edwards lowest load it can be seen that an increase in surface fluid pressure decreases the final strain reached for the same load. Immediately as a load is applied to the cartilage the fluid in the deepest layer is pressurised to the value of the applied load, whereas at the surface the fluid takes no pressure and the load is supported by the matrix. If the surface fluid is at a pressure above zero gauge pressure, the pressure differential in the fluid between the deepest and the surface layers is less and the resultant out-flow of fluid is correspondingly less. This is not a linear relationship as seen from figure 5.27. A surface fluid pressure of about $\frac{1}{3}$ the applied pressure does not result in a $\frac{1}{3}$ reduction of the final strain. However in the extreme case of the surface fluid pressure equalling the applied load, there is no resultant strain of the specimen which is as would be expected since there is no resulting pressure differential set up in the fluid and consequently no fluid flow.

The way the deformation of the cartilage is accomplished with time is shown by the way the strain varies with the depth from the surface as the time increases. Figure 5.28 shows this variation, again for a constant applied pressure of $1.02 \times 10^6 N/m^2$ and for the case of zero gauge pressure of the

fluid at the surface. In this case all the load at the surface must be supported by the matrix and so immediately the strain at the surface becomes the value of the final strain. As time increases the fluid seeps out and the strain in the deeper layers increases. Eventually at an infinite time in theory the whole specimen is at the final strain and no more deformation takes place. The near vertical lines on the graph show the positions of various points in the solid with respect to the surface as time increases. If the surface fluid pressure were not zero, of course this variation would not be the same, the main difference being that for the same load the strain at the surface at all times would be the new final strain for that surface fluid pressure.

Figure 5.29 shows the magnitude of the fluid pressures through the depth as deformation and time increase. Initially most of the load is carried by the fluid pressures except at the surface where the gauge pressure is zero. The fluid pressure decreases with time throughout the depth as the strain increases and the matrix carries a larger portion of the load. Eventually the matrix carries all the load, the fluid pressure throughout is zero and the final strain has been reached everywhere. When the surface fluid pressure is not zero a similar transfer of load carriage between fluid and matrix is carried out, but instead of the fluid pressures converging on a zero value at equilibrium, they converge to the value of the surface fluid pressure, and the graph of figure 5.29 appears condensed on the vertical axis.

Figure 5.30 shows the comparison between the computer model and the results obtained by Edwards for all the loading conditions. Agreement for the loading phase is reasonably good, but in the unloading cases the computer model is heavily dependent on several variables, most especially permeability, and a small alteration in these measured values would make agreement significantly better or worse.

Confined compression tests, as reported in section 5.1 on bovine and human cartilage have produced qualitively similar results to those of Edwards. The data from the experiments has been used in the computing and yielded the graphs of figures 5.31 - 5.33 for bovine and figures 5.34 - 5.36 for human specimens.

For all the bovine specimens the data was

Porosity	0.68	
a	$0.28 \times 10^{6} N/m^2$	from figure 5.11
b	1.47	

Stress levels and specimen thicknesses were individual to each test. The value of permeability is the most important variable and for this reason the results are presented with a band of likely permeabilities. Munding (1975) measured the permeability of the bovine cartilage being used and produced results scattered around a mean of $8.5 \times 10^{-19} m^2$. This value and double this value ($1.7 \times 10^{-18} m^2$) were used to plot the practical results, although this latter value is probably rather high.

With the dimensionless group $T = \frac{Kqt}{\eta z_o^2}$ incorporating the value of K only one line is produced by the computer for each loading case. Litchfield when plotting against real time, showed that doubling the parameter $\frac{K}{z_o^2}$, halved the time to reach a certain strain. However, in this dimensionless study doubling the parameter $\frac{K}{z_o^2}$ does not alter the plotting of the ϵ v T graph, but for each value of $\frac{K}{z_o^2}$ chosen the value of T represents a different real time. In this case, to show the effect of altering the permeability it is the practical results that must be plotted using the two extremes of the permeability range. At the lowest load, figure 5.31, the computed curve falls within the band of experimental results, but as load increases, figures 5.32 and 5.33, the computed results fall outside this band. In all of these cases the effect on the computed curve of keeping the

permeability constant with strain is shown, and this is obviously a far too severe constraint as in all cases it is very far from the practical results.

For the human patella specimens the data was

Porosity	0.68	
a	0.455×10^6	from figure 5.11
b	1.5	

Again stress levels and specimen thicknesses were individual to each test. Once more the important variable is permeability. As no tests have been performed in this study on the permeability of patella cartilage, a guide to the possible value was taken from the figures given by Maroudas (1973) for femoral condyle cartilage. For comparison with the computed $\dot{\varepsilon}_v$ T curve the range of permeability of $4.25 - 8.5 \times 10^{-19} m^2$ was used, with the latter of these being again on the high side. Figures 5.34 - 5.36 show a similar trend as for the bovine results, with the agreement to the computed curve being closest at the lower applied stress levels.

From the curves of figures 5.21 - 5.27 it can be seen how very many variables have an effect on the strain v. time characteristics of articular cartilage. No doubt by combining the effects of many of these, and altering some values the computed and practical results could be made extremely close. However this would then be a case of curve fitting and not modelling.

5.4 Theoretical Results - Oscillating Loading

Due to computational difficulties Litchfield (1974) found it very difficult to run the axial flow programme with oscillating loading. Therefore to acquire some idea of the magnitude of the oscillating strain amplitude produced by fluid flow, the phase lags and the effect of frequency on both of these, it was decided to use only the radial flow programme for these calculations. Some relationship was therefore required between the strain/time

characteristics produced by axial flow only, and those produced by radial flow only.

Both programmes in their corrected and non-dimensional forms were run with the same data. An arbitrary cylindrical specimen size was chosen with $R = 2.5$ mm and $z_o = 1.0$ mm. The values of a and b used were those obtained from the tests on bovine specimens and a value of $5 \times 10^{-19} m^2$ was used for permeability as this seems to fall reasonably in line with the values given by McCutchen (1962) and Munding (1975). This value was used both as axial and radial permeability as several workers (see literature review) have found these to be approximately equal. Porosity was taken as 0.68 and the non-dimensional stress level used was 2.0.

The resulting graphs of T and T^* against strain are shown in figure 5.37

where $T = \frac{Kat}{\gamma z_o^2}$ and $T^* = \frac{Kat}{\gamma R^2}$

It can be seen that although the radial flow programme, $\epsilon \vee T^*$, is much quicker to react initially it takes longer to reach the final strain, whereas the axial flow programme predicts a slower initial increase, but reaches the final strain ahead of the radial flow case.

From figure 5.37 it can be seen that up to around a strain of 0.2 there is the relationship of $T \simeq 50T^*$ Therefore up to this value of strain $\frac{R^2}{z_o^2} = 5.0$ or $\frac{R}{z_o} = 2.236$.

Therefore it can be postulated that if a specimen was chosen having $R = 2.236 z_o$ the axial and radial flow characteristics would be similar in the initial stages.

For obtaining some details about the effect on strain amplitudes of fluid flow due to oscillating loads the radial flow programme was then used on the assumption that up to a strain about 0.2 and for an idealised specimen

having $R = 2.236 z_0$ it could be counted as similar to the axial flow.

Figure 5.38 shows the first few cycles of the strain response to an oscillating applied load at a frequency of 1Hz with an amplitude of $\frac{\sigma}{a} = 4.0$ around a mean load of $\frac{\sigma}{a} = 2.0$. This magnitude of loading is much greater than is likely to be encountered in most physiological situations, but it was found necessary to use such grossly exaggerated loads for the computing, as the strains due to fluid flow were so small. Figure 5.38 shows up this condition. In about the first ten cycles of loading, the creep strain has reached 5×10^{-3} whereas the amplitude of the strain due to the oscillating component of the load is around 0.15×10^{-3}, more than an order of magnitude smaller.

Figures 5.39 - 5.41 show this same response. Figure 5.39 for the first two cycles, figure 5.40 for the 601 cycle and figure 5.41 for the 3600 cycle. The strain amplitudes decrease with the increase in creep strain and also the phase lag decreases. See table below

Cycle	1 - 2	601 - 602	3601 - 3602	
	0.14×10^{-3}	0.44×10^{-4}	0.93×10^{-5}	Strain Amplitude
	1.0×10^{-3}	0.14	0.28	Creep Strain
	63	63	36	Phase Angle ^{o}

These very small values of strain amplitude due to fluid flow support the view put in section 5.2 that the measured oscillating strains are due almost entirely to gross compressibility and not to fluid flow at frequencies around 1Hz, the walking frequency.

From the experimental work of section 5.2 an average was taken of results from the first 1 - 1.5 minutes of the loading cycle. The mean creep strain in this period was 0.13 and the mean 'A.C.' strain amplitude was 1.5×10^{-3}. Comparing these values with those of the above table of computed results, show that the effect of fluid flow is about two orders of magnitude

smaller than the experimentally obtained values for the A.C. strain amplitude, again showing that at these frequencies fluid flow plays a negligible part in the oscillating deformation.

Comparing the phase angles too, shows the fluid flow reaction to the oscillating load is lagging by as much as 63^{o}, whereas in practice the phase angles recorded were similar to those of rubber. The elasticity effect of the cartilage at these frequencies again overrides the effect of fluid flow.

Purely for comparison purposes the computer programme was run with loading frequencies of 0.2, 1 and 5 Hz. These are the same as the experimental test frequencies. As the loading used in the computing was far in excess of the practical loadings, the values of strains produced will not be quoted directly, but a modulus will be quoted. This could be termed the 'oscillating load fluid flow modulus' which is given by:- $\frac{\text{Applied stress amplitude}}{\text{Resulting strain amplitude due to fluid flow}}$

Figure 5.42 shows the value of this modulus plotted against creep strain for the three frequencies. One obvious conclusion from this is that at all these frequencies the value of this Modulus is one or two orders of magnitude greater than any of the experimentally obtained results, so that even slowing the frequency down to 0.2 Hz still does not give the fluid flow sufficient time to take a major part in the deformation of the cartilage.

Unlike figure 5.18 however, where the frequency had no effect on the modulus, figure 5.42 shows that frequency does affect the fluid flow modulus. The greater the frequency the smaller the role played by fluid flow in cartilage deformation. This conclusion is obvious since slowing the frequency down to the extreme of zero would produce the characteristics of the static load case, where it is known that fluid flow plays the major role in the deformation.

6 Discussion

Many of the points for discussion have been put forward and dealt with in the relevant sections of Chapter 5. The discussion here is to stress certain of the points raised and introduce new topics of discussion not already covered.

The results of the constant load tests can be seen to be broadly in agreement with those of other workers. The similarities recorded and previously discussed between confined and unconfined results may not be as surprising as originally thought. The specimens used in the unconfined tests of this work were all from bovine femurs. The cartilage on the trochlea was around 1 mm thick and the test specimen, as removed, had a diameter of about 5.6 mm. For the unconfined tests the cartilage is left attached to the subchondral bone. Considering this geometry the 'unconfined' tests cannot be considered to be entirely 'radially free', because of the large diameter to thickness ratio and the bone fixation on one face. The quantitative differences between the results recorded in section 5 and say those of Johnson (1974) for unconfined tests could therefore be partly accounted for by the fact that his tests were more realistically unconfined. The diameter to thickness ratio of his specimens would be about half that of the specimens used here.

The comparison made in figure 5.11 between the equilibrium stress-strain curves for confined tests on three different species show the response of each species to be similar in form but widely different in magnitude. The dog tibial cartilage used by Edwards proves to be much stiffer than either the human or bovine cartilage, with the bovine cartilage appearing softest.

With regard to a value for Poisson's ratio for cartilage, there have been several figures quoted for this. Kempson et al (1971) give the average

Poisson's ratio as 0.48 from tension tests on canine articular cartilage. Hayes and Mockross (1971) calculated values from the experimentally obtained shear compliance coefficients and bulk creep compliances. They quote values of 0.42 for one second after loading, and 0.37 for a long term value.

It is interesting to note that Hayes and Mockross note a significant decrease in Poisson's ratio between short and long term tests. From the experimental work of this thesis, under dynamic conditions i.e. short term loading, the cartilage does appear to be behaving similarly to an 'ideal' material which maintains constant volume when stressed elastically, and therefore has a Poisson's ratio close to 0.5. However from the micrometer test reported in section 5.1 the conclusion can be drawn that the long term or 'slow' Poisson's ratio is approaching zero, as the axial applied stress has the ultimate result of producing only axial strain. The resultant loss of volume, when stressed, in a material with Poisson's ratio close to zero is, in the case of cartilage, achieved by expressing the interstitial fluid.

Considering now the dynamic load experiments, the creep strains achieved, due to the mean constant load applied, appear to be the same as the strains achieved for a similar static load. The strain/time curves and stress/strain curves of section 5.1 are relevant to either the static load tests or the dynamic load tests. This result is in contrast to the findings of Simon (1971) and Linn (1967) who, as reported in the literature review, found that the final strains attained in oscillatory load tests were less than in static load tests.

The oscillating load/deflection characteristics are essentially linear, as shown by the hysteresis loops. However the slope of the relationship (the calculated modulus) increases as the creep strain increases. In trying to explain this increase in modulus with creep strain it is interesting to consider an alternative modulus, E' . This alternative modulus is based

on a strain calculated from the current length, l, of the specimen as opposed to the original length, l_o.

$$\epsilon = \frac{\delta l}{l_o}$$

correct the strain to $\epsilon' = \frac{\delta l}{l}$

since $l = l_o(1-\epsilon)$

$$\epsilon' = \frac{\delta l}{l_o(1-\epsilon)} = \frac{\epsilon}{(1-\epsilon)}$$

Therefore this alternative modulus $E' = \frac{\Delta\sigma}{\Delta\epsilon'} = \frac{\Delta\sigma}{\Delta\epsilon}(1-\epsilon)$

which gives $E' = E(1-\epsilon)$

Figures 6.1 - 6.3 show the variation of E and E' with creep strain .

Although E' still increases with creep strain, the increase is far less than the increase in E . This seems a reasonable conclusion because as the specimen strains the composition of the specimen is altering. The ratio of matrix to interstitial fluid is increasing. Both E and E' are moduli recorded for the combination, but with increased creep strain the modulus must become more dependent on the modulus of the matrix. This perhaps suggests that the modulus of the matrix alone is higher than any of the moduli calculated from these experimental results.

Considering now the effect of loading frequency on cartilage stiffness, refer to figures 5.18 and 5.42. The frequencies chosen were those fairly representative of fast 100 m sprinting, ordinary walking, and a slow dawdle. At these frequencies the experimental results, figure 5.18, which are the combined effect of fluid flow and elastic deformation, show very little variation in the recorded stiffness due to change in frequency. However frequency must ultimately have an effect on the calculated modulus, for, in the extreme, where the frequency is zero, the equilibrium moduli are of the order of $1 \times 10^6 N/m^2$, whereas in the oscillatory tests, for the range of

frequencies used the modulus is around 1 - 10 x $10^8 N/m^2$. This must be a result of fluid flow. In the computer predicted relationships between stiffness and frequency, figure 5.42, which of course only deal with fluid flow, it can be seen that as frequency increases the cartilage stiffens. However it seems reasonable to state that over the range of frequencies chosen, although fluid flow increases its effect at the lower end of the frequency range, it is still the elastic component which plays the dominant role in the deformation of the cartilage.

It would seem fair to state that the comparison between the experimental results and the predictions of the computer model are qualitatively rather disappointing. However the computational work has yielded some useful information.

The computer model predicts solely the fluid flow contribution to deformation, and these are shown in section 5.3 to be not particularly close to the actual deformations recorded in cartilage under constant load. However when considering dynamic loading, the predictions of the model tend to fall much more closely in line with the experimental conclusions about the deformation process. Qualitatively then it seems reasonable to accept the predictions of the model as the correct fluid flow phenomena under dynamic loading. Above all the computer model confirms that for short duration loading, around the frequency of the walking cycle, fluid flow plays virtually no part in the dynamic component of the deformation.

From the relationships of figures 5.21 - 5.27 it is seen that the computer predictions are very dependent on the relationships between the variables in the analysis, and on the values of these variables, for instance the relationship of $k = f_n(\epsilon)$. A linear relationship similar to that proposed by Mansour and Mow (1976) can be seen in figure 5.22, to produce very different characteristics from the Litchfield relationship where $k = f_n(\epsilon^3)$

It is relationships such as these that would seem to be partly responsible for the innaccuracies of the computer predictions for static loading. If these relationships were indisputably determined and values of such properties as porosity and permeability were determined absolutely for each specimen, then perhaps the predicted results would be more accurate for each loading case.

It seems now possible to describe the mechanical behaviour of articular cartilage in terms of the over simplified rheological model of figure 6.4. In this case spring A is a non-linear elastic spring representing the equilibrium behaviour of slow or long term compression tests, such as in figure 5.11. Spring B is a rubber-like material which cartilage would be if all the fluid content were immobilised, and C is viscous dashpot in which the clearance decreases with displacement. Spring B is much stiffer than A at small strains and the dashpot C is virtually locked at frequencies in the range of one cycle per second and above; at such frequencies therefore the behaviour is dominated by spring B, with A and C contributing to long term changes viz. creep strain. However as seen from experimental work the cartilage stiffness to oscillatory loads increases as creep strain increases. Therefore spring B in this rheological model must be such that it increases in stiffness as creep strain increases, i.e. when components A and C are contributing more to the response.

Under loads of short duration the response of the model will be much like that of rubber, with a high resistance to volumetric strain and a relatively low resistance to shear strain.

7 Conclusions

The experimental work has led to the following conclusions about the action of articular cartilage in the body under normal physiological conditions.

It appears that during a normal working day, including walking, standing sitting, etc., the cartilage will become thinner and stiffer. The average loading during the period would determine a daily working thickness for the cartilage, with the cartilage resuming its unstrained dimensions during a night's rest. This 'daily working thickness' may not be achieved in the same way as the equilibrium thickness arrived at during the laboratory tests. In the laboratory tests the fluid flow was axial and into a region of atmospheric pressure; however, in a joint the synovial fluid in the contact region will be pressurised, and so flow will presumably be less in the axial direction, i.e. straight into the contact zone, and radial flow will occur.

During the day then the cartilage becomes thinner and consequently stiffer, i.e. takes on a higher elastic modulus, see figures 6.1 - 6.3. Fluctuations in loading during this period will induce only elastic responses of the cartilage. In terms of the oversimplified rheological model previously mentioned, during the day spring A compresses, the dashpot is at its lowest clearance or tightest and spring B has a higher stiffness.

The dynamic elastic modulus, E , of cartilage appears to be of the order of $1 \times 10^8 N/m^2$ when the cartilage has zero creep strain. This value might increase, depending on the species from which the cartilage was taken, towards a value of the order of $1 \times 10^9 N/m^2$. Each species of cartilage has its own characteristics to dynamic and static loading.

As cartilage has been shown to react in a linear elastic manner to dynamic loading the conclusion of Radin and Paul (1970) is as one would expect.

This is that cartilage contributes little to the load attenuation properties of joints. There is only a thin covering of cartilage on the bone ends, the volume of cartilage is small compared with the volume of the bone, and its damping is very small at normal physiological loading frequencies.

The cartilage covering on bone ends would seem therefore to have the functions:-

1) providing a compliant surface to enlarge the load-supporting area and reduce the contact stress level.
2) protect the underlying bone from mechanical damage that would be caused by direct bone to bone contact.
3) providing a low friction bearing surface within the joints to aid the elegant mechanical functioning of articulating joints.
4) along with synovial fluid playing an important role in the mechanics of the lubrication of joints.

Appendix I

Short study of subchondral bone

This short study of the deflection characteristics of subchondral bone arose from the oscillating load tests on articular cartilage. As stated in section 5.2 the very small deflections recorded in oscillatory tests led to the scrutiny of the whole of the apparatus and procedure, as any deflection external to the deflection of the cartilage alone, would introduce errors.

The subchondral bone is cancellous bone overlayed with a thin layer of compact bone. Currey (1970) gives the following description of cancellous bone:

"Cancellous bone is found predominantly under synovial joints and areas in which forces are applied over large areas. This indicates that its main function may be to transmit forces, where the stresses, if the bone were solid, would be ridiculously low (and the weight of the bone correspondingly high), yet where the morphology of the situation does not allow a mere thinning of the cortex of the bone; this would produce a too fragile shell."

Many papers have been published on the properties of bone and on the relationship of such features as mineral content and collagen fibre orientation on these mechanical properties. However most published work has been on compact bone tissue or even complete bones from various species and most of this work involved the use of dried or chemically treated bone. The interest in this short study was on wet subchondral bone only, that was, like the cartilage, removed from the animal shortly after slaughter, and not allowed to dry.

Currey (1970,1974) in these two papers not only quotes values of mechanical properties found by other researchers, but puts forward many points relating to bone and especially cancellous bone that are of interest here. He says that "bone is viscoelastic, but from the point of view of its function this viscoelasticity is not nearly so important as it is for the more pliant materials. This is because, except in the extremis, it is not the function

of bone to store or to dissipate energy." He maintains that the reaction of bone in compression is vastly different from tension, and for cancellous bone failure in compression is accompanied by considerable buckling. Cancellous bone is considerably weaker and more pliant than compact bone when tested on its own; however a statement such as this is not especially meaningful as cancellous bone is always surrounded by a thin shell of compact bone. When making calculations on the properties of cancellous bone, it is generally accepted that the total cross-section may be used, even though some of the cross section is occupied by the spaces in the bone. Therefore properties calculated tend to refer to the whole specimen not the bone material alone. With increase in mineralisation of bone, stiffness and static strength increase, but the amount of energy absorbed in static loading and impact rises and then falls. Currey showed that nature selects the ammount of mineralisation required in individual bones to meet their function.

In this research, similar tests to those on cartilage were performed on small cylindrical plugs of subchondral bone. The bone studied was from the same sites as the bovine cartilage. In the specimens tested, the reported covering of compact bone was of negligible thickness. The test specimens were removed with a trephine in a similar way to the cartilage and bone specimens. The cartilage was then removed from the specimen with a scalpel blade.

As stated previously this was to be a minor investigation. Three primary tests were performed. These were confined oscillating load tests, with the load oscillating around a mean constant level. The response of the bone to this constant load can be seen in figure A1 which has been corrected for deflection of the rig. From the point of application of the load there appeared an immediate elastic response producing the majority of the final strain. Up to about 4 minutes after load application there was a continued increase in strain, but thereafter the strain increased only very slightly for the duration of the test, longer than 50 minutes. The most notable point gained from this is that the ultimate strains reached for these loads is far smaller

than the ultimate strains recorded for cartilage at these loads. The deflections of the bone is insignificant compared to the cartilage deflections in constant load cases, therefore the effect of the bone can be disregarded in the cartilage tests.

Figure A2 shows a constant incremental load test in which one bone specimen was repeatedly loaded and unloaded. The points on the curve were taken immediately after load application; however this graph does include the deflection of the rig. It can be seen that after the first load application, successive unloading and loading produced a repeatable curve. After the final unloading the bone was left and the residual deformation did decrease with time. It would appear then that wet subchondral bone acts in an elastic fashion to quickly applied loads, with time dependant responses being slow.

The oscillating component of the applied load allowed elastic moduli of the bone to be calculated. This was done exactly as for cartilage using the stress and strain amplitudes read off the oscilloscope photographs, after correcting for rig deflections. As so few tests were undertaken, plotting the results against creep strain or time yields no significant information. The only trend obvious from the results is that the elastic modulus of subchondral bone is higher than that of cartilage by about one order of magnitude. It appeared also that during the first few minutes after load application, i.e. in the time taken to achieve most of the equilibrium strain, the modulus was lower than for the rest of the loaded period.

The average values of the modulus recorded were:-

before the equilibrium strain, $0.63 \times 10^9 N/m^2$

after the equilibrium strain, $2.12 \times 10^9 N/m^2$

Currey (1970) quotes the following values for the elastic modulus of bone. From tests on prisms of cancellous bone, taken from all parts of human femora the average value of E is $0.245 \times 10^9 N/m^2$, the value being $0.176 \times 10^9 N/m^2$

for specimens above 71 years of age and 0.32 x $10^9 N/m^2$ for specimens below 71 years of age (Evans and King). These values are around $1/30$ of the modulus of compact bone. Values ranging from 6.7 - 21.0 x $10^9 N/m^2$ are quoted for the elastic modulus of cubes of compact bone from an ox femur in compression at low strain rate (Bird, Becker, Healer and Messer) and 18.6 x $10^9 N/m^2$ for similar specimens under similar conditions (McElhaney). A higher value 29.0 x $10^9 N/m^2$ (McElhaney, Fogle, Byars and Weaver) from compression tests on an ox femur is recorded, although Currey reports that this value could be abnormally high due to the testing conditions.

From these quoted figures, and the experimental work done for this research, it would seem that in tests of cartilage, where the cartilage is not removed from the bone, it is not permissible to ignore deflections of the bone. Other workers, especially those performing the unconfined type of test on cartilage have chosen to ignore bone deflections in their calculations. This may be understandable if they were accepting the higher figures for the elastic modulus, i.e. that for compact bone, as the elastic modulus for the subchondral bone. However it has now been shown that the modulus of subchondral bone is lower, and close enough to the modulus of cartilage to require consideration.

References

Balazs, E.A., Bloom, G.D., Swann, D.A. (1966) Fine structure and glycosaminoglycan content of the surface layer of articular cartilage, Fed. Proc., 25, 1813.

Camosso, M.G., Marotti, G. (1962) The mechanical behaviour of articular cartilage under compressive stress, J. Bone Jt. Surg. 44A, 699.

Charnley, J. (1959) The Lubrication of animal joints, Symp. on Biomechanics, Inst. Mech. Engrs., London. 12.

Currey, J.D. (1970) The mechanical properties of bone, Clin. Orthopaed, 73, 210.

Currey, J.D. (1974) Bone:- Lecture given at Biomechanics short course on joints and joint replacements. University of Leeds, March.

Dowson, D. (1967) Modes of Lubrication in human joints. Proc. Instn. Mech. Engrs, 181, 3J, 45.

Dowson, D., Unsworth, A., Wright, V. (1970) Analysis of 'boosted lubrication' in human joints, J. Mech. Eng. Sci., 12, 364.

Edwards, J. (1967) Physical Characteristics of articular cartilage, Proc. Inst. Mech. Engrs., 181, 16.

Elmore, S.M., Sokoloff, L., Norris, G., Carmeci, P. (1963) The nature of 'imperfect' elasticity of articular cartilage, J. Appl. Physiol. 18, 393

Fein, R.S. (1967) Are synovial joints squeeze-film lubricated? Proc. Inst. Mech. Engrs., 181, 3J, 125.

Freeman, M.A.R., Swanson, S.A.V., Manley, P.T. (1975) Stress-lowering function of articular cartilage, Med. and Biol. Eng., March, 245.

Hassell, A.H. (1849) Microscopic anatomy of the human body, Vol. 1, Pub. Samuel Highley, London.

Hayes, W.C., Mookrose, L.F. (1971) Viscoelastic properties of human articular cartilage, J. Appl. Physiol., 31, 562.

Higginson, G.R., Norman, R. (1974) A model investigation of squeeze-film lubrication in animal joints, Phys. Med. Biol., 19, 785.

Higginson, G.R., Litchfield, M.R., Snaith, J.E. (1976) Load/deformation/time characteristics of articular cartilage, In press.

Hirsch, C. (1944) The pathogenisis of chondromalacia of the patella, Acta. Chir. Scand., 90, Suppl. 83, 9.

Hunter, W. (1743) Of the structure and diseases of articulating cartilages, Phil. Trans., 42, 514.

Johnson, G.R. (1974) Dynamic properties of articular cartilage and loading of the ankle joint, Ph.D. Thesis, University of Leeds.

Kempson, G.E., Miur, H., Swanson, S.A.V., Freeman, M.A.R. (1970) Correlations between stiffness and the chemical constituents of cartilage on the human femoral head, Biochim. Biophys. Acta., 215, 70.

Kempson, G.E., Freeman, M.A.R., Swanson, S.A.V. (1971) The determination of a creep modulus for articular cartilage from indentation tests on the human femoral head, J. Biomechanics, 4, 239.

Kempson, G.E., Spivey, C.J., Swanson, S.A.V., Freeman, M.A.R. (1971a) Patterns of cartilage stiffness on normal and degenerate human femoral heads, J. Biomechanics, 4, 597.

Leidy, J. (1849) On the intimate structure and history of the articular cartilages, Am. J. Med. Sc., 17, 277.

Linn, F.C. (1967) Lubrication of animal joints, I: The arthrotripsometer, J. Bone Jt. Surg., 49A, 1079.

Linn, F.C., Sokoloff, L. (1965) Movement and composition of interstitial fluid of cartilages, Arth. and Rheum., 8, 481.

Litchfield, M.R. (1974) The mechanical properties of a liquid-filled porous solid with reference to articular cartilage, Ph.D. Thesis, University of Durham.

McCall, J.G. (1969) Load deformation response of the microstructure of articular cartilage, In: Lubrication and wear in joints, Sector Pub., London, 39.

MacConaill, M.A. (1932) The function of intra-articular fibro-cartilages, J. Anat., 66, 210.

McCutchen, C.W. (1959) Mechanism of animal joints: Sponge-hydrostatic and Weeping Bearings, Nature, 184, 1284.

McCutchen, C.W. (1962) The frictional properties of animal joints, Wear, 5, 1.

McCutchen, C.W. (1966) Boundary lubrication by synovial fluid: demonstration and possible osmotic explanation, Fred. Proc., 25, 1061.

McCutchen, C.W. (1967) Physiological Lubrication, Proc. Instn. Mech. Engrs., 181, 3J, 55.

Maroudas, A. (1968) Physico-chemical properties of cartilage in the light of ion exchange theory, Biophysics, J., 8, 575.

Maroudas, A. (1973) Adult articular cartilage, Edited by Freeman, M.A.R., Pitmans, London, 231.

Maroudas, A. (1973a) In: Adult articular cartilage, Edited by Freeman, M.A.R., Pitmans, London, 156.

Maroudas, A., Bullough, P. (1968) Permeability of articular cartilage, Nature, 219, 1260.

Maroudas, A., Bullough, P., Swanson, S.A.V., Freeman, M.A.R. (1968) The permeability of articular cartilage, J. Bone Jt. Surg., 50B, 166.

Mansour, J.M., Mow, V.C. (1976) The permeability of articular cartilage under compressive strain and at high pressures, J. Bone Jt. Surg., 58A, 509.

Mansour, J.M., Mow, V.C. (1976a) On the natural lubrication of synovial joints: normal and degenerate, Joint A.S.M.E. - A.S.L.E. Conference, 5th - 7th October, U.S.A.

Meachim, G., Stockwell, R.A. (1973) In: Adult articular cartilage, Edited by Freeman, M.A.R., Pitmans, London, 35.

Minns, R.J., Stevens, F.S. (1976) The collagen fibril organization in human articular cartilage, J. Anat. (in press).

Munding, R.H. (1975) The mechanical properties of adult articular cartilage, 3rd year undergraduate project, University of Durham.

Radin, E.L., Paul, I.L., Lowy, M. (1970) A comparison of the dynamic force transmitting properties of subchondral bone and articular cartilage, J. Bone Jt. Surg., 52A, 444.

Radin, E.L., Paul, I.L. (1970) Does cartilage compliance reduce skeletal impact loads? Arth. Rheum., 13, 139.

Schäfer, E.S. (1920) The essential of histology, Ed. by H.M. Carleton, Pub. Longmans, Green and Co., London, 114.

Simon, W.H. (1971) Scale effects in animal joints. II: Thickness and elasticity in the deformation of articular cartilage, Arth. Rheum., 14, 493.

Sisson, S., Grossman, J.D. (1948) The anatomy of domestic animals, Third edition, Pub. W.B. Saunders Company, Philadelphia and London.

Sokoloff, L. (1966) Elasticity of aging cartilage, Fed. Proc., 25, 1089.

Tanner, R.I. (1966) An alternative mechanism for the lubrication of Synovial joints, Phys. Med. Biol., 11, 119.

Walker, P.S., Dowson, D., Longfield, M.D., Wright, V. (1968) 'Boosted Lubrication' in synovial joints by fluid entrapment and enrichment, Ann. Rheum. Dis., 27, 512.

Yannas, I.V. (1970) Involvement of articular cartilage in a linear relaxation process during walking, Nature, 227, 1358.

FIG 2·1

Schematic view of the collagen fibrillar organisation in human A C. in the full thickness block, from the surface to the deep subchondral bone, approximately 50x full size

Reproduced by kind permission of Minns and Stevens (1976)

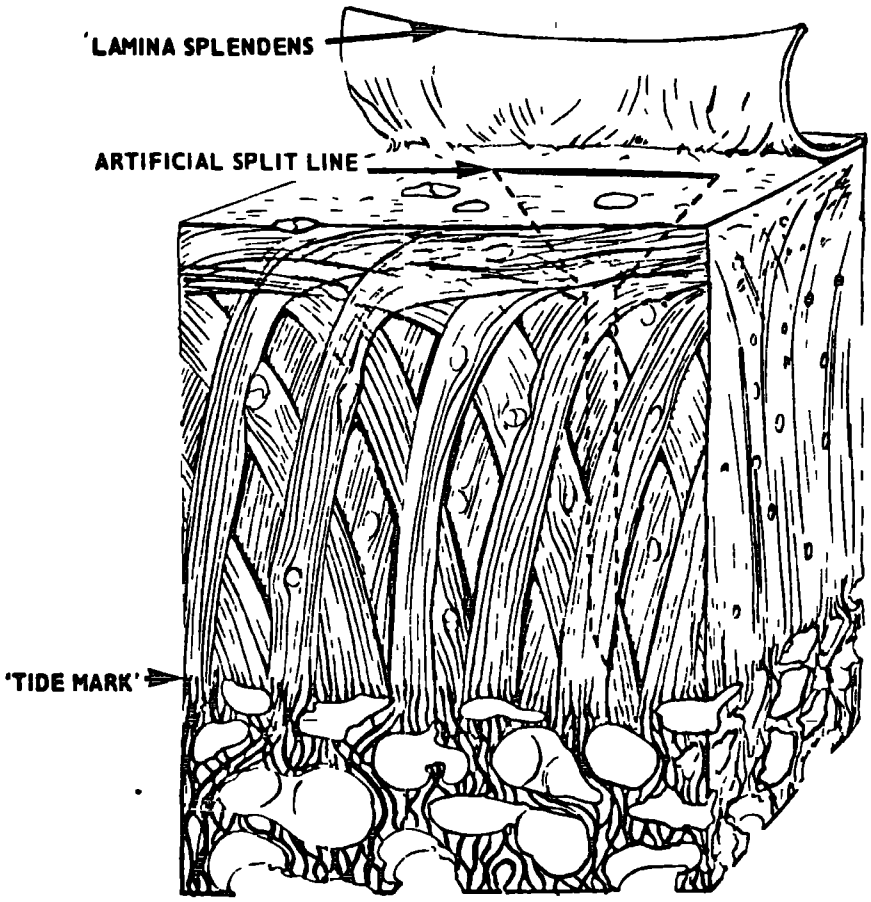

FIG 3·1 METHOD OF OBTAINING FINITE DIFFERENCE EQUATIONS FOR UNEQUAL STEP LENGTHS OF ΔZ

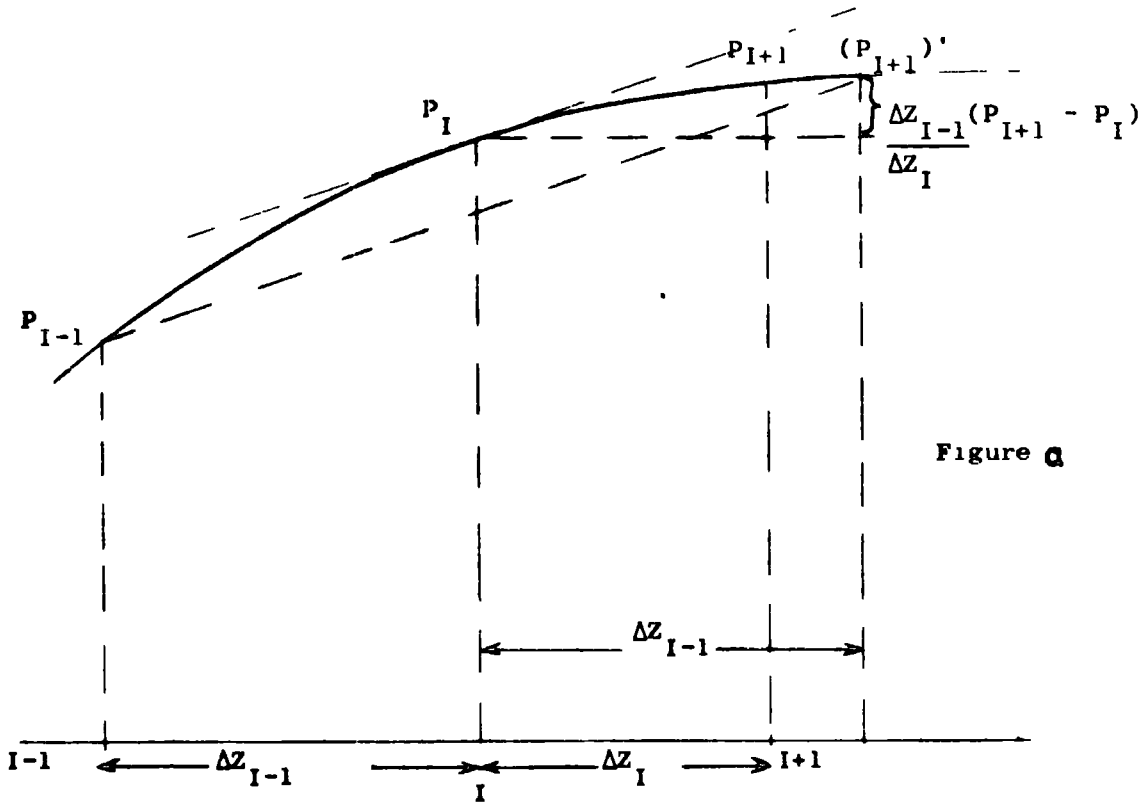

Figure a

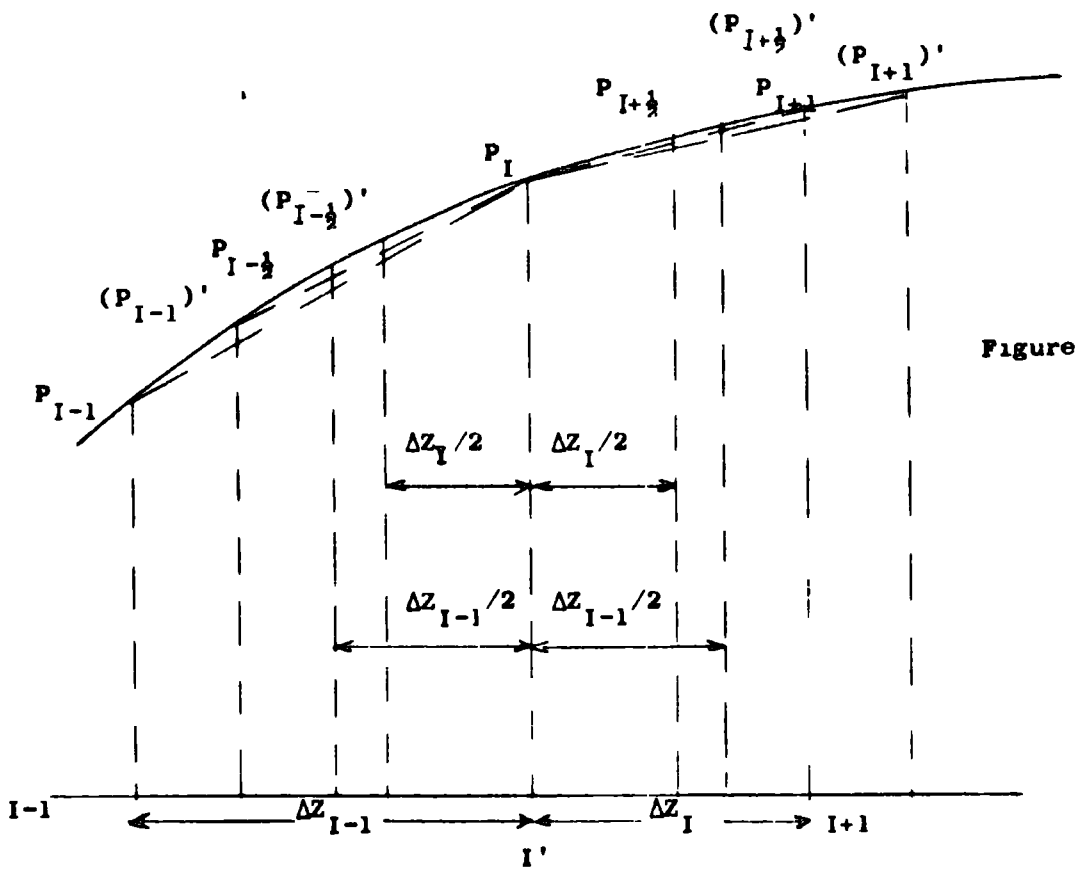

Figure b

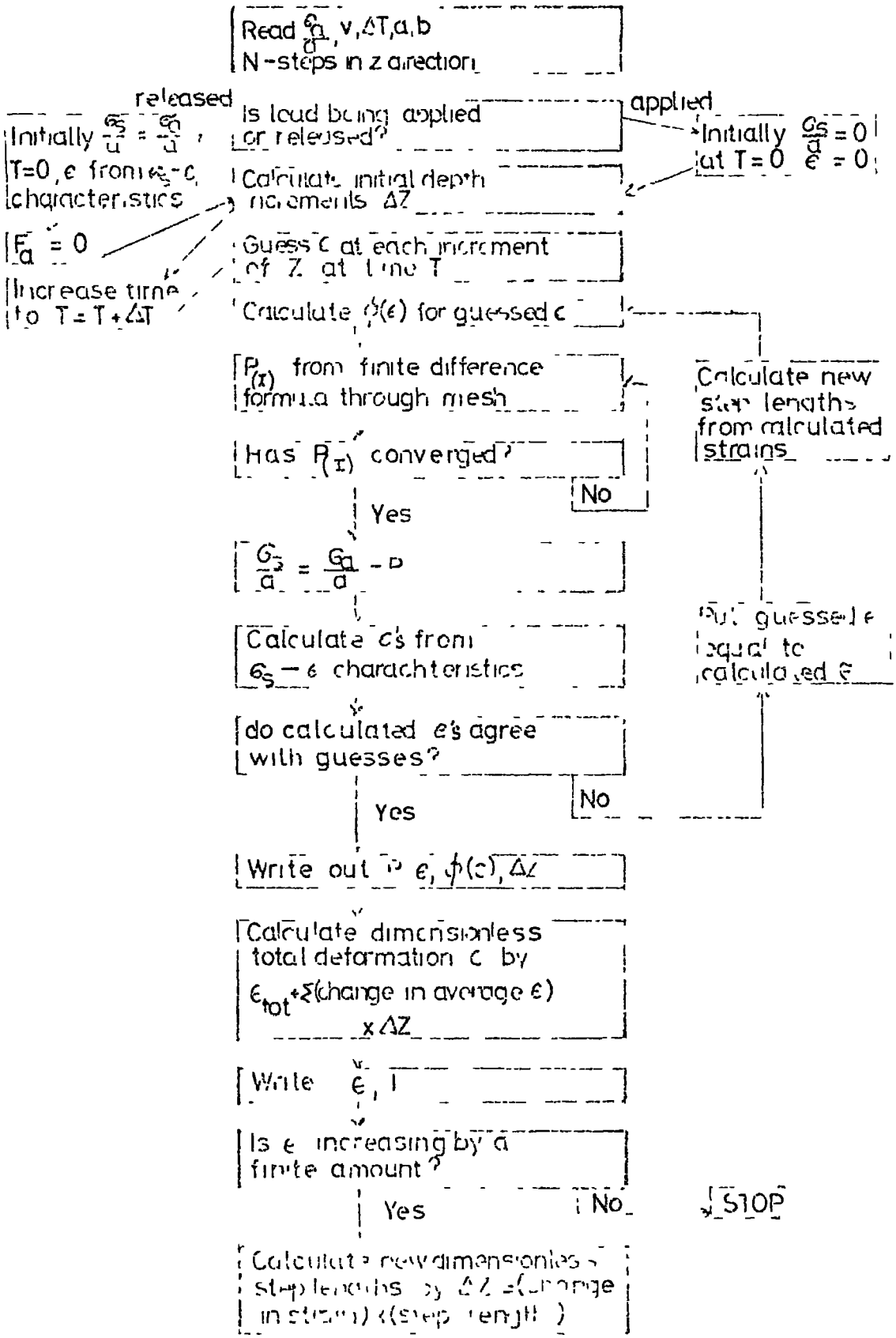

FIG 5.2 FLOW DIAGRAM FOR DIMENSIONLESS AXIAL FLOW PROGRAMME

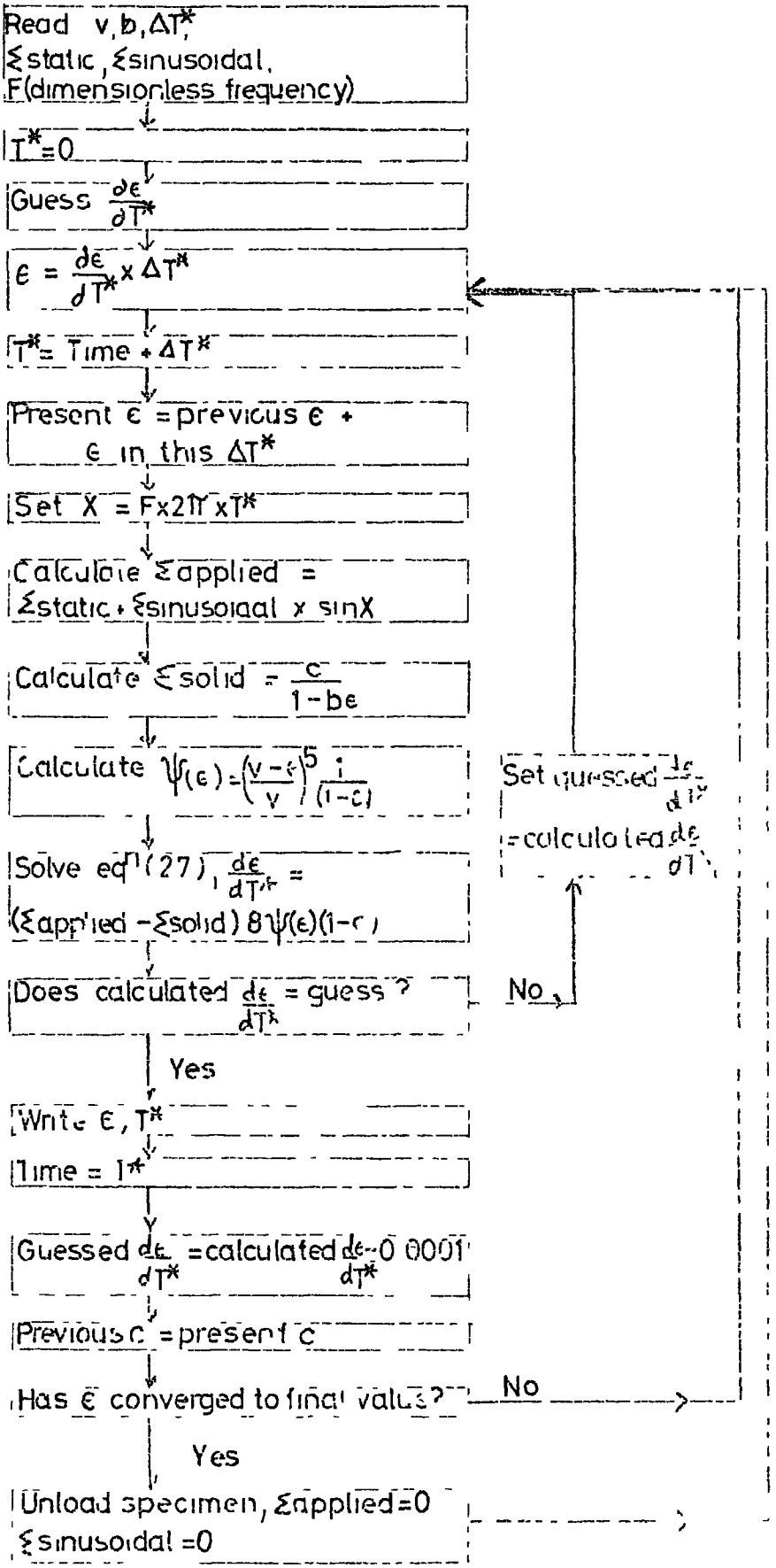

FIG 3.3 FLOW DIAGRAM FOR DIMENSIONLESS RADIAL FLOW PROGRAMME

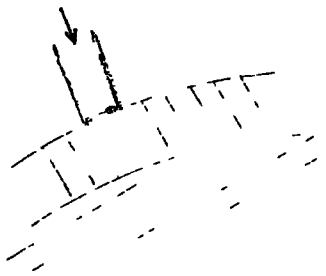

$\epsilon_z \not\gg \epsilon_r, \epsilon_\theta$

FLOW IN r, θ and z DIRECTIONS

a) INDENTATION

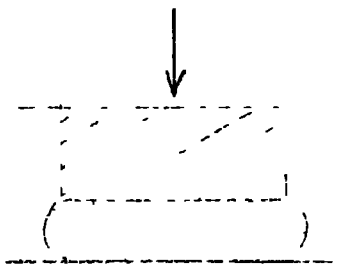

$\epsilon_z \not\gg \epsilon_r, \epsilon_\theta$

FLOW IN r DIRECTION ONLY

b) UNCONFINED

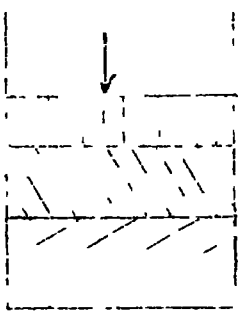

$\epsilon_z \gg \epsilon_r, \epsilon_\theta$

FLOW IN z DIRECTION ONLY

c) CONFINED

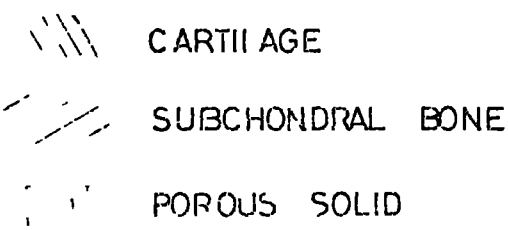

FIG 4·1 THREE TYPES OF COMPRESSION TEST

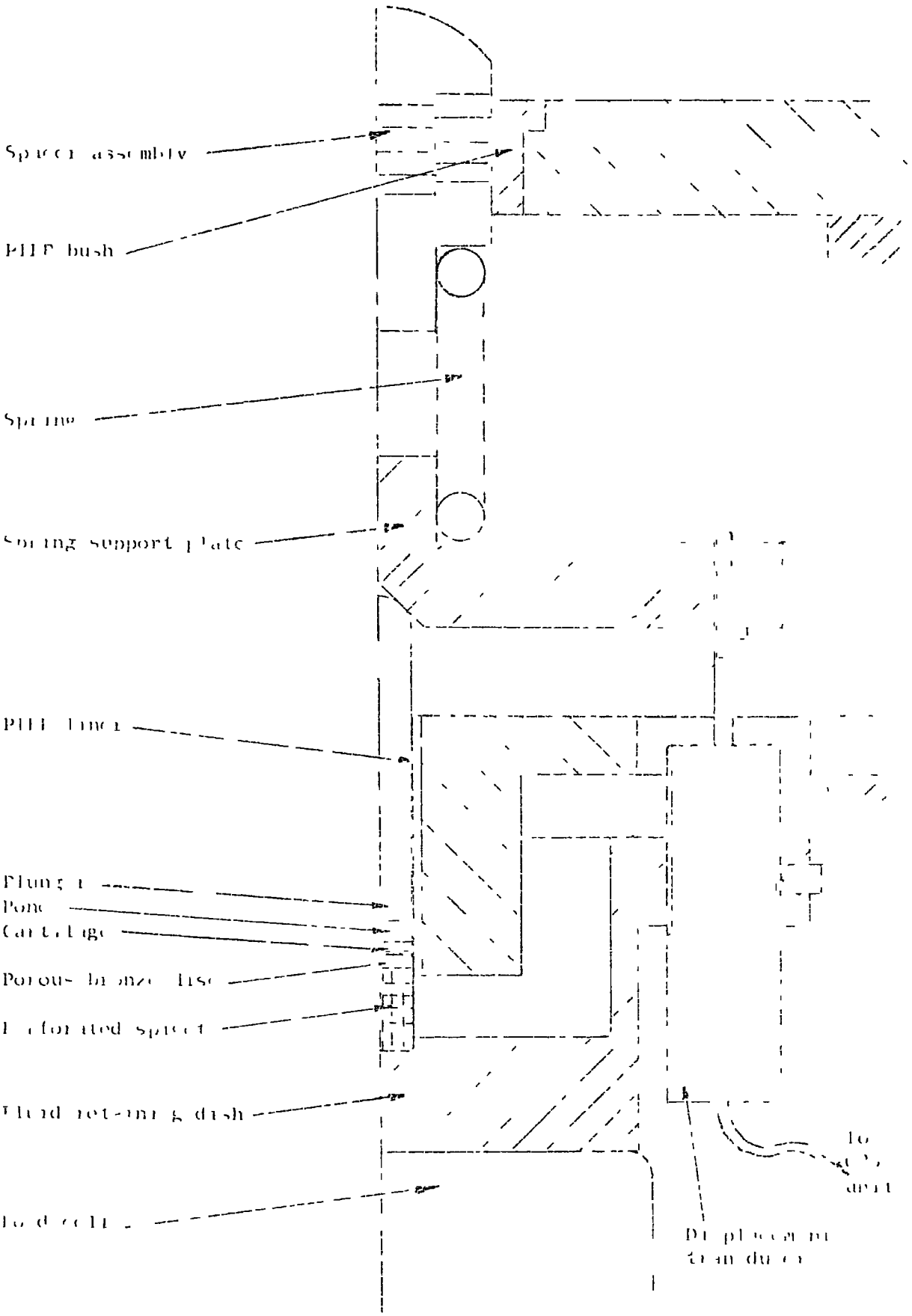

Figure 4.2 SPECIMEN HOLDER ASSEMBLY
Half Section showing Split Ring

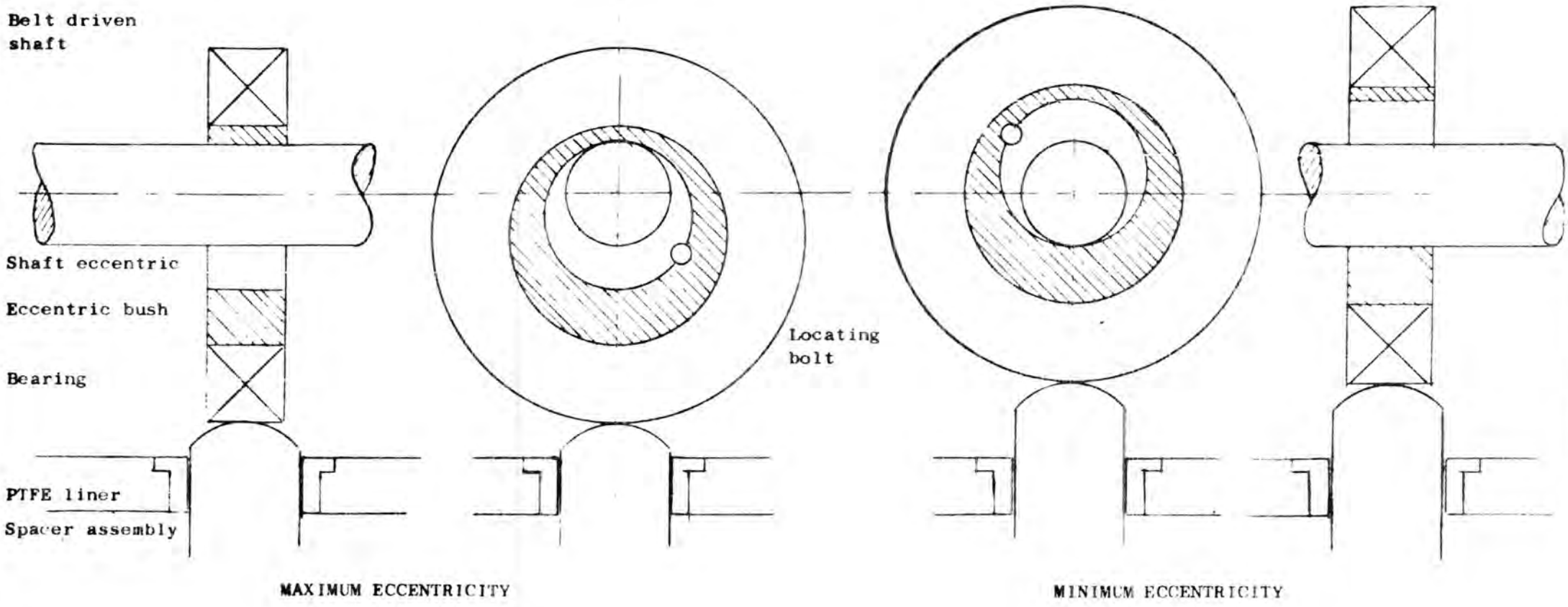

Figure 4·3 : CONFIGURATION OF RIG FOR SINUSOIDAL LOAD APPLICATION

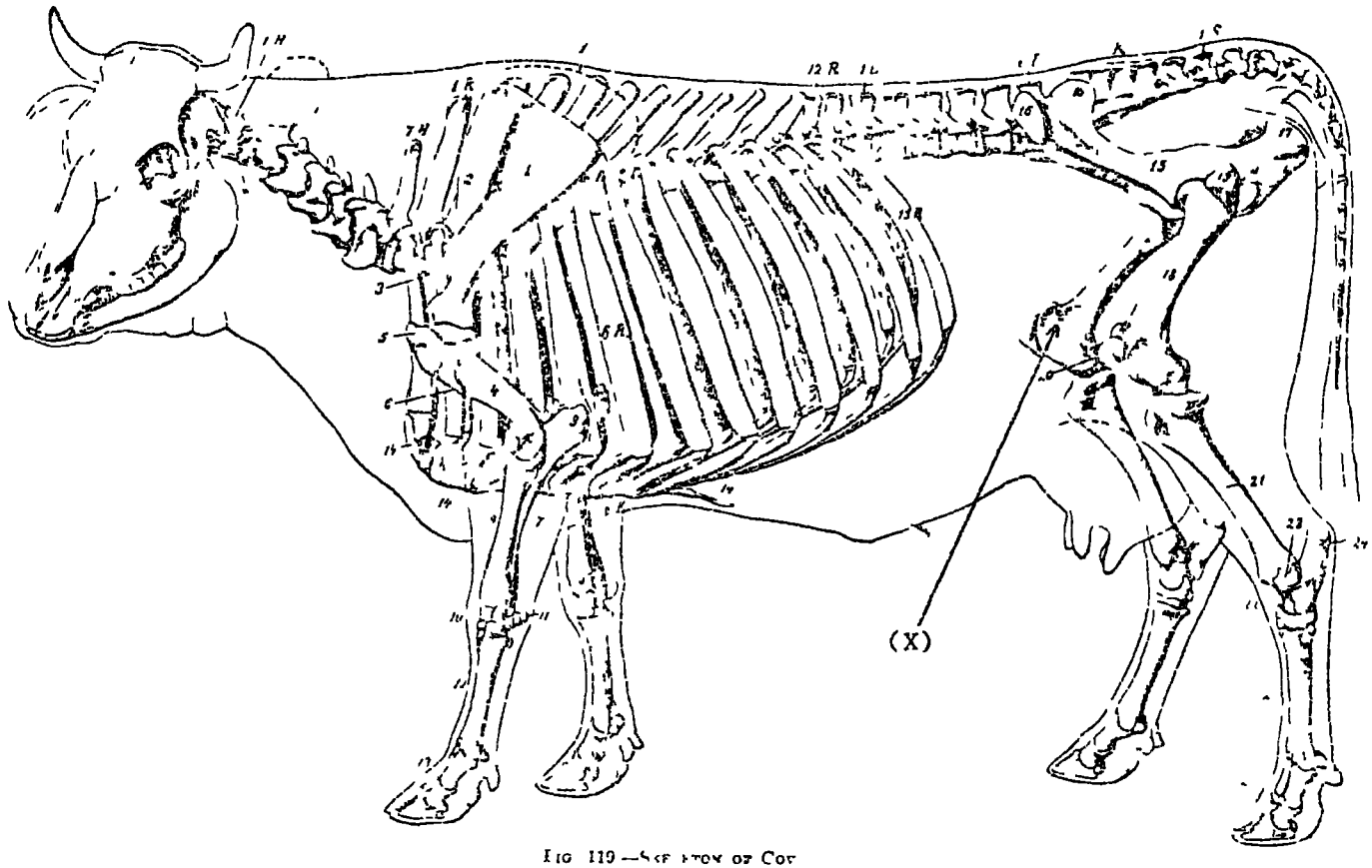

FIG 119.—SKELETON OF COW

1 H Atlas *7 H* seventh cervical vertebra *1 R* first thoracic vertebra *9 P* scapula *12 R* twelfth thoracic vertebra *13 P* ilium *1 L* first *6 L* last lumbar vertebra *K* sacrum *15* first coccygeal vertebra *16 K* tuber coxae *17* wing of ilium *1* scapula *2* tuberosity of scapula *3* spine of scapula *4* acromion *5* humerus *6* lateral tuberosity of humerus *6'* deltoid tuberosity *7* ulna *8* olecranon *9* radius *10* carpus *11* accessory carpal bone *12* metacarpus *13* phalanx *14* sternum *14'* manubrium *14''* xiphoid cartilage *15* thigh *16* tuber coxae *16'* tuber sacrale *17* tuber ischii *18* patella *19* tuber major *20* patella *21* tibia *21'* lateral condyle of tibia, *22* tarsus *23* distal end of fibula, *24* tuber calcis *25* metatarsus *26* phalanges The bones of the fore limb are placed too high in relation to the thorax (after Ellenberger-Baum, Atlas für Kursäler)

FIG 44 BOVINE SKELETON BONE USED FOR SPECIMENS (X)
Reproduced from Sisson and Grossman (1948)

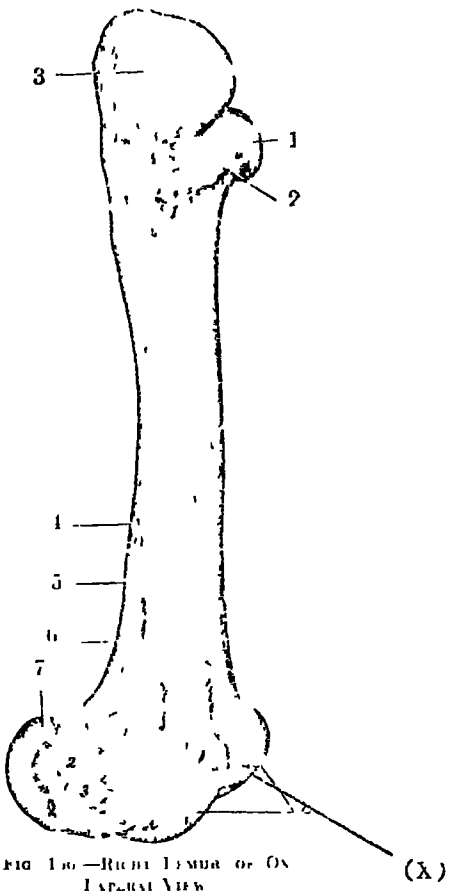

FIG 1 to —RIGHT FEMUR OF OX
LATERAL VIEW

Numbers round bone 1 Head 2 neck 3 trochanter major 4 lateral border 5 lateral supracondyloid crest 6 supracondyloid fossa 7 lateral condyle 8 trochlea Numbers on bone 1 Impression for trochanteric bursa of tensor profundus 2 lateral epicondyle 3 depression for origin of popliteus muscle 4 extensor fossa

FIG 4 5 BOVINE FEMUR
INDICATING SITE OF SPECIMENS (X)
Reproduced from Sisson and Grossman (1948)

FIG 4 6 INK STAIN PATTERNS ON HUMAN PATELLA SPECIMENS

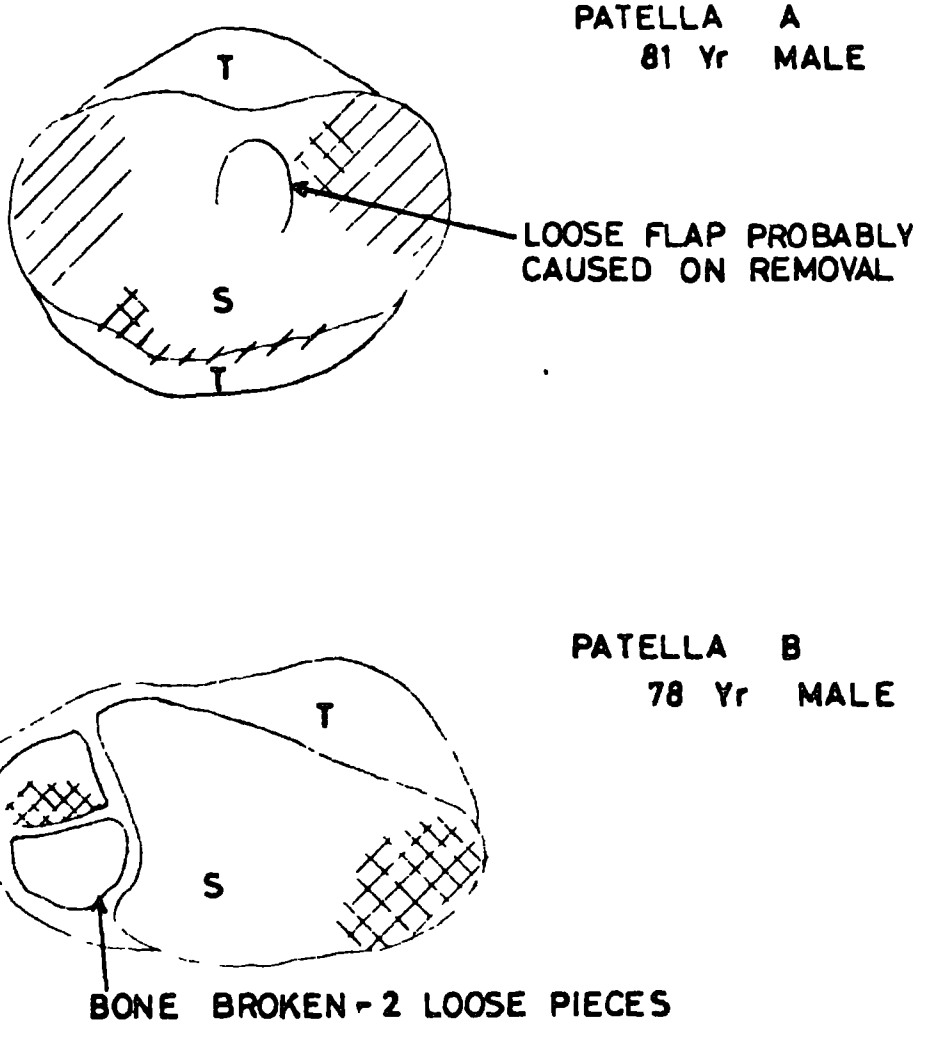

FIG 5·1 STRAIN v TIME BOVINE CARTILAGE CONFINED
LOADING AND RECOVERY

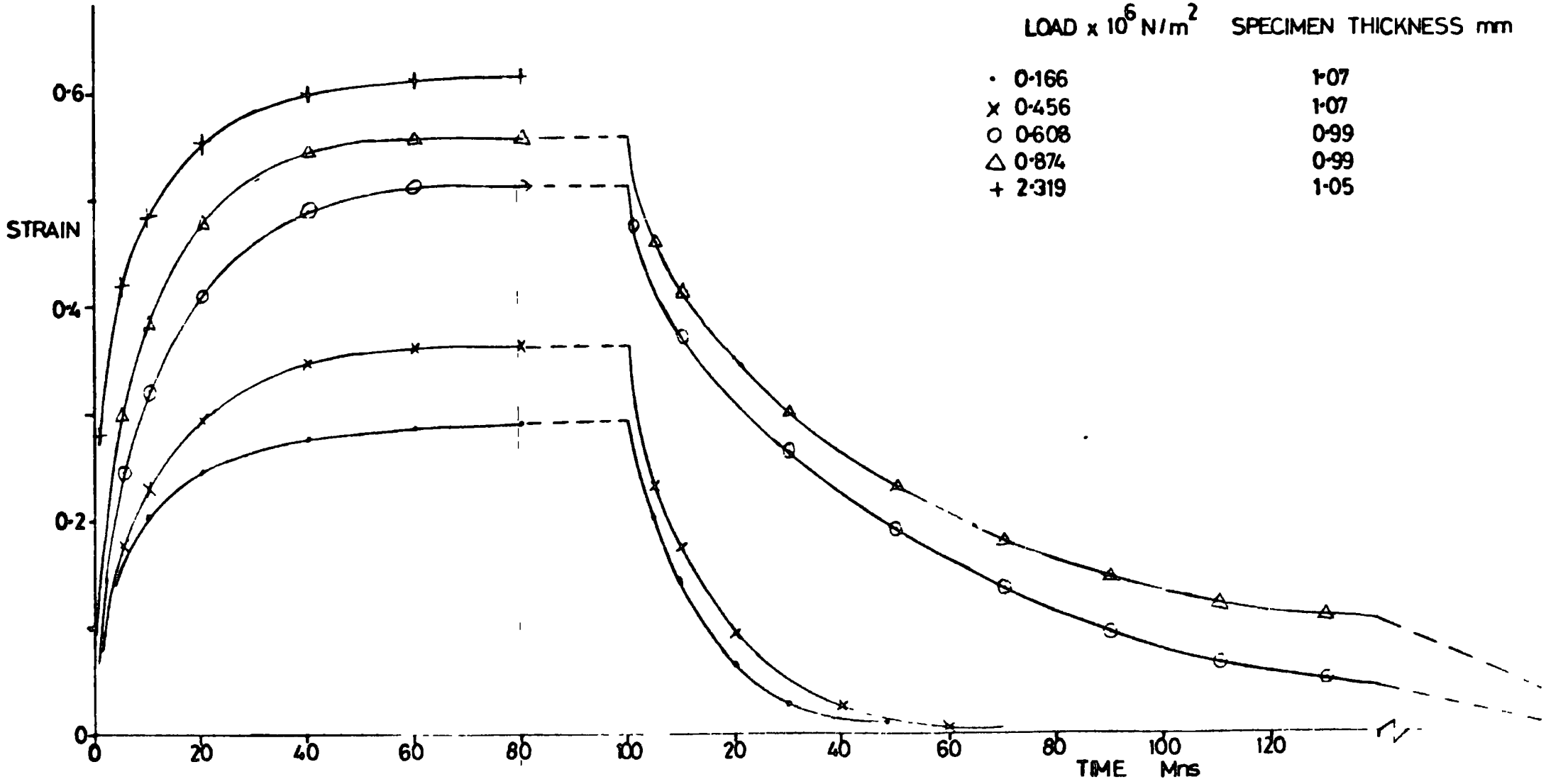

FIG 5·2 STRAIN v TIME HUMAN CARTILAGE CONFINED
LOADING | AND RECOVERY

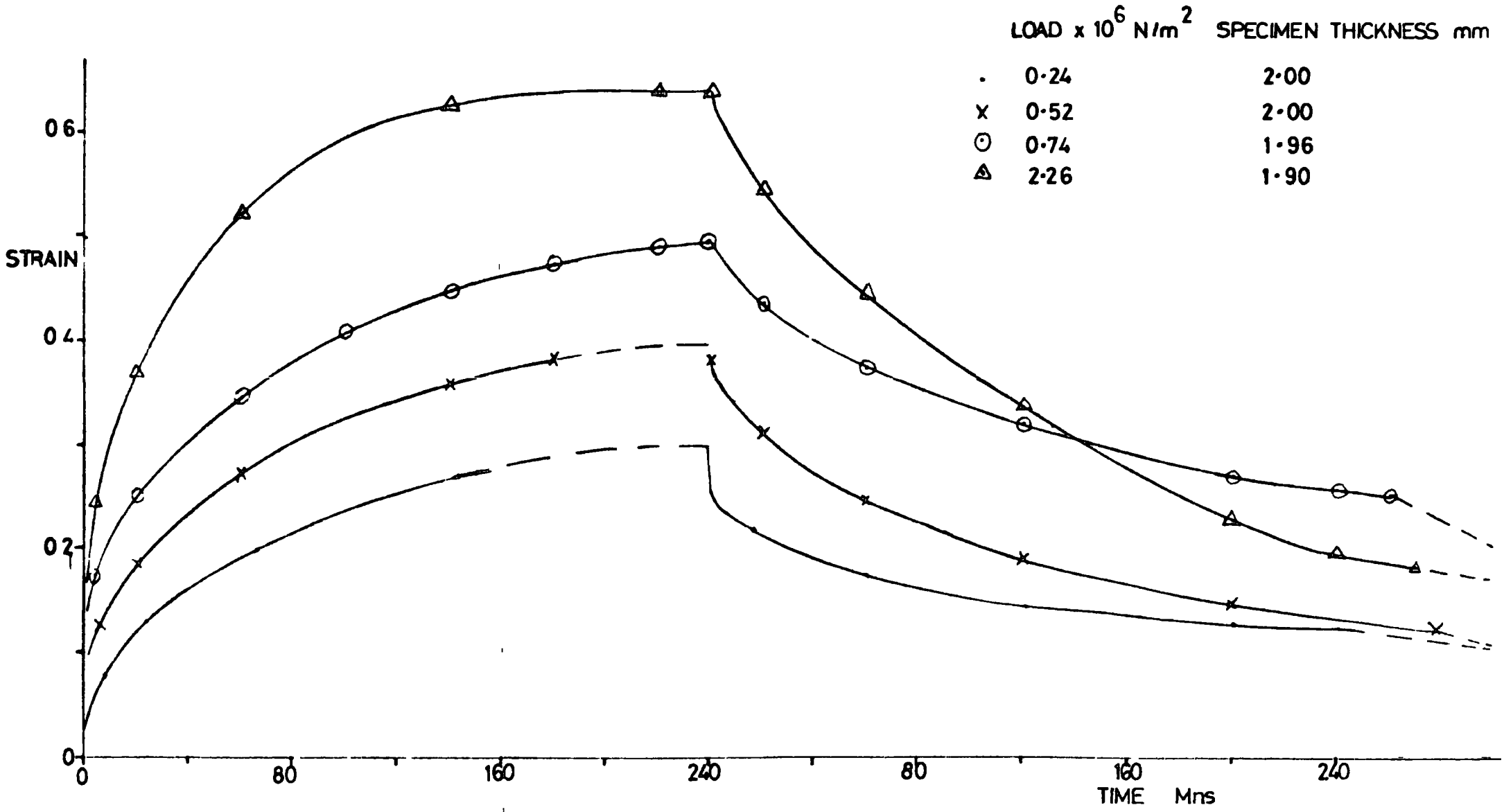

FIG 5·3 STRAIN v TIME BOVINE CARTILAGE UNCONFINED
LOADING AND RECOVERY

	LOAD x 10^6 N/m^2	SPECIMEN THICKNESS mm
x	2·015	1·15
⊙	0·68	1·15

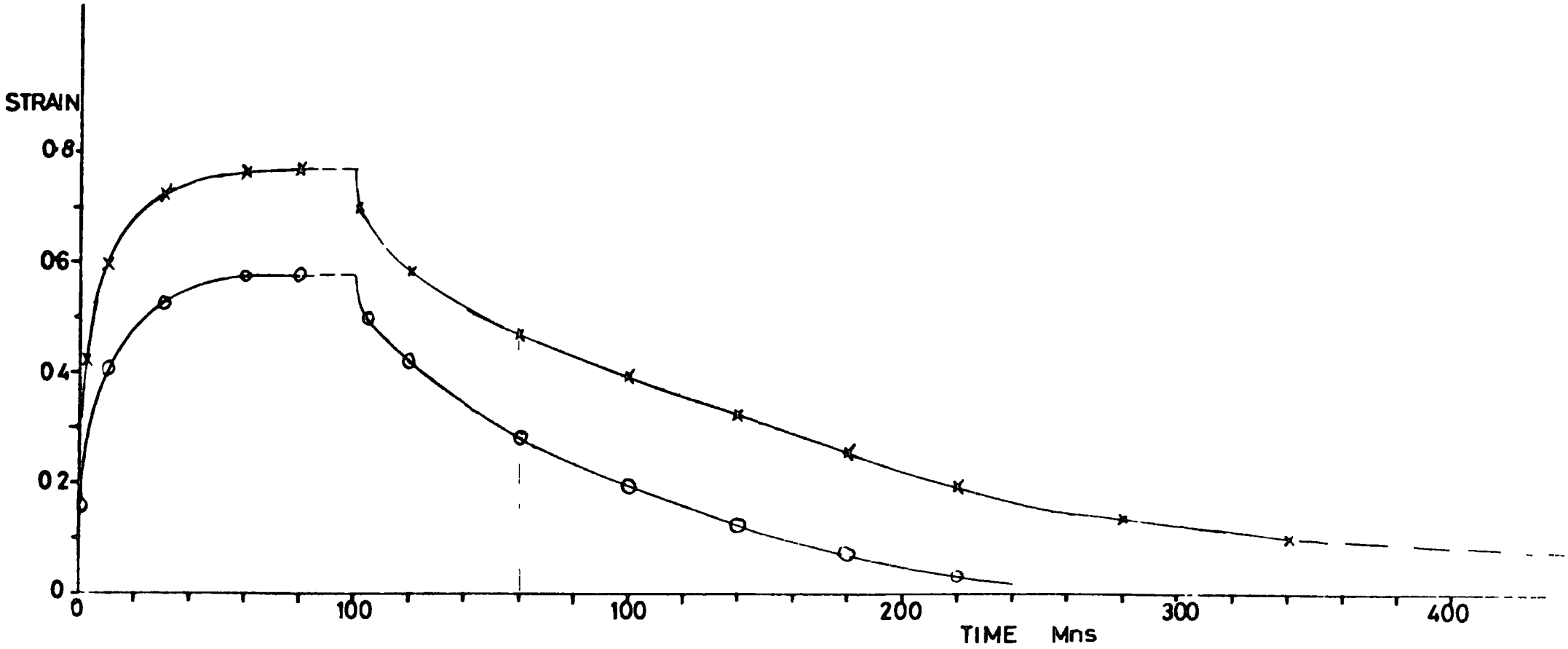

FIG 5·4 STRAIN v TIME BOVINE CARTILAGE UNCONFINED
LOADING ONLY

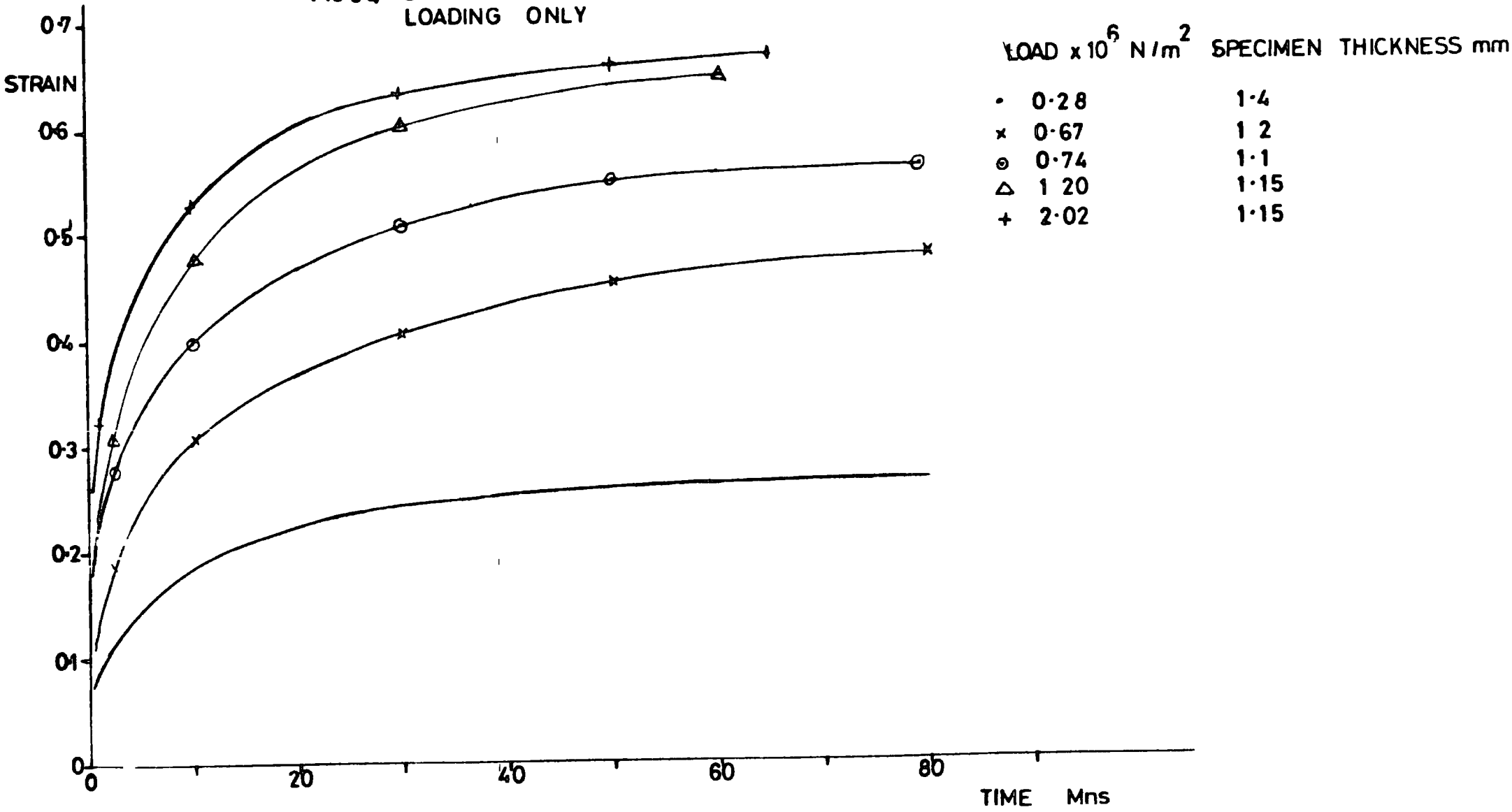

FIG 5-5 STRESS v STRAIN BOVINE CARTILAGE
SELECTED CONFINED TESTS

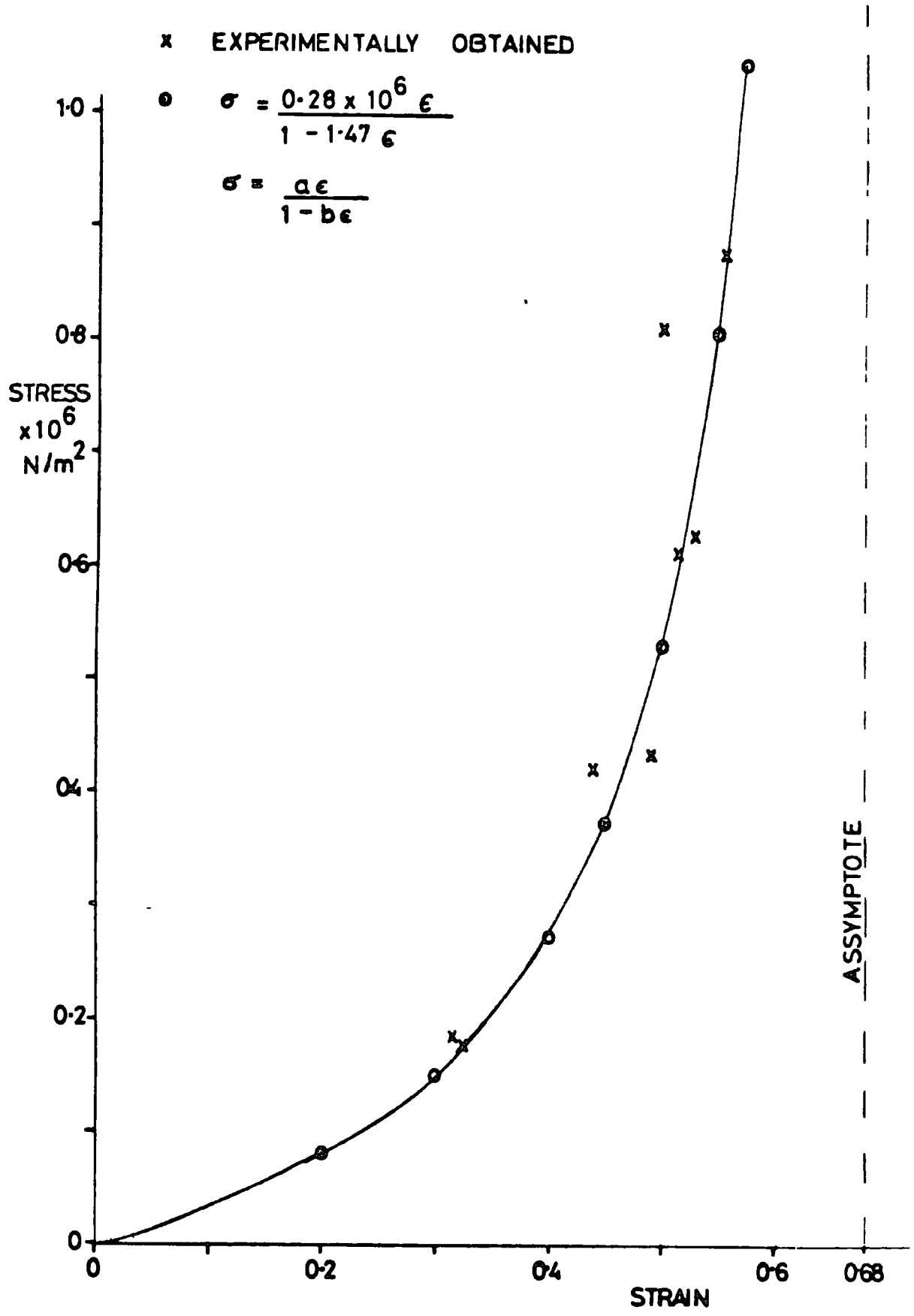

FIG 5·6 STRESS v STRAIN BOVINE CARTILAGE CONFINED

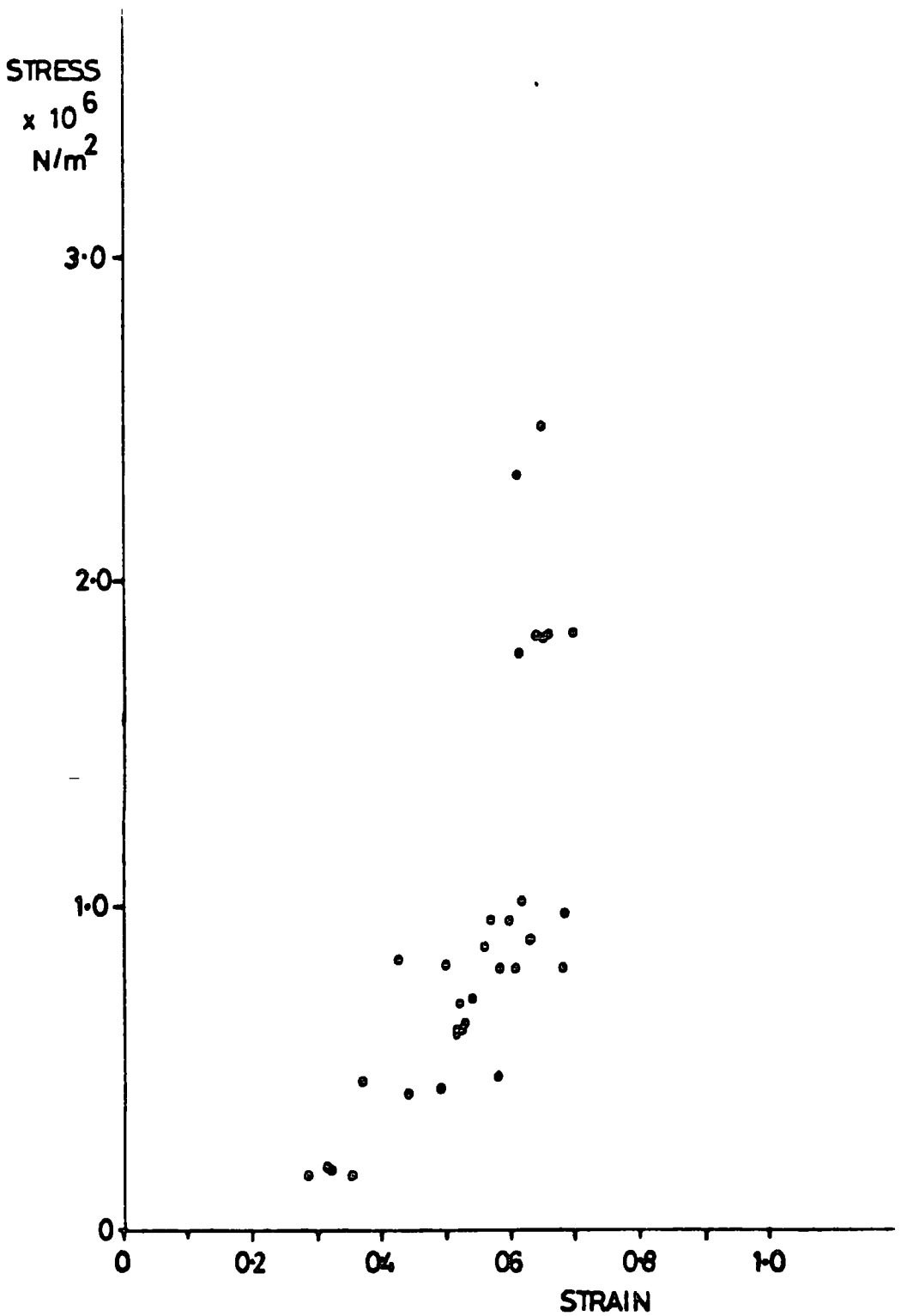

FIG 5·7 STRESS v. STRAIN BOVINE CARTILAGE
UNCONFINED

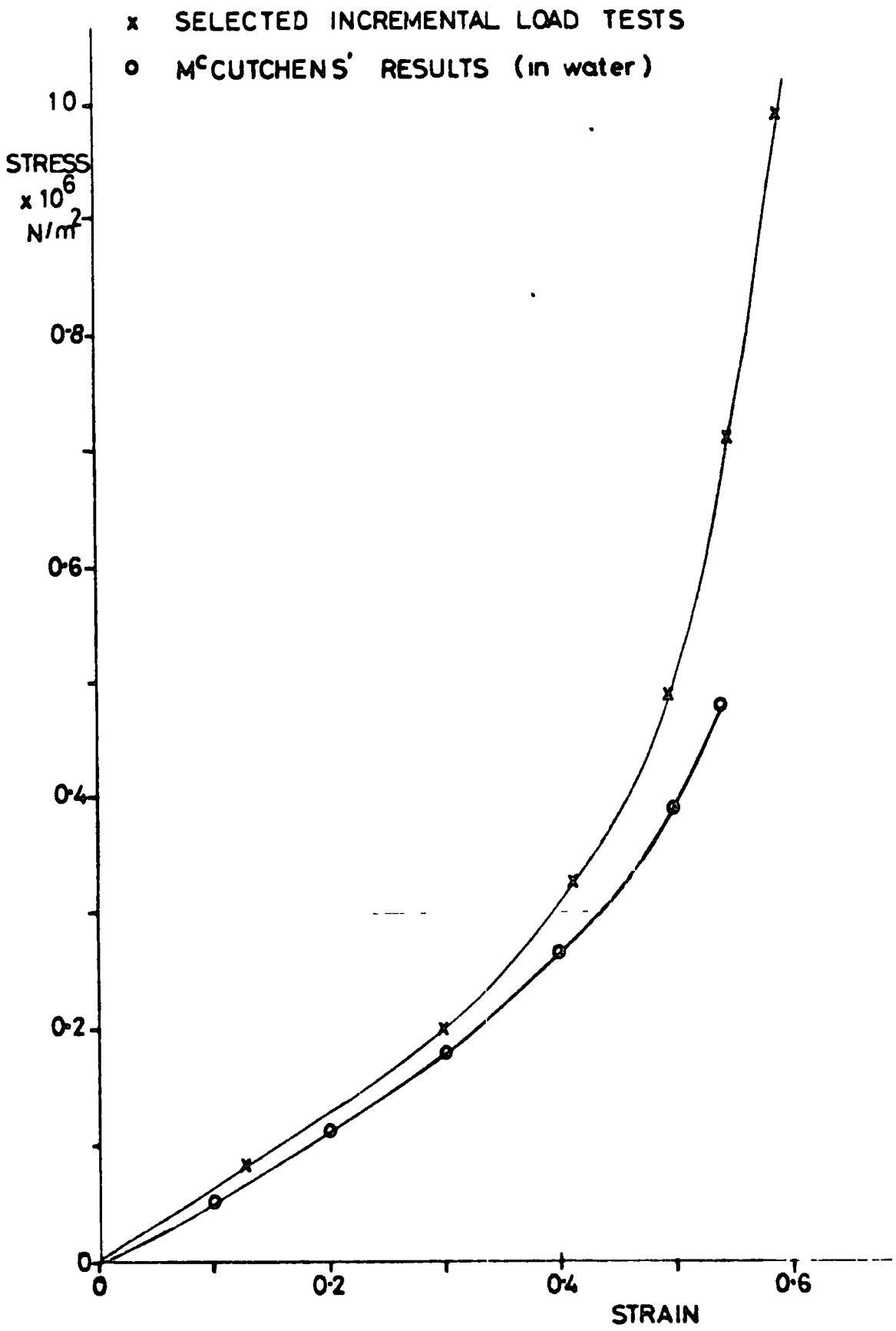

FIG 5-8 STRESS v STRAIN UNCONFINED BOVINE CARTILAGE

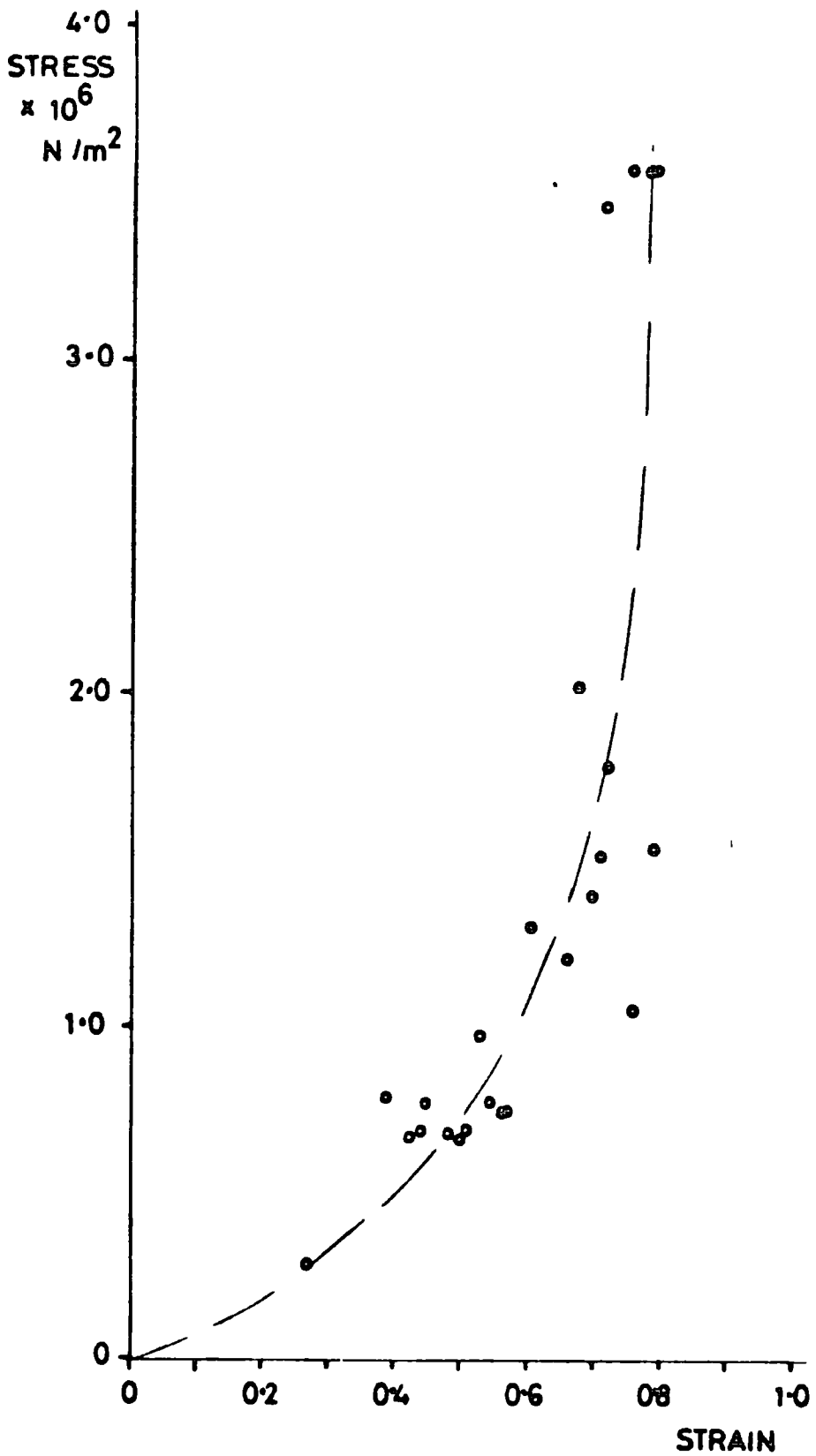

FIG. 5·9 DECREASE IN DIAMETER WITH TIME, UNDER CONSTANT AXIAL STRAIN UNCONFINED

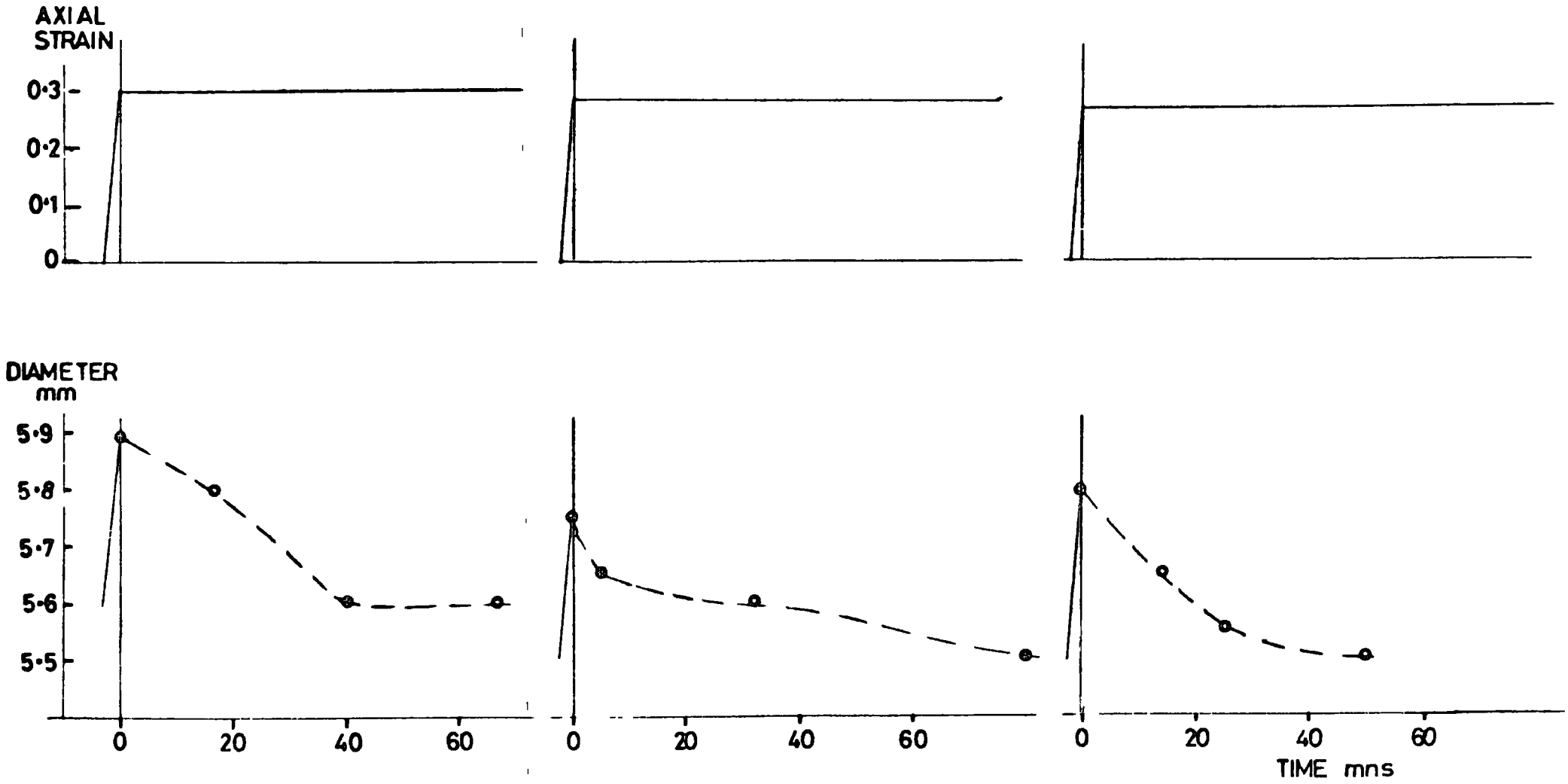

FIG 5·10 STRESS v STRAIN HUMAN CARTILAGE
CONFINED

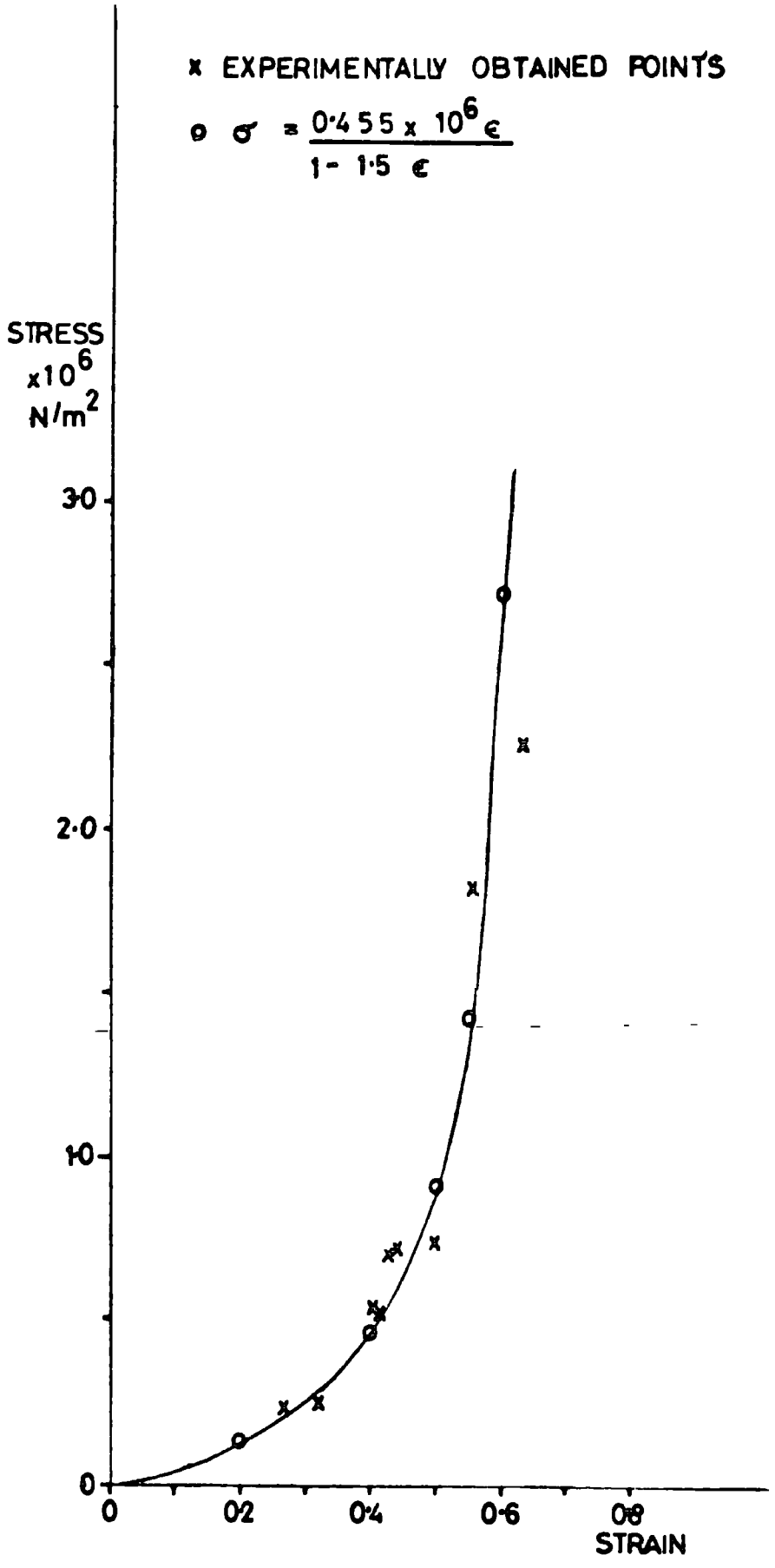

FIG. 5 11 STRESS v STRAIN
STATIC LOAD TESTS
CONFINED

		RELATIONSHIP FOR COMPUTER MODEL
o	DOG TIBIA (EDWARDS')	$\sigma = \frac{1 \cdot 655 \times 10^6 \epsilon}{1 - 1 \cdot 825 \epsilon}$
Δ	HUMAN PATELLA	$\sigma = \frac{0 \cdot 455 \times 10^6 \epsilon}{1 - 1 \cdot 5 \epsilon}$
x	COW FEMUR	$\sigma = \frac{0 \cdot 28 \times 10^6 \epsilon}{1 - 1 \cdot 47 \epsilon}$

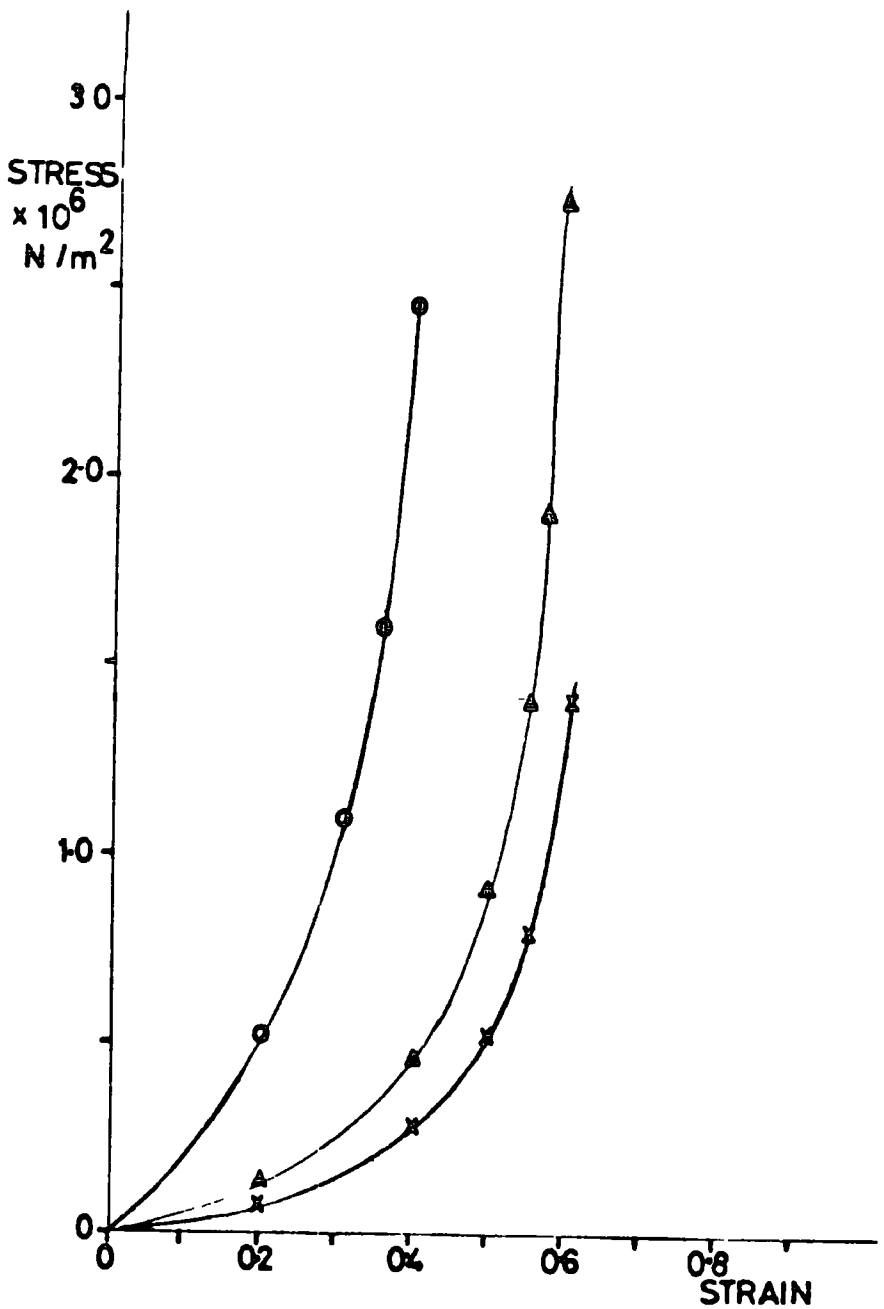

FIG. 5-12 RIG DEFLECTION CHARACTERISTICS

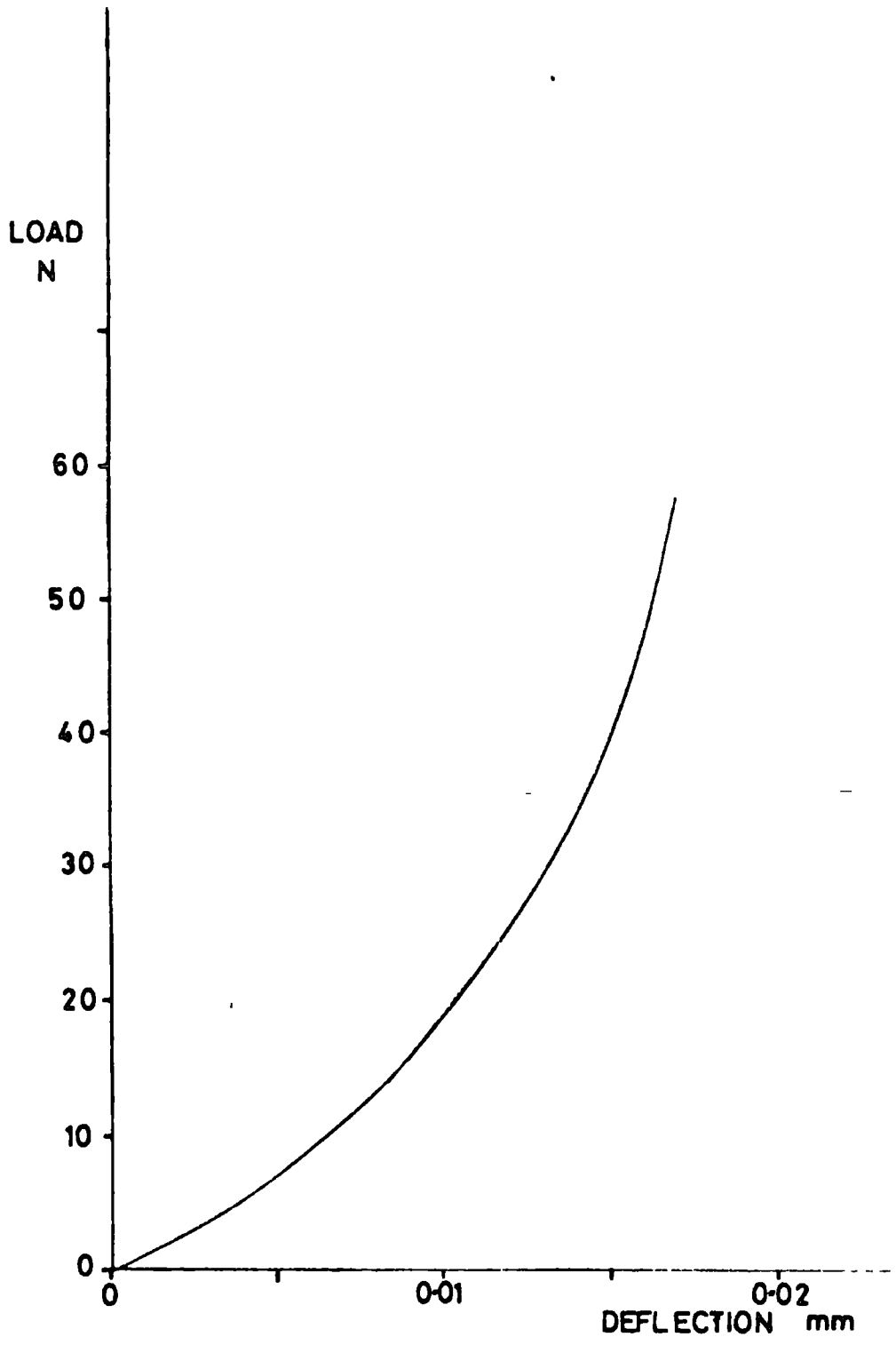

FIG 5·13 HYSTERESIS LOOPS CONFINED TESTS

A BOVINE
STRESS AMP 1.23 MN/m^2
STRAIN AMP 0.0083
PHASE 5°

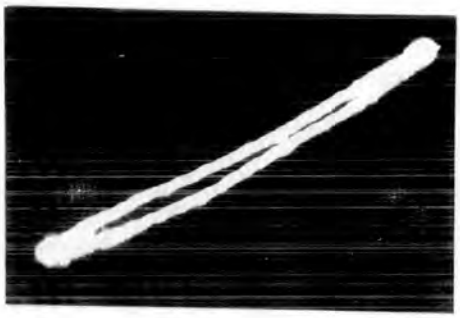

B BOVINE
STRESS AMP 0.66 MN/m^2
STRAIN AMP 0.0071
PHASE 9°

C HUMAN
STRESS AMP 0.16 MN/m^2
STRAIN AMP 0.0013
PHASE 0°

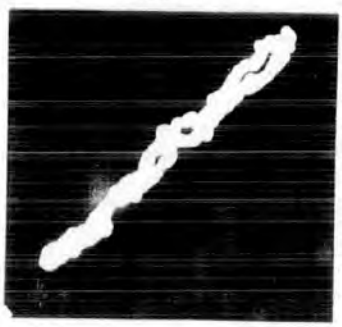

D HUMAN
STRESS AMP 0.14 MN/m^2
STRAIN AMP 0.0023
PHASE 7°

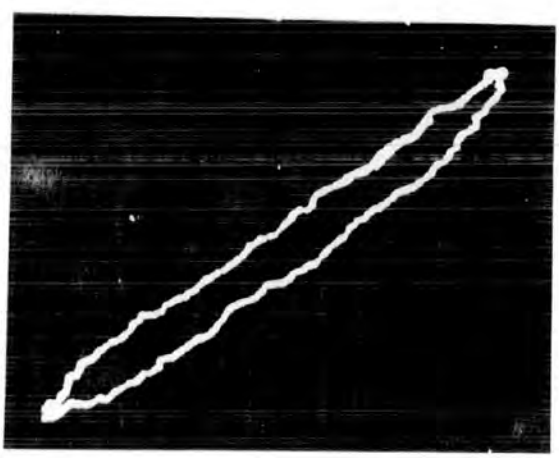

E RUBBER
STRESS AMP 0.54 MN/m^2
STRAIN AMP 0.0106
PHASE 15°

FIG 5.14 ELASTIC MODULUS v CREEP STRAIN
CONFINED TESTS BOVINE CARTILAGE
FREQUENCY 0·83 Hz.

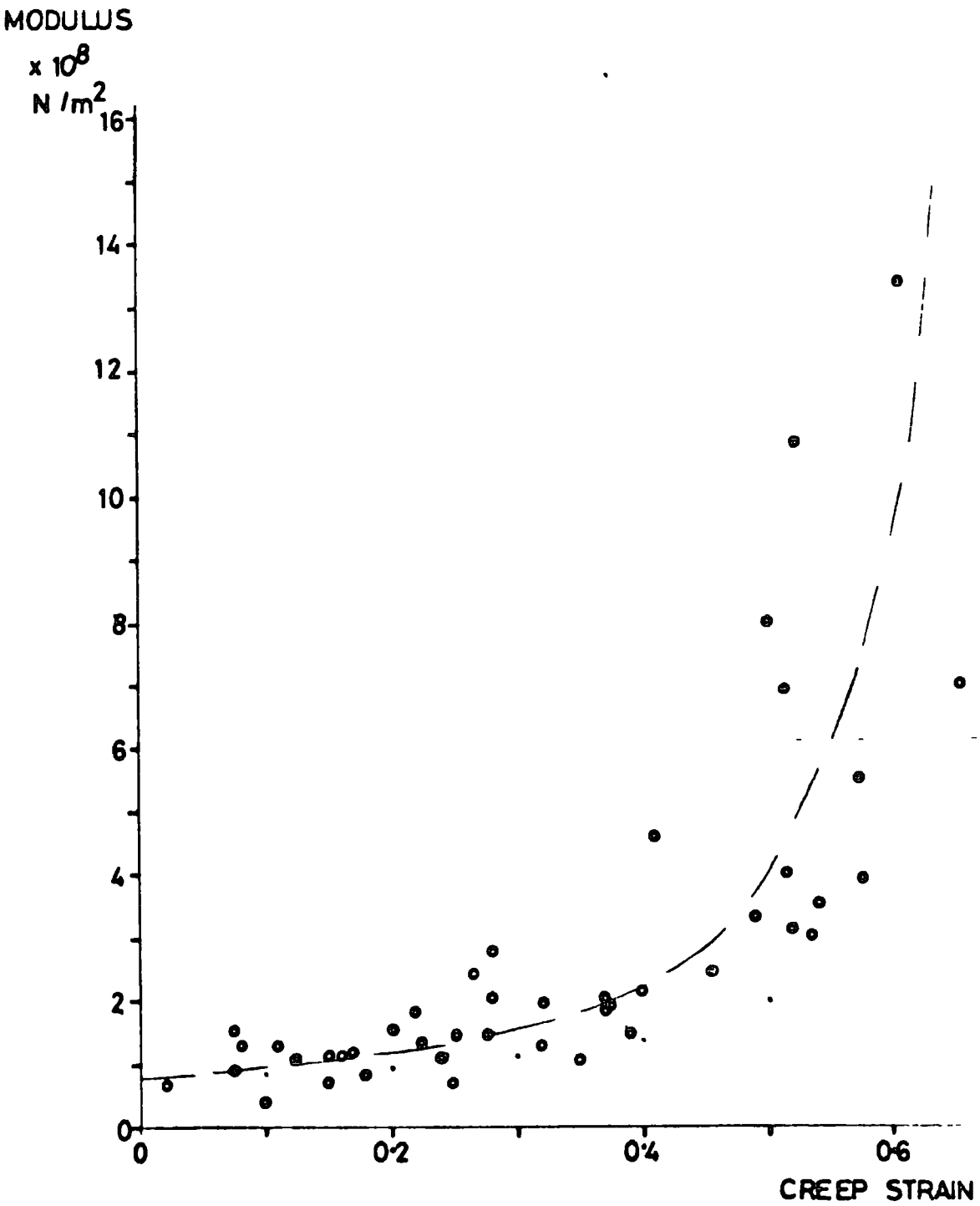

FIG 5·15 ELASTIC MODULUS v CREEP STRAIN
CONFINED TESTS HUMAN CARTILAGE
FREQUENCY 0·83 Hz

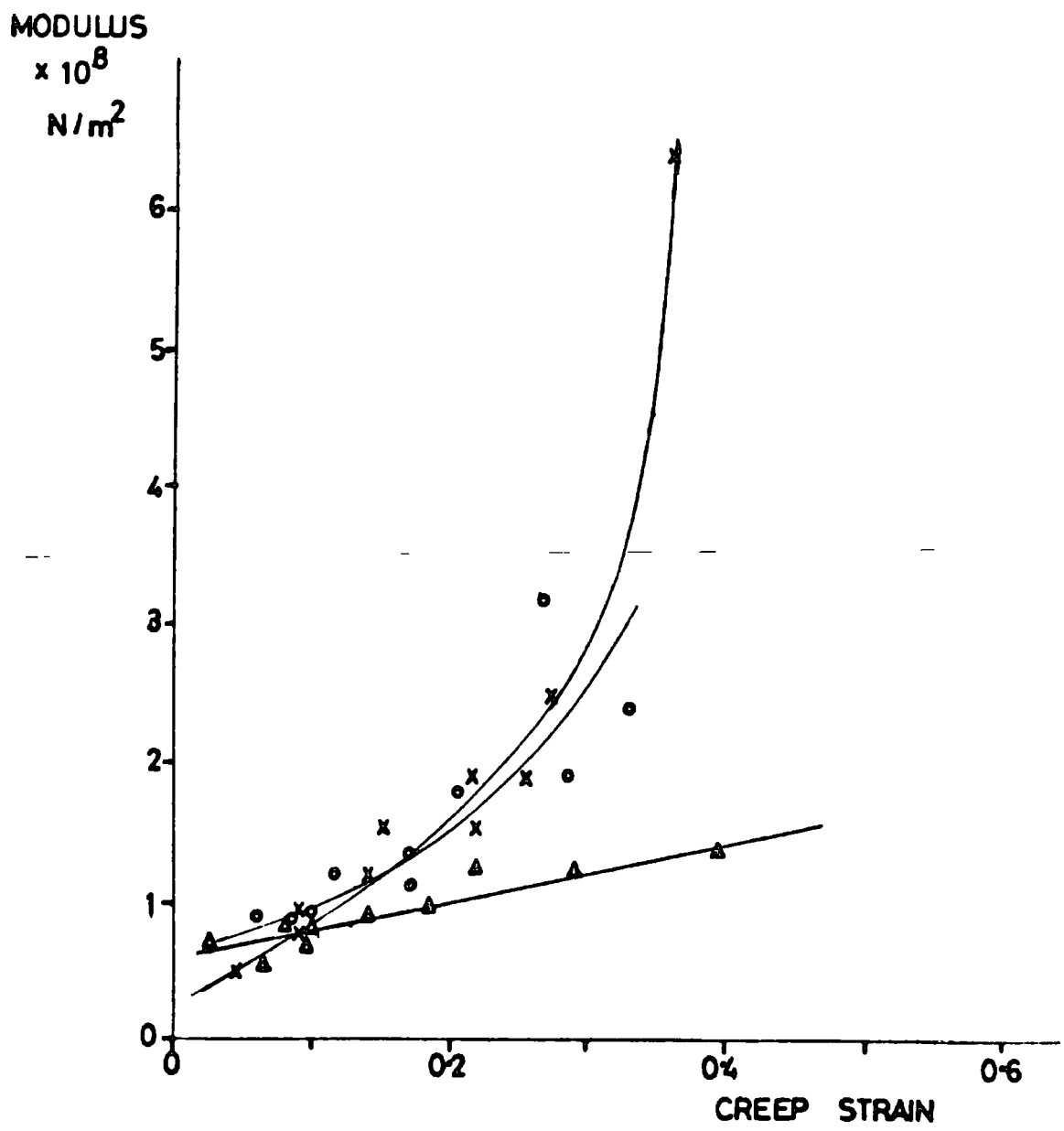

FIG 5·16 HYSTERESIS LOOPS UNCONFINED TESTS

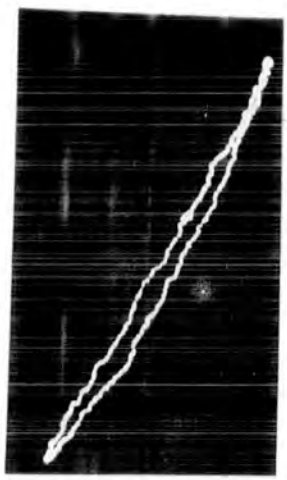

A BOVINE
STRESS AMP 0.64 MN/m^2
STRAIN AMP 0.0024
PHASE 6^o

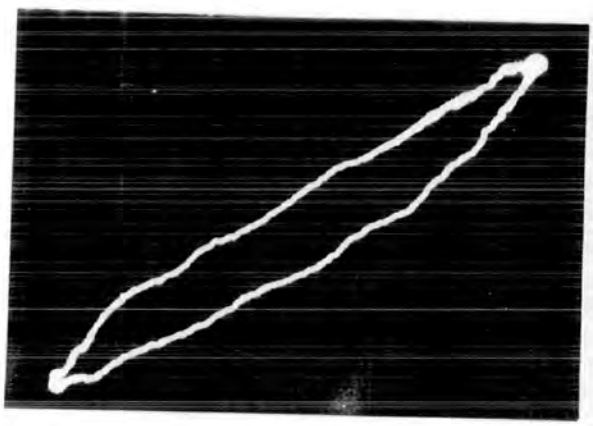

B BOVINE
STRESS AMP 0.43 MN/m^2
STRAIN AMP 0.0093
PHASE 21^o

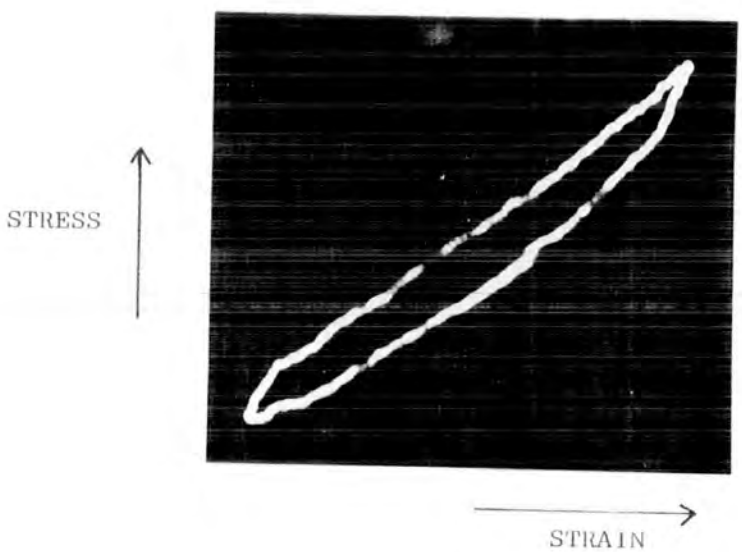

C RUBBER
STRESS AMP 0.57 MN/m^2
STRAIN AMP 0.0324
PHASE 17^o

FIG 5·17 ELASTIC MODULUS v. CREEP STRAIN
UNCONFINED TESTS BOVINE CARTILAGE
FREQUENCY 0·83 Hz.

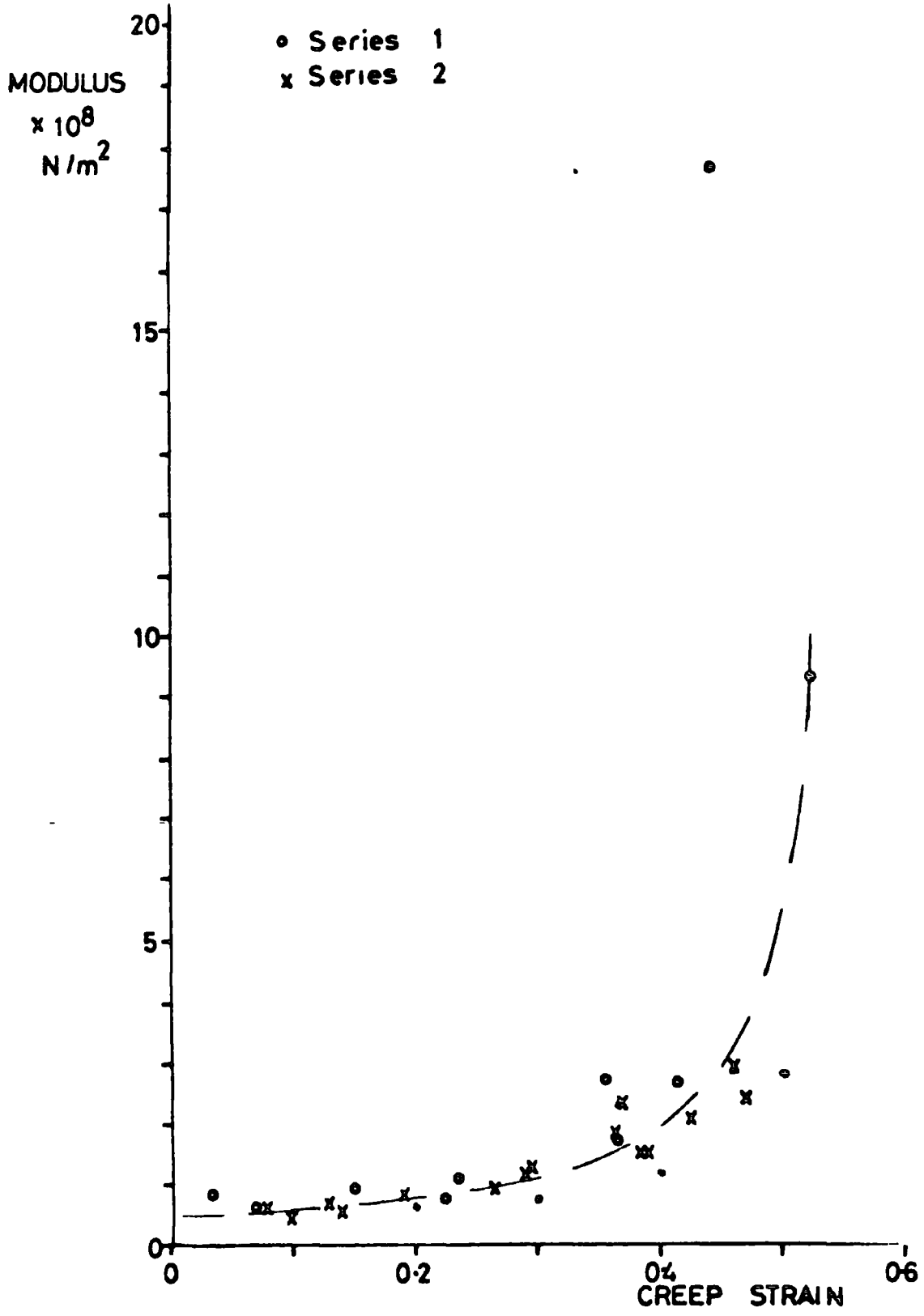

FIG 518 EFFECT OF LOADING FREQUENCY ON CARTILAGE STIFFNESS
ELASTIC MODULUS v CREEP STRAIN

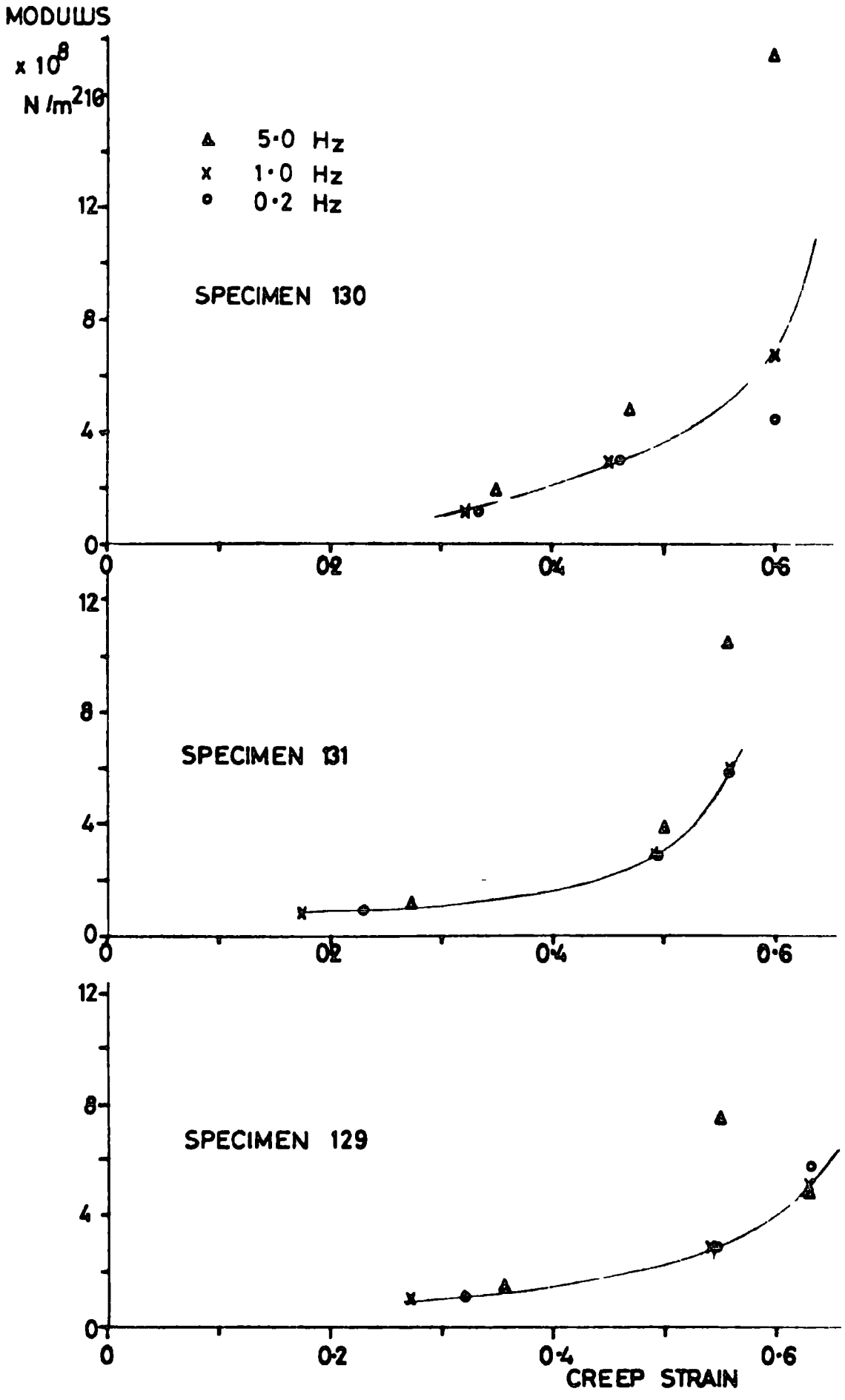

FIG 5·19 EFFECT OF LOADING FREQUENCY ON CARTILAGE STIFFNESS

ELASTIC MODULUS v CREEP STRAIN

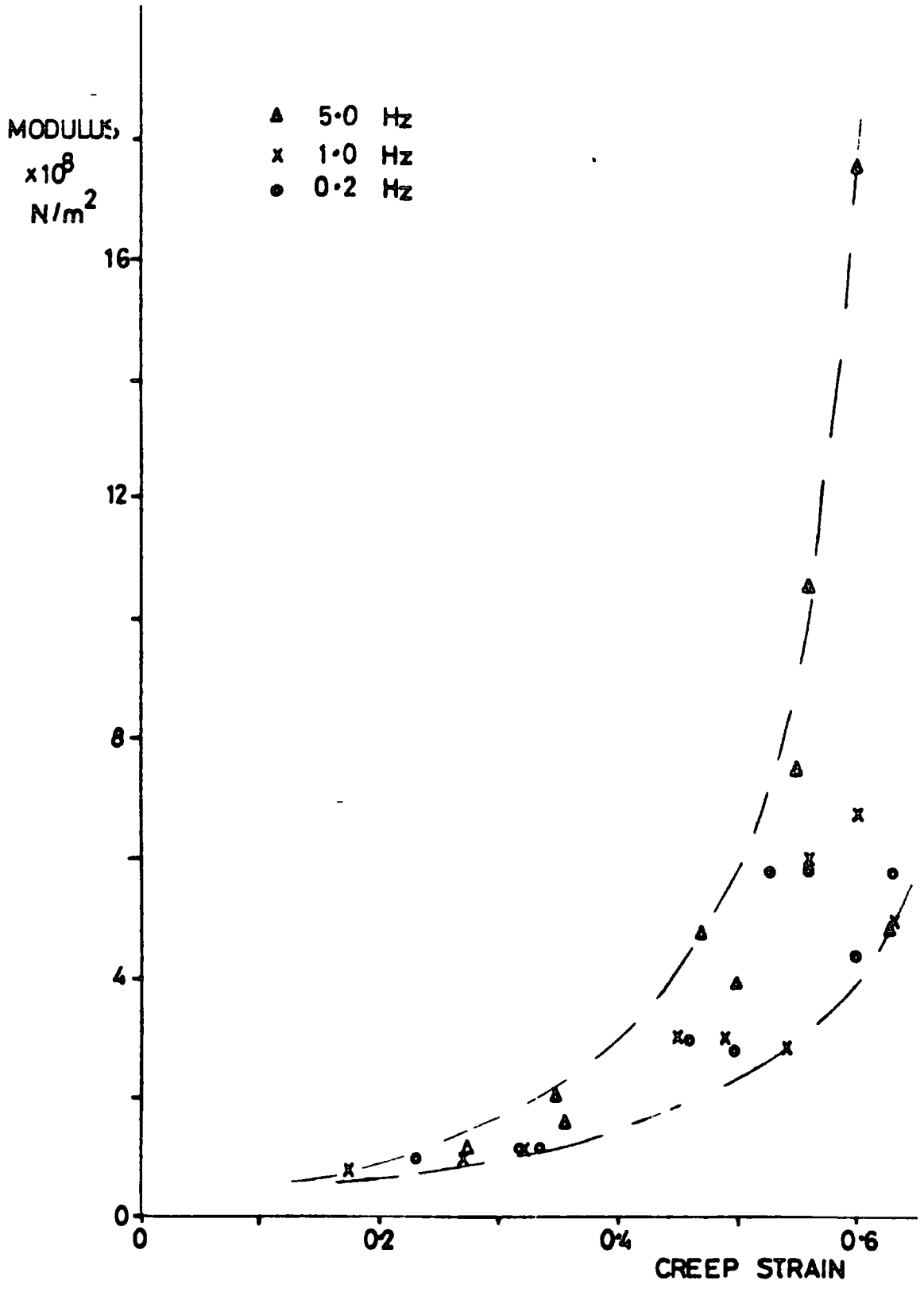

FIG 5·20 EFFECT OF MODIFYING THE COMPUTER MODEL

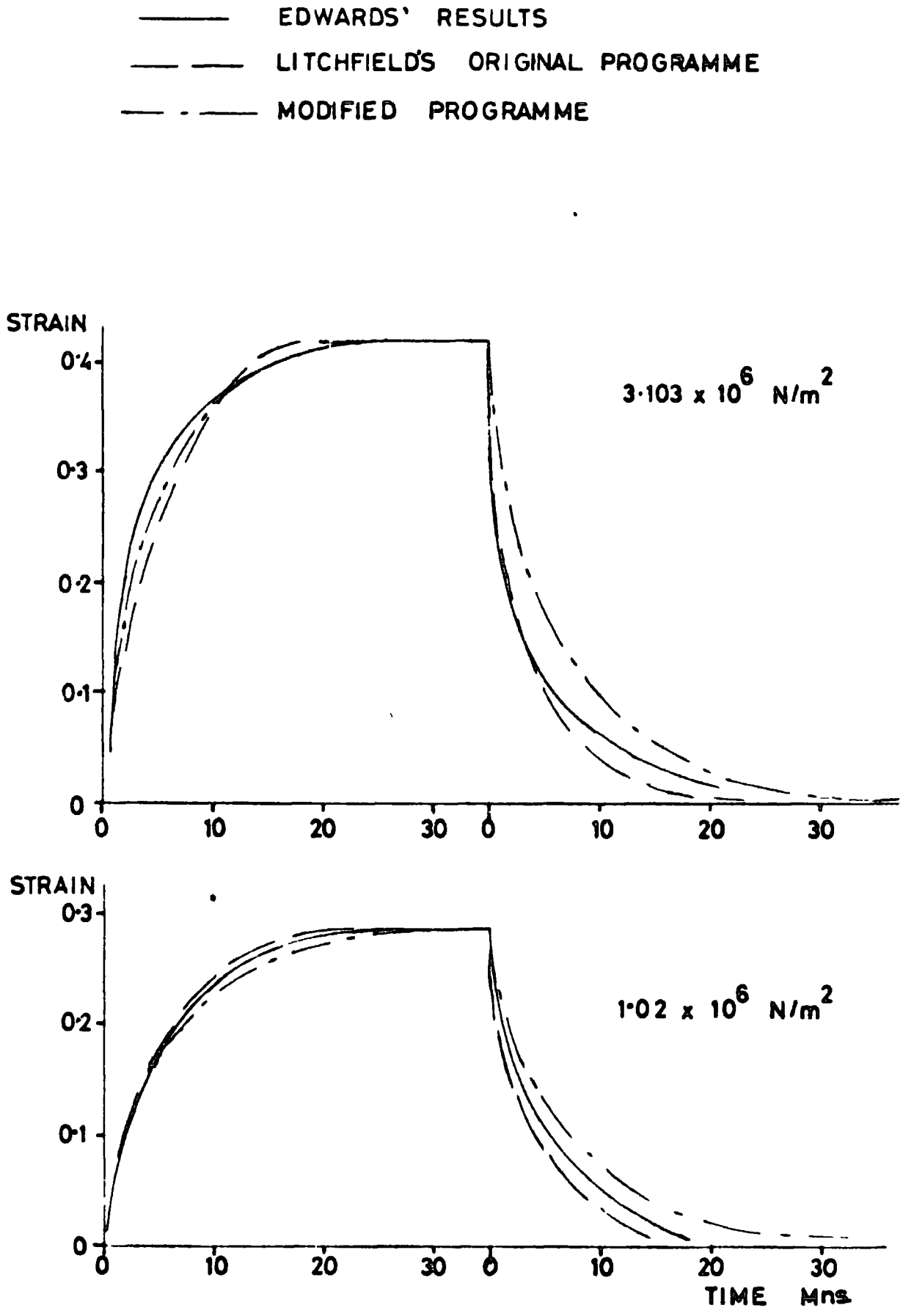

FIG. 5·21 EFFECT OF POROSITY ON COMPUTED STRAIN

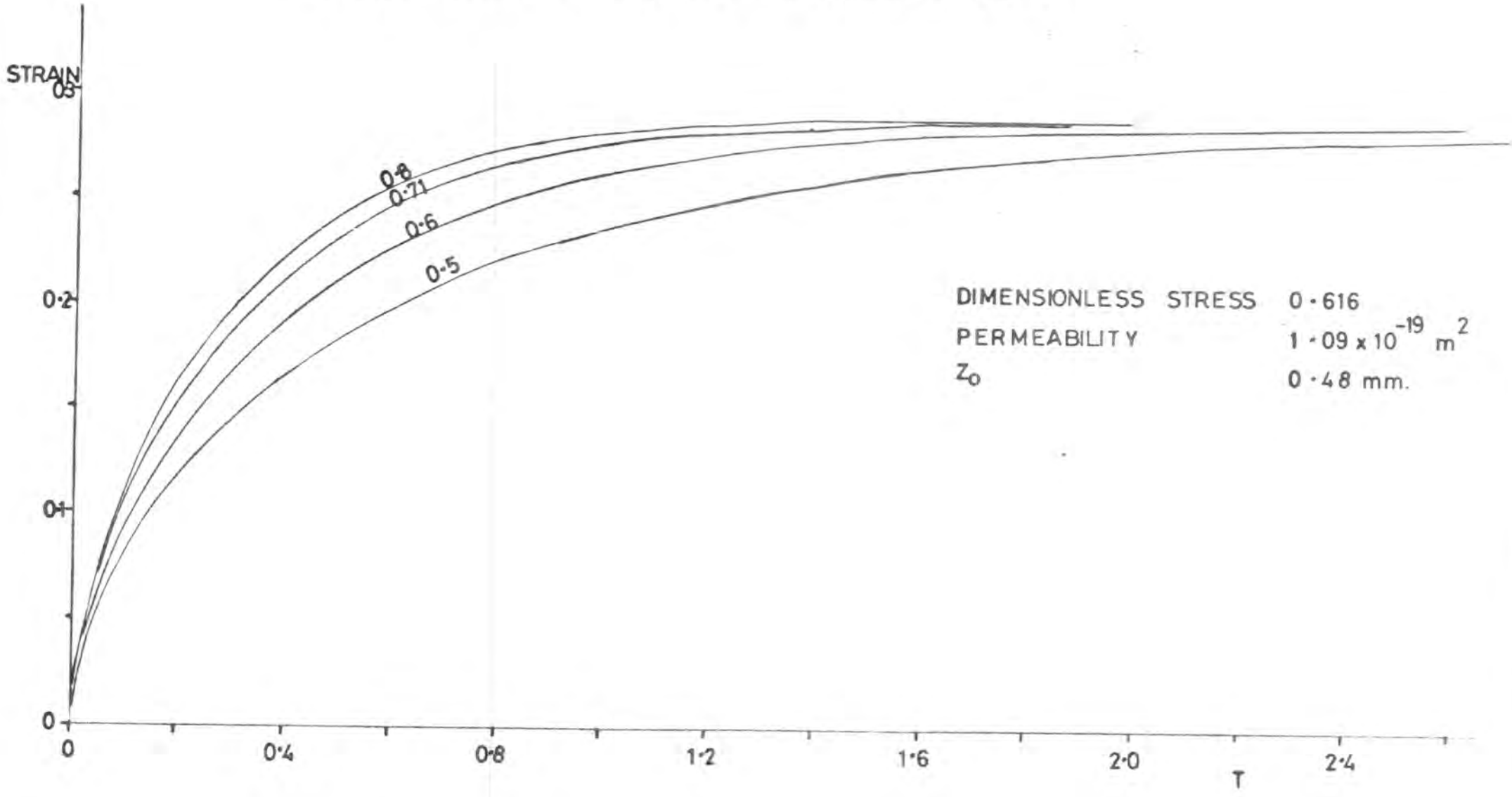

FIG 5·22 EFFECT OF THE RELATIONSHIP BETWEEN PERMEABILITY AND STRAIN ON COMPUTED STRAIN

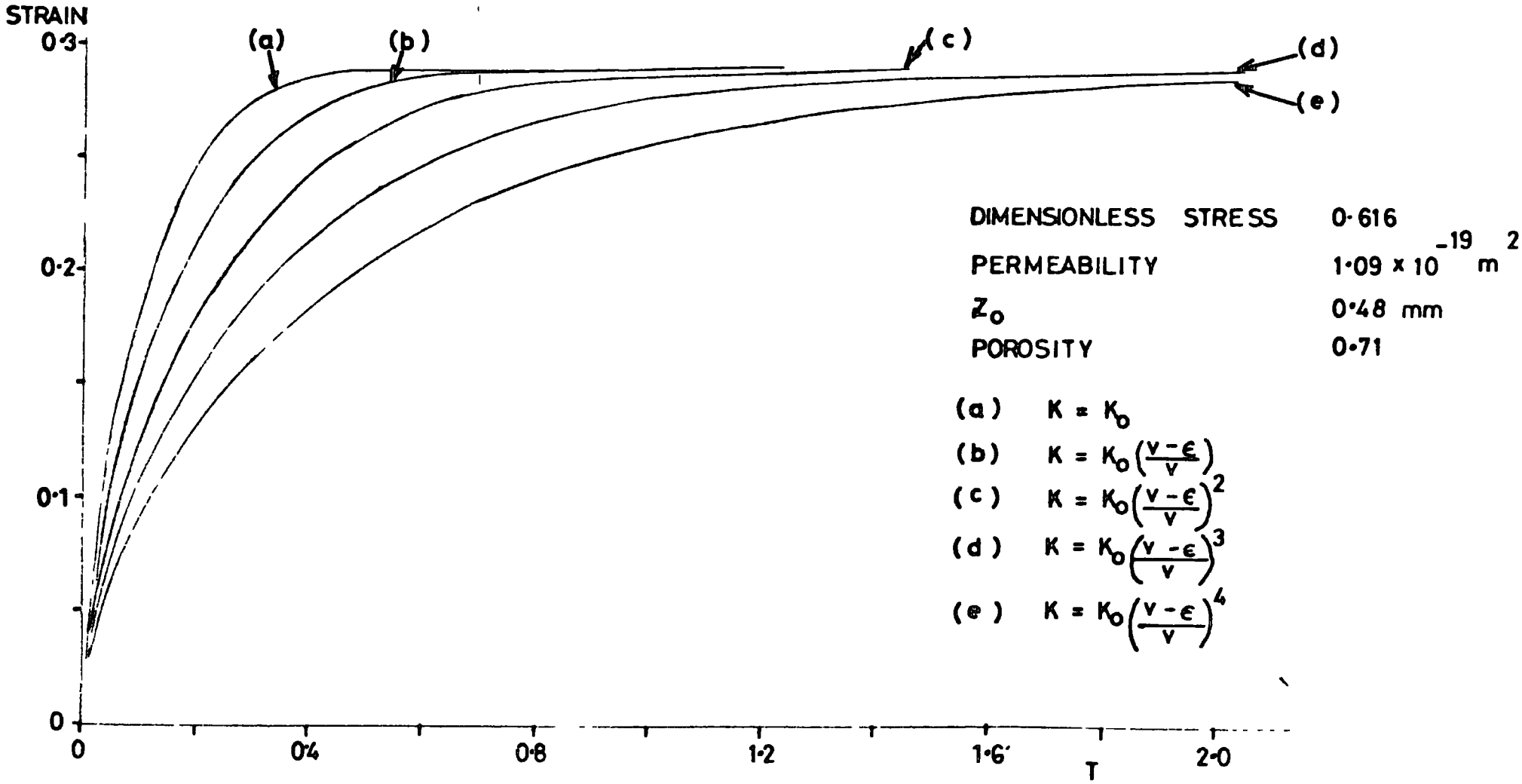

FIG 5 23 PERMEABILITY AGAINST DEPTH FROM SURFACE
MAROUDAS (1973)

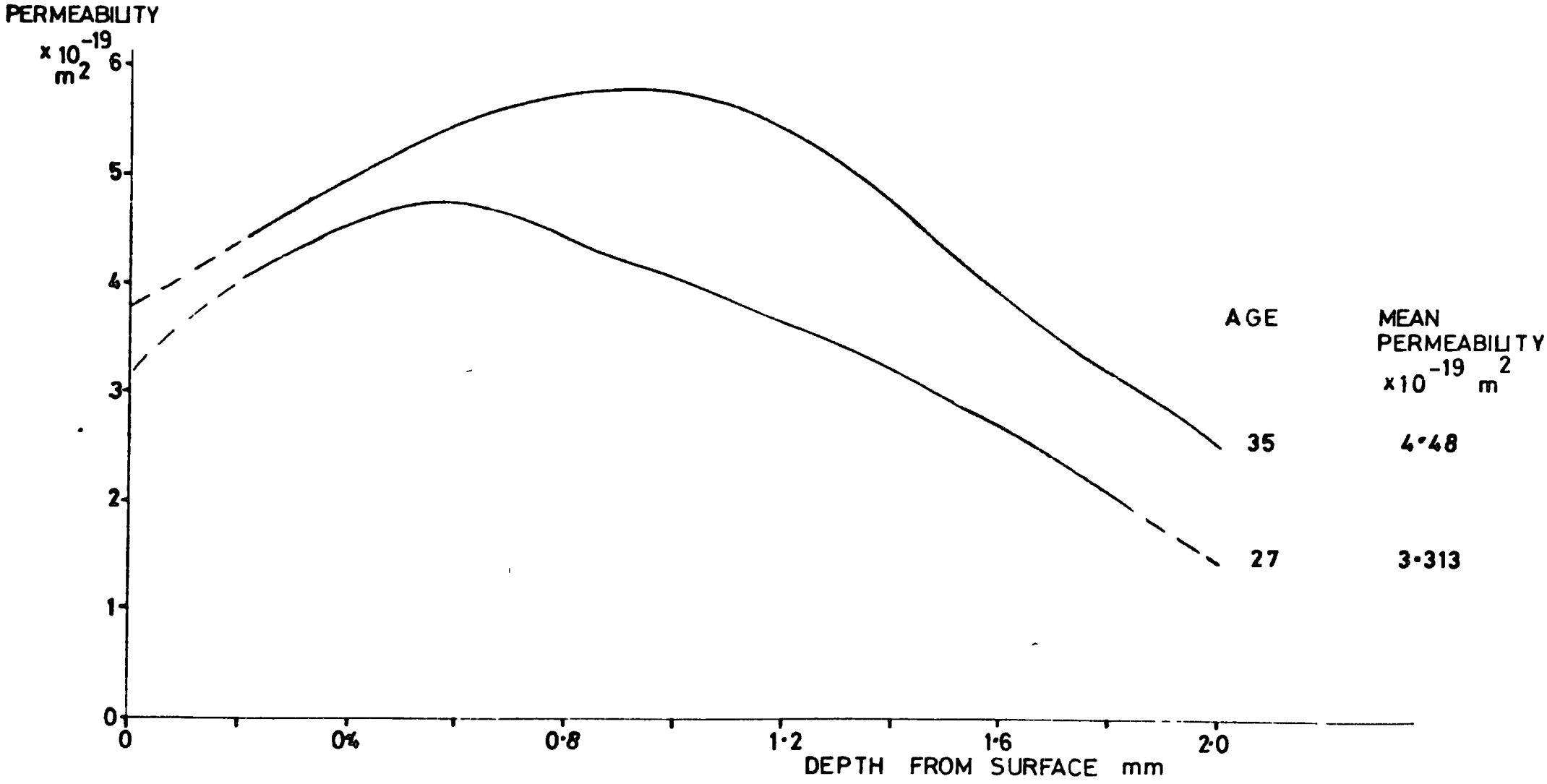

FIG 5·24 EFFECT OF VARIATION OF PERMEABILITY THROUGH THE DEPTH ON COMPUTED STRAIN

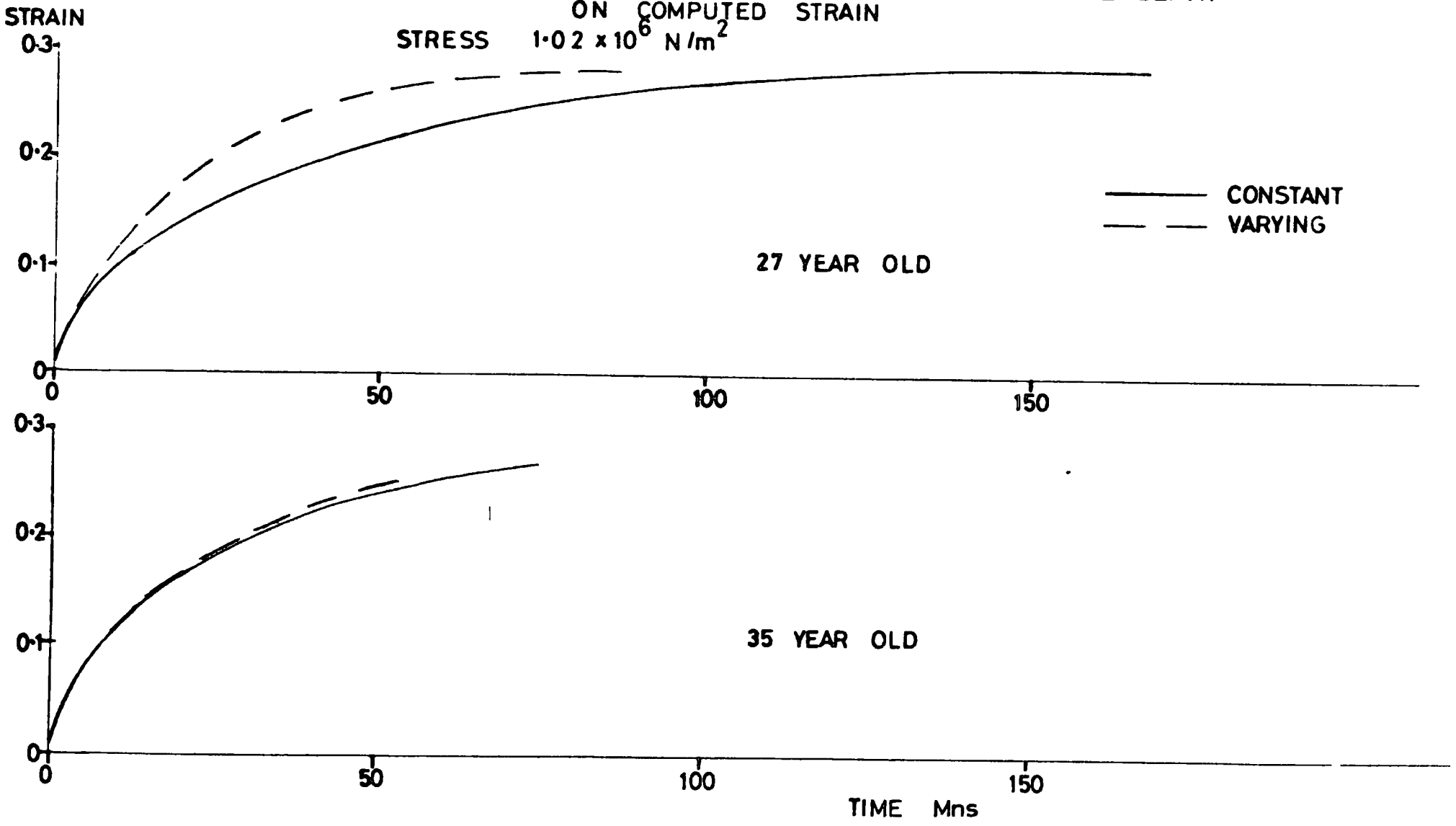

FIG 5·25 PROPOSED DISTRIBUTION OF PERMEABILITY THROUGH THE DEPTH

$$K = (C + 20X - 20X^2) \times 10^{-19}$$

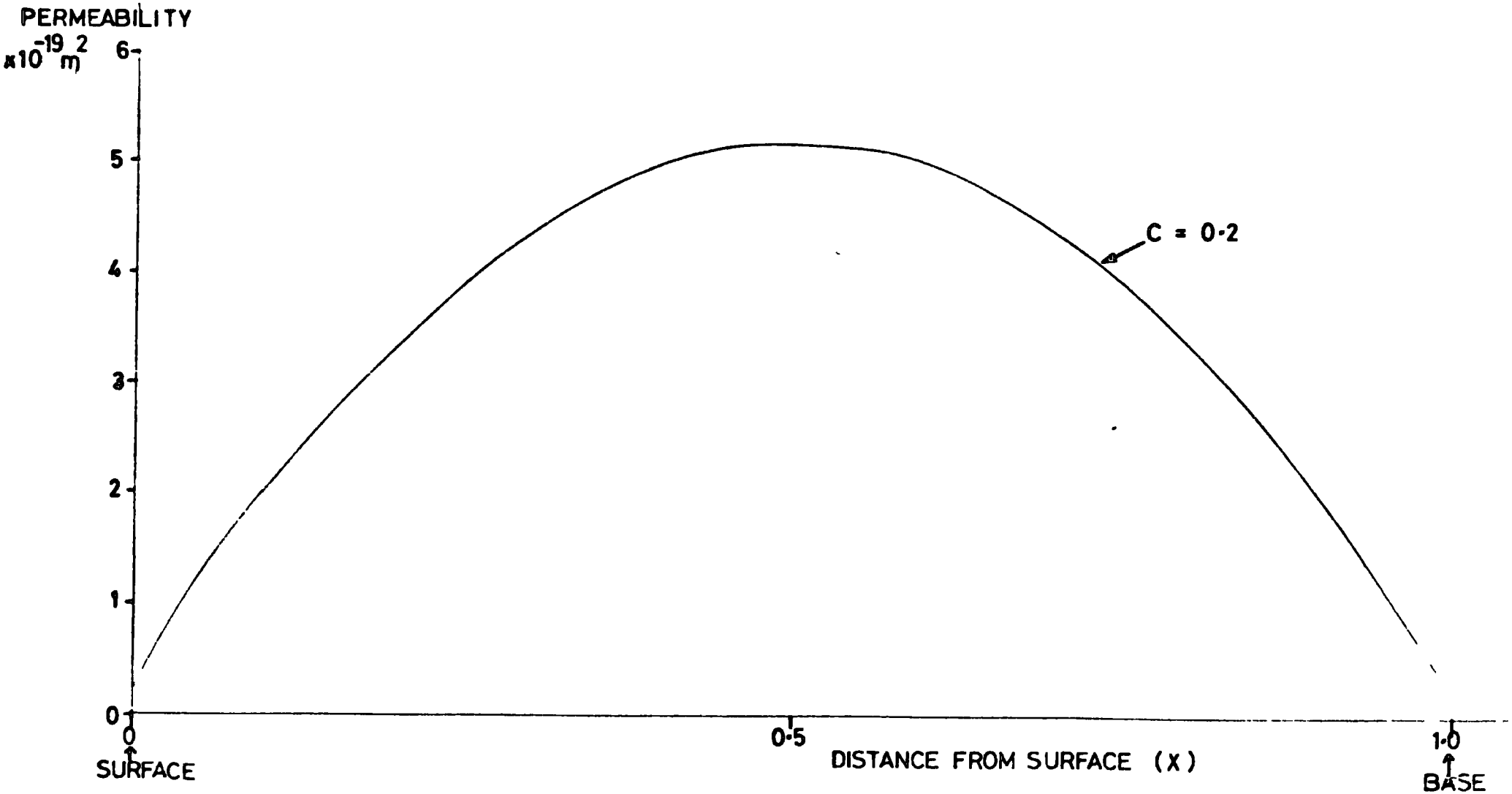

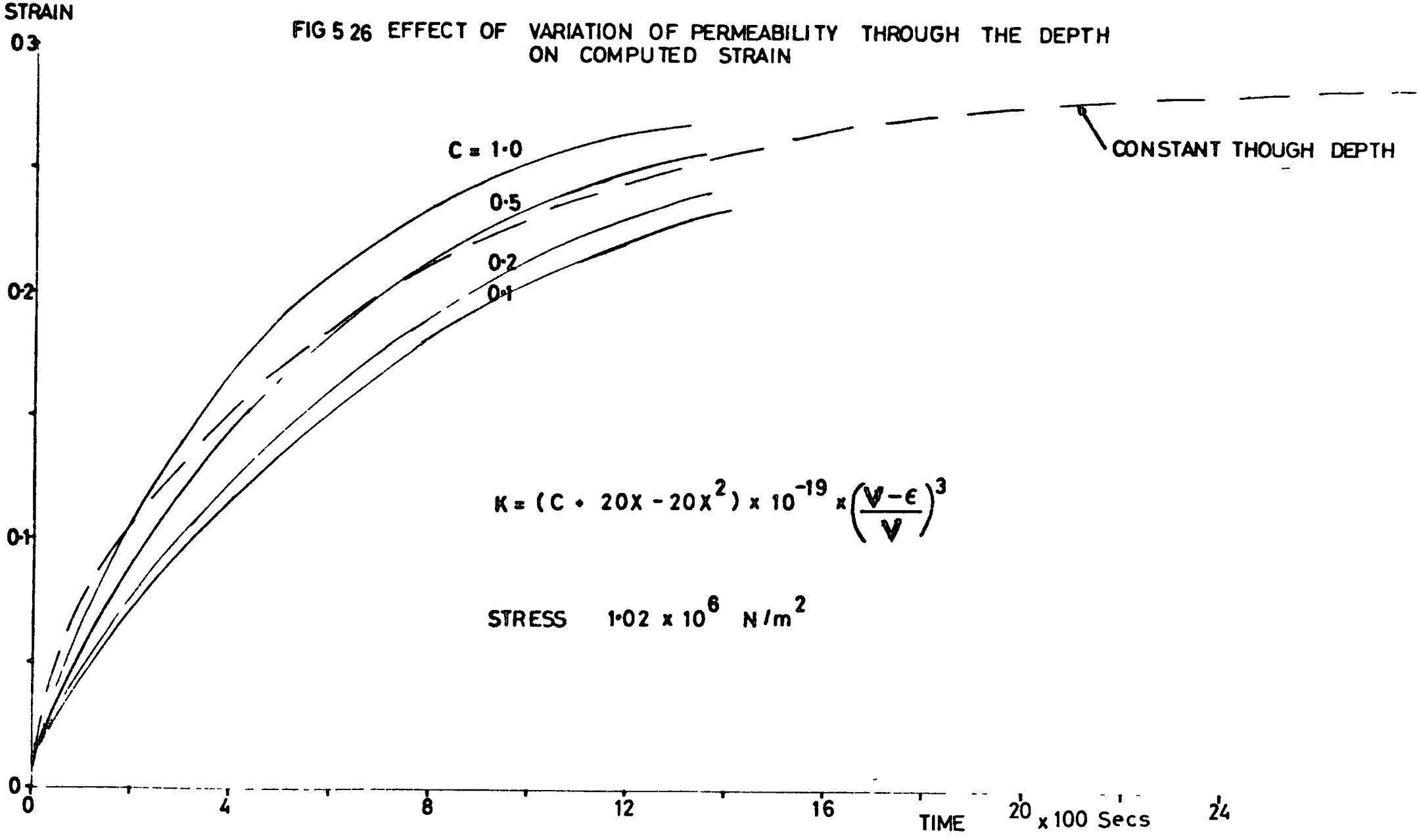

FIG 5 26 EFFECT OF VARIATION OF PERMEABILITY THROUGH THE DEPTH ON COMPUTED STRAIN

FIG 5·27 EFFECT OF SURFACE FLUID PRESSURE ON COMPUTED STRAIN

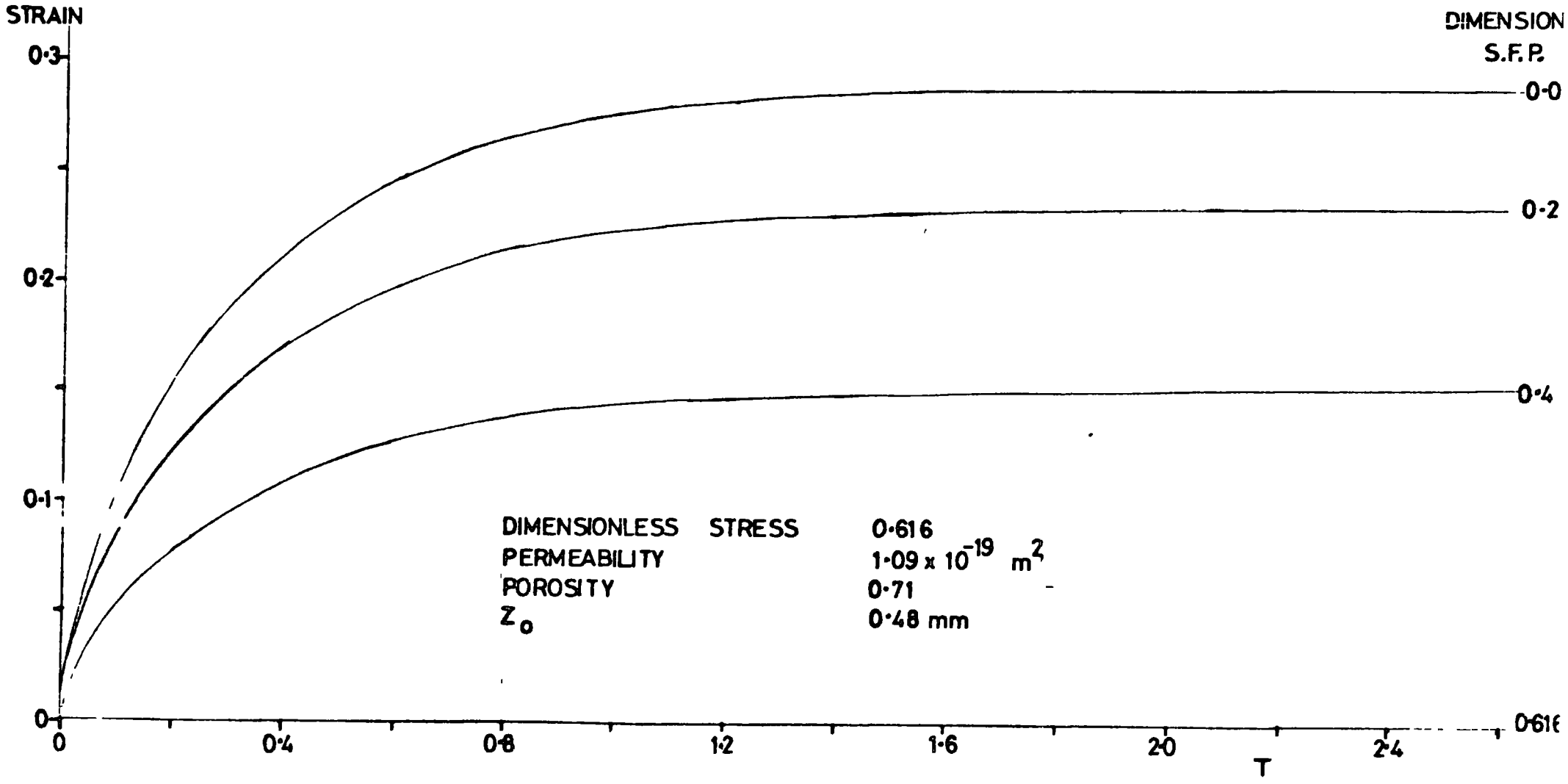

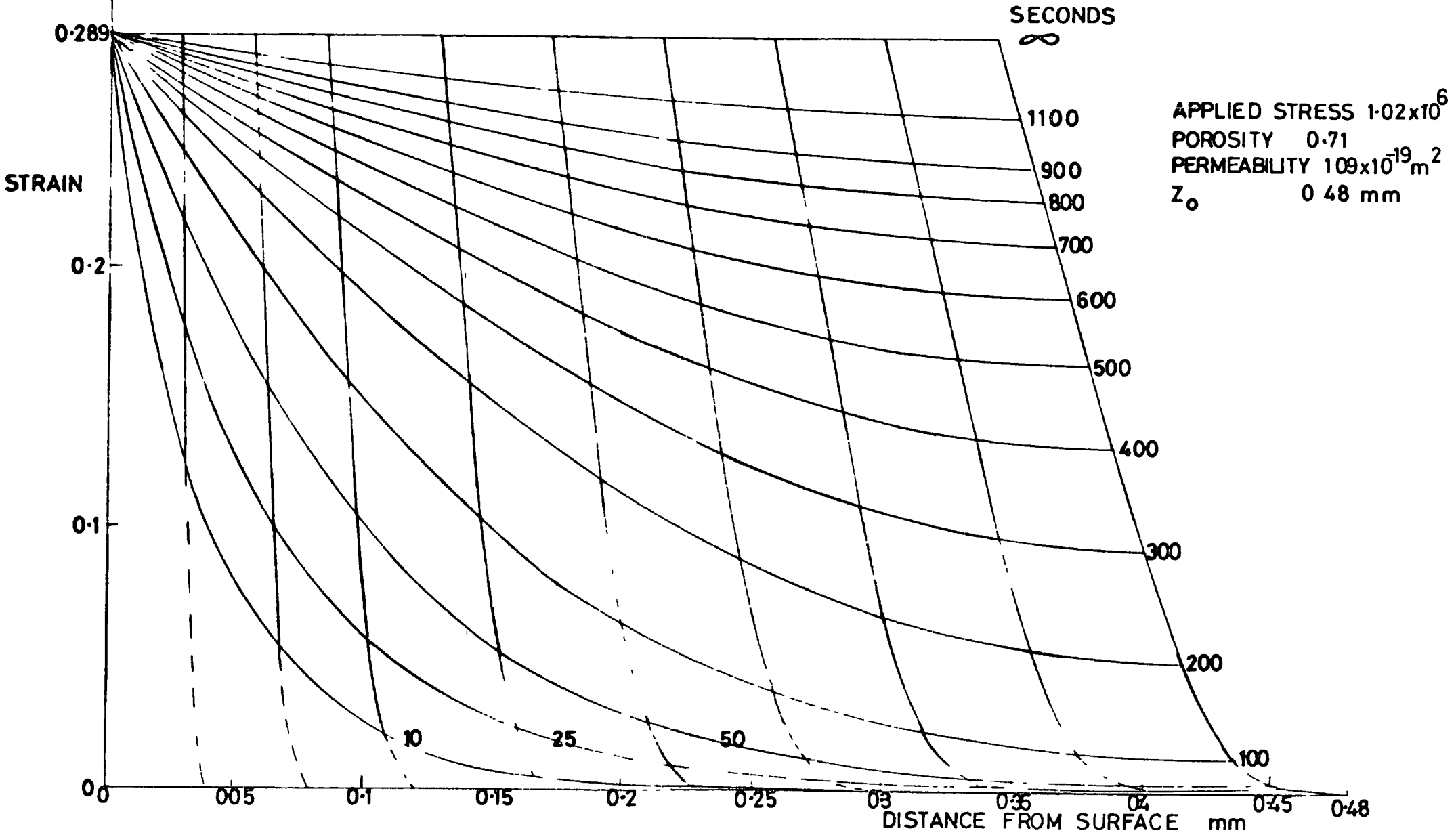

FIG.5·28 VARIATION OF STRAIN THROUGH THE DEPTH WITH TIME (UNDER LOAD)

FIG 5·29 VARIATION OF FLUID PRESSURE THROUGH THE DEPTH WITH TIME (UNDER LOAD)

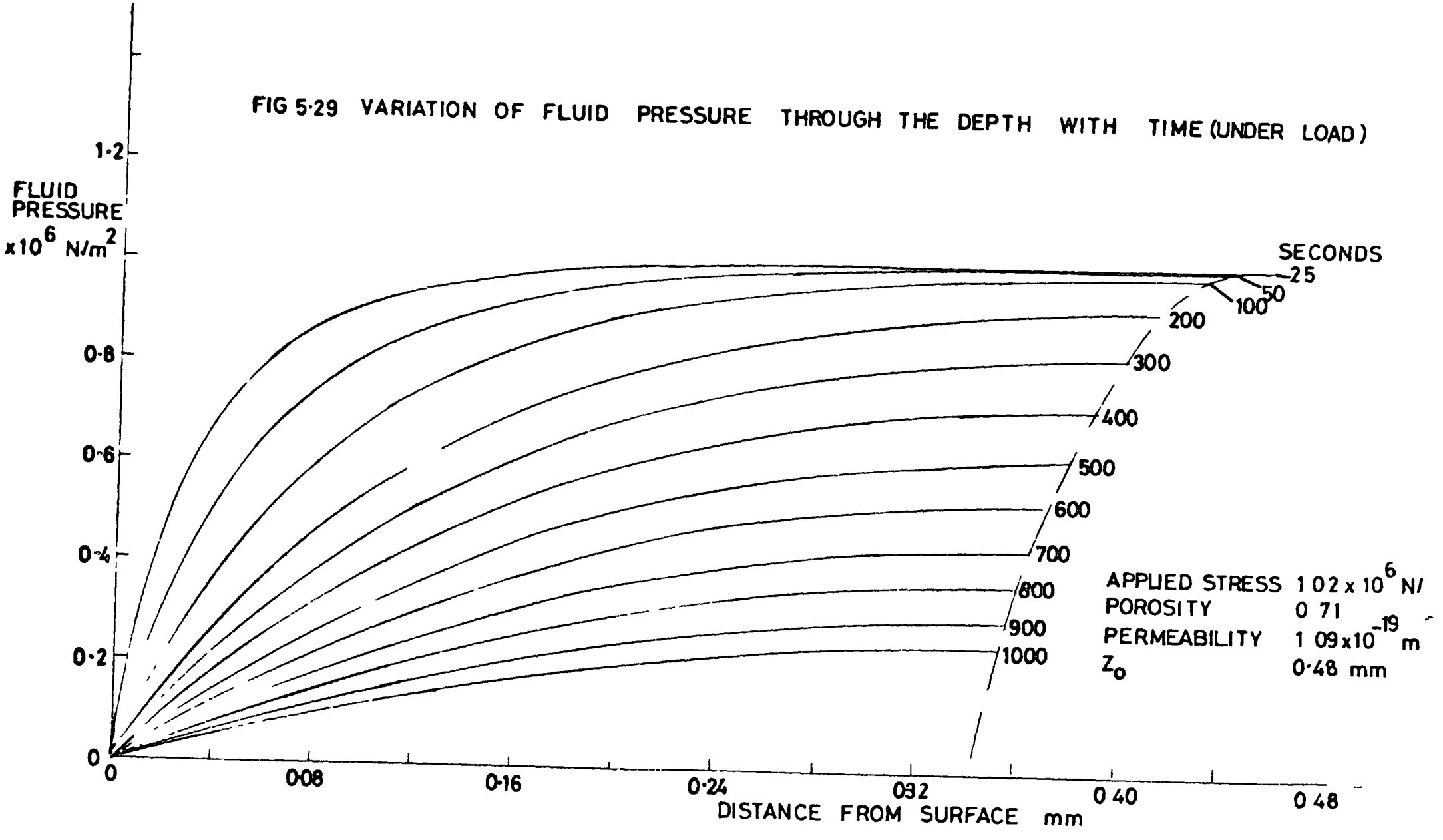

FIG 5·30 COMPARISON WITH MODEL

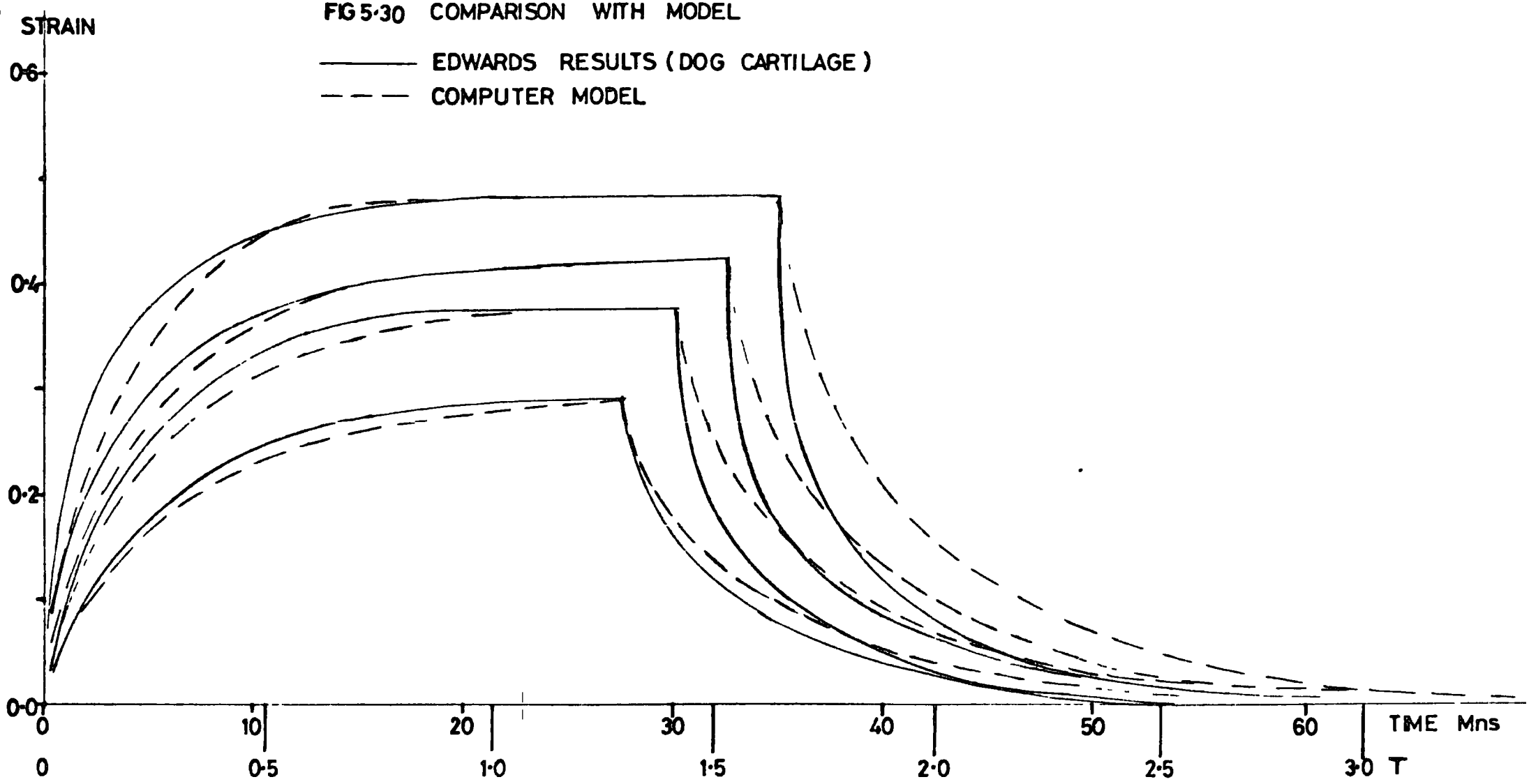

FIG 5·31 COMPARISON WITH MODEL
BOVINE CARTILAGE

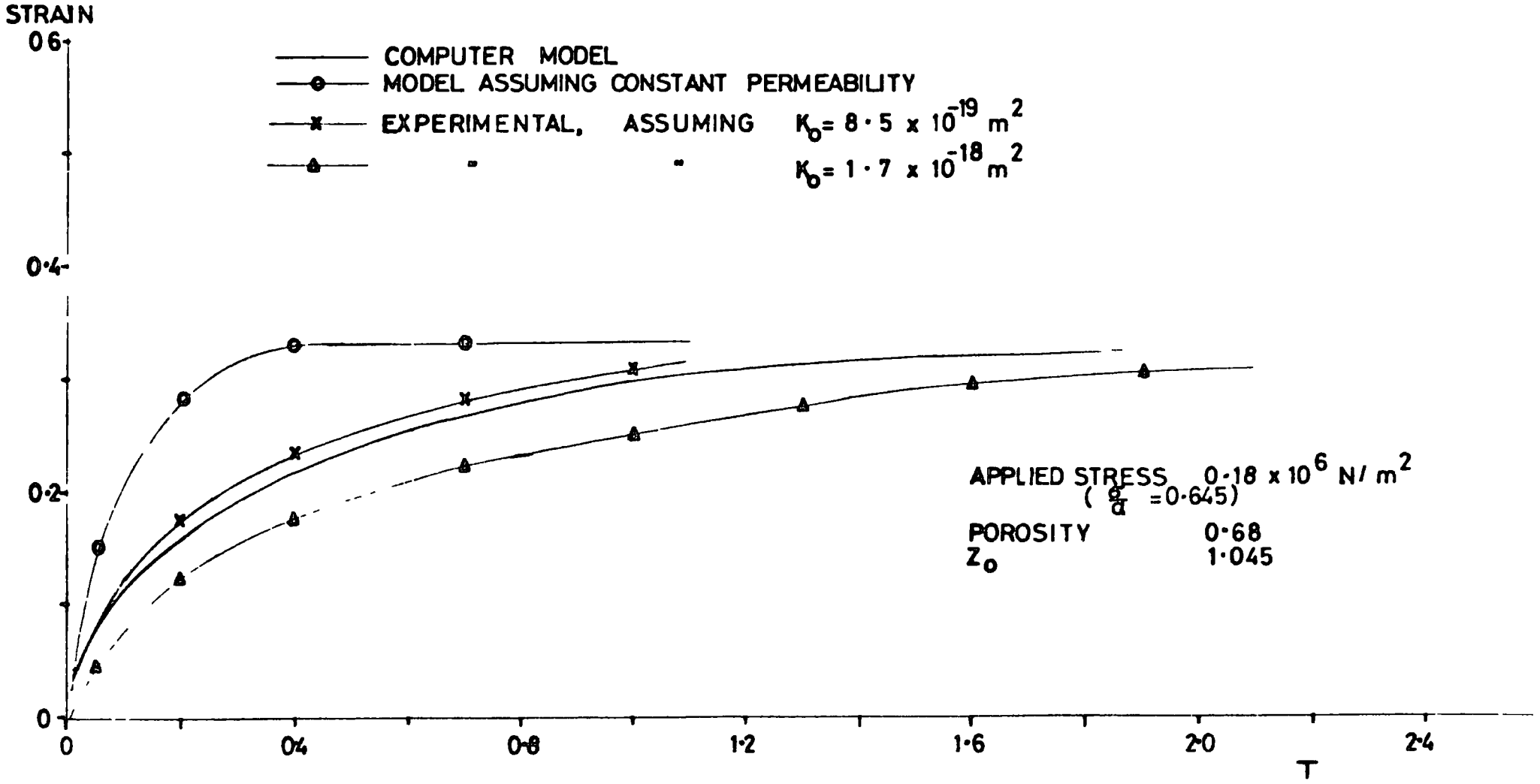

FIG 5·32 COMPARISON WITH MODEL
BOVINE CARTILAGE

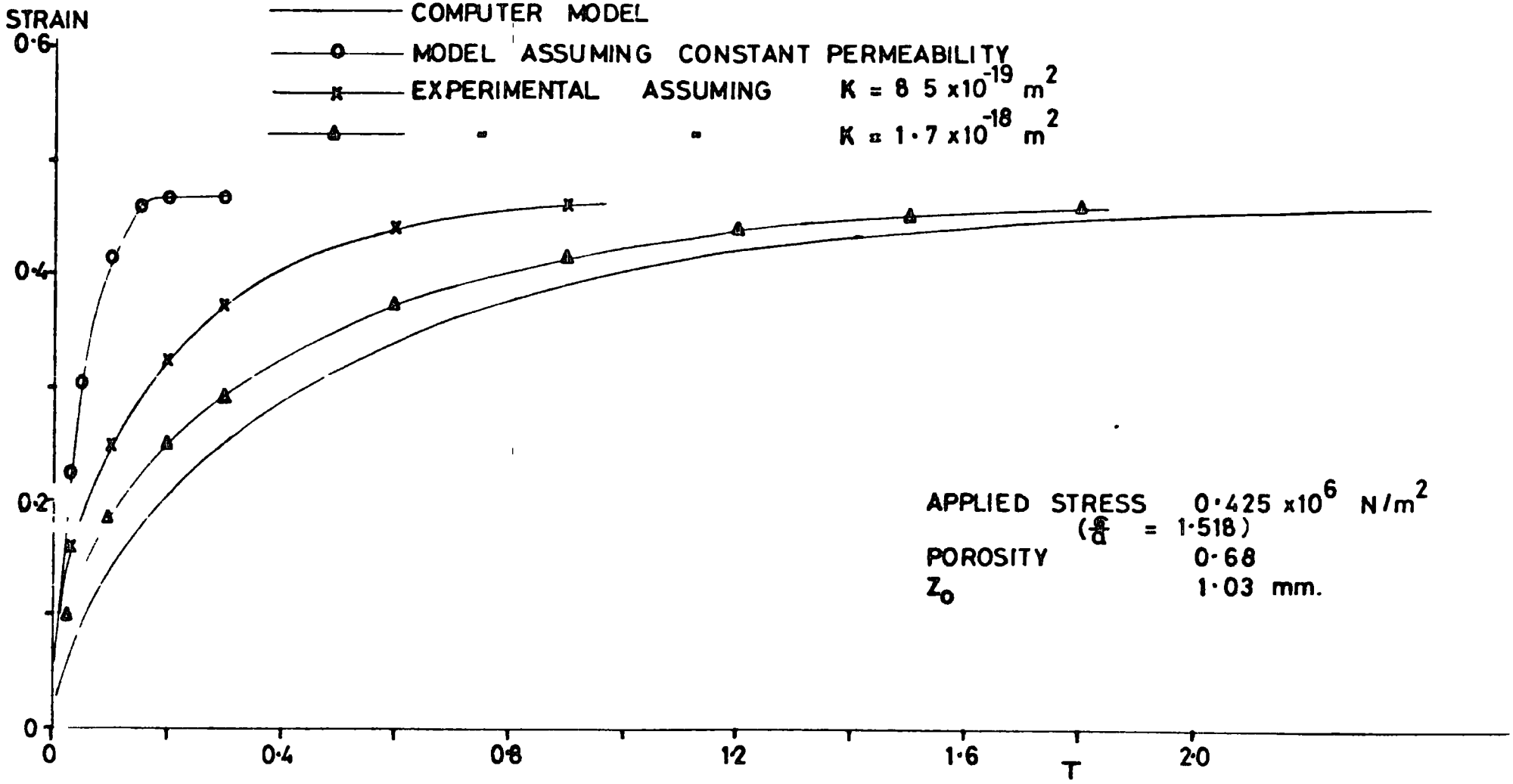

FIG 5·33 COMPARISON WITH MODEL
BOVINE CARTILAGE

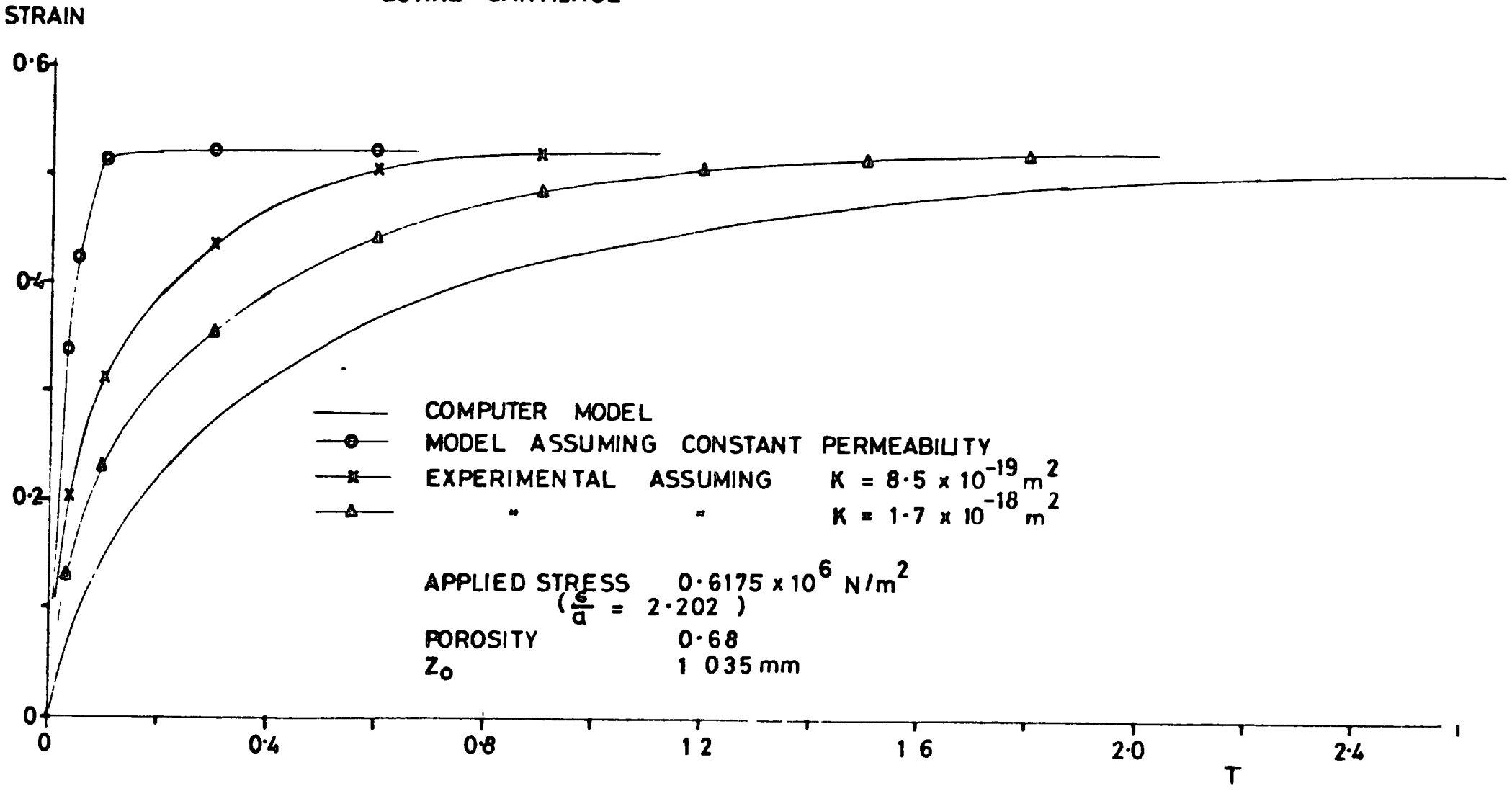

FIG 5·34 COMPARISON WITH MODEL HUMAN CARTILAGE

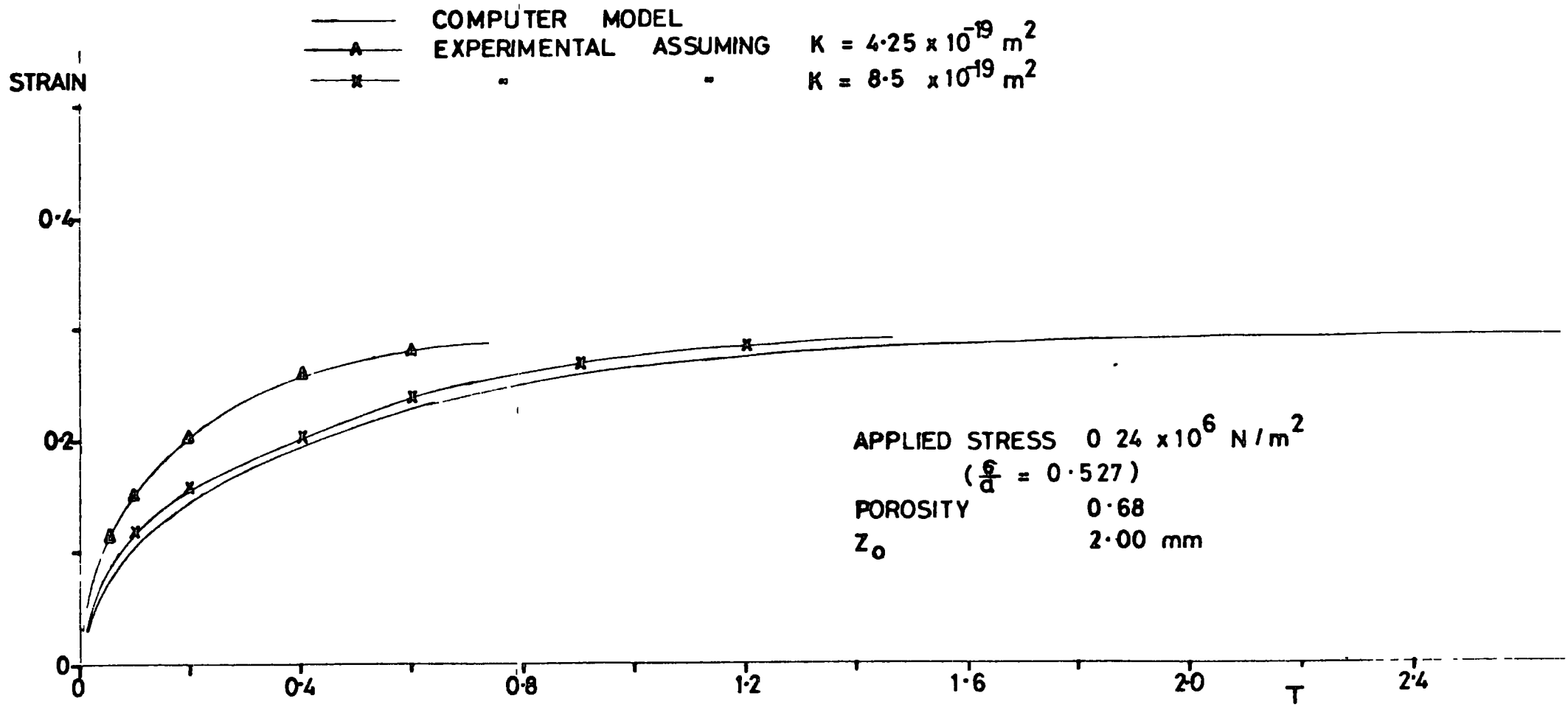

FIG 5·35 COMPARISON WITH MODEL
HUMAN CARTILAGE

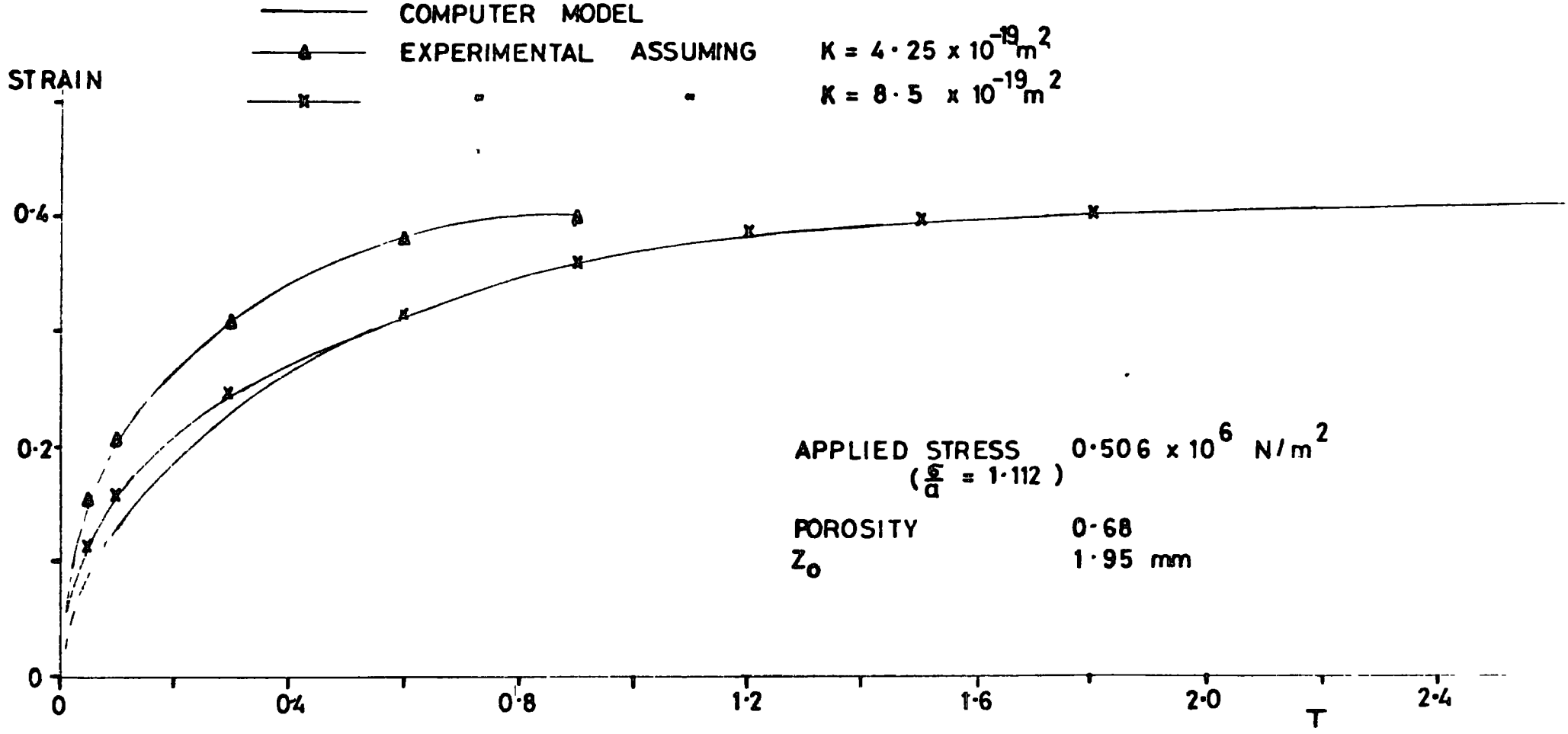

FIG 5·36 COMPARISON WITH MODEL HUMAN CARTILAGE

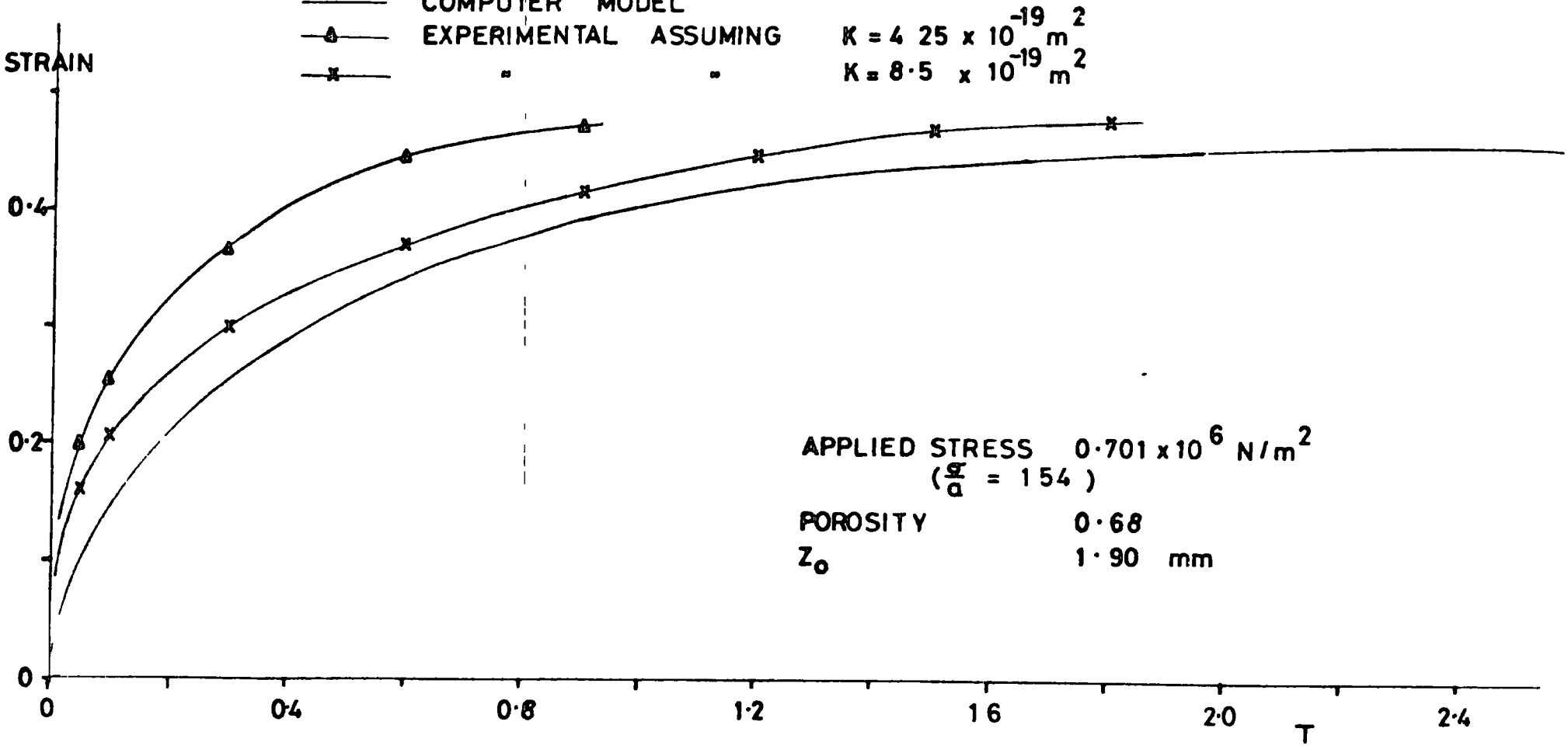

FIG 5·37 COMPARISON OF AXIAL AND RADIAL FLOW MODELS

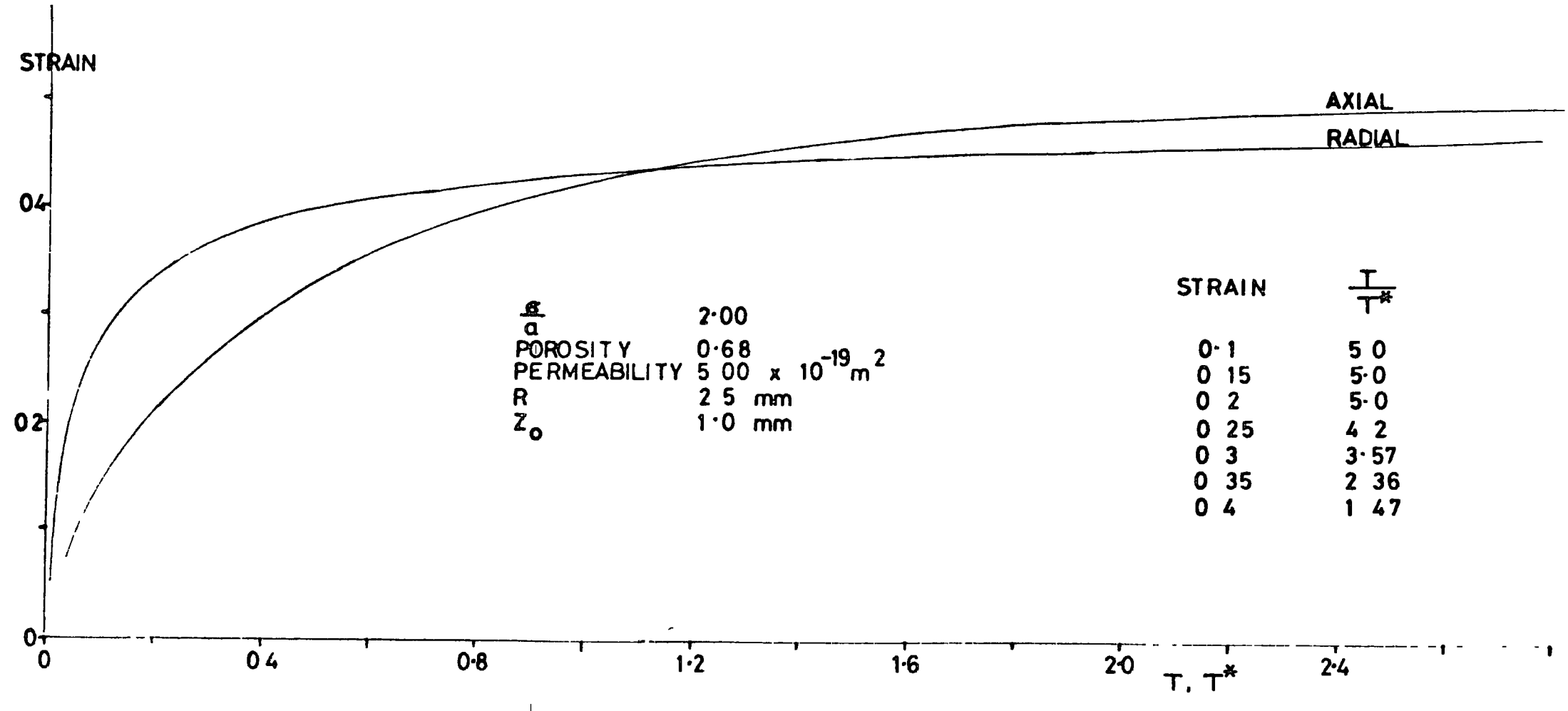

FIG 5·38 THEORETICAL STRAIN ARISING FROM RADIAL FLUID FLOW UNDER AN OSCILLATING STRESS OF $0-10^6$ N/m^2 AT 1 Hz

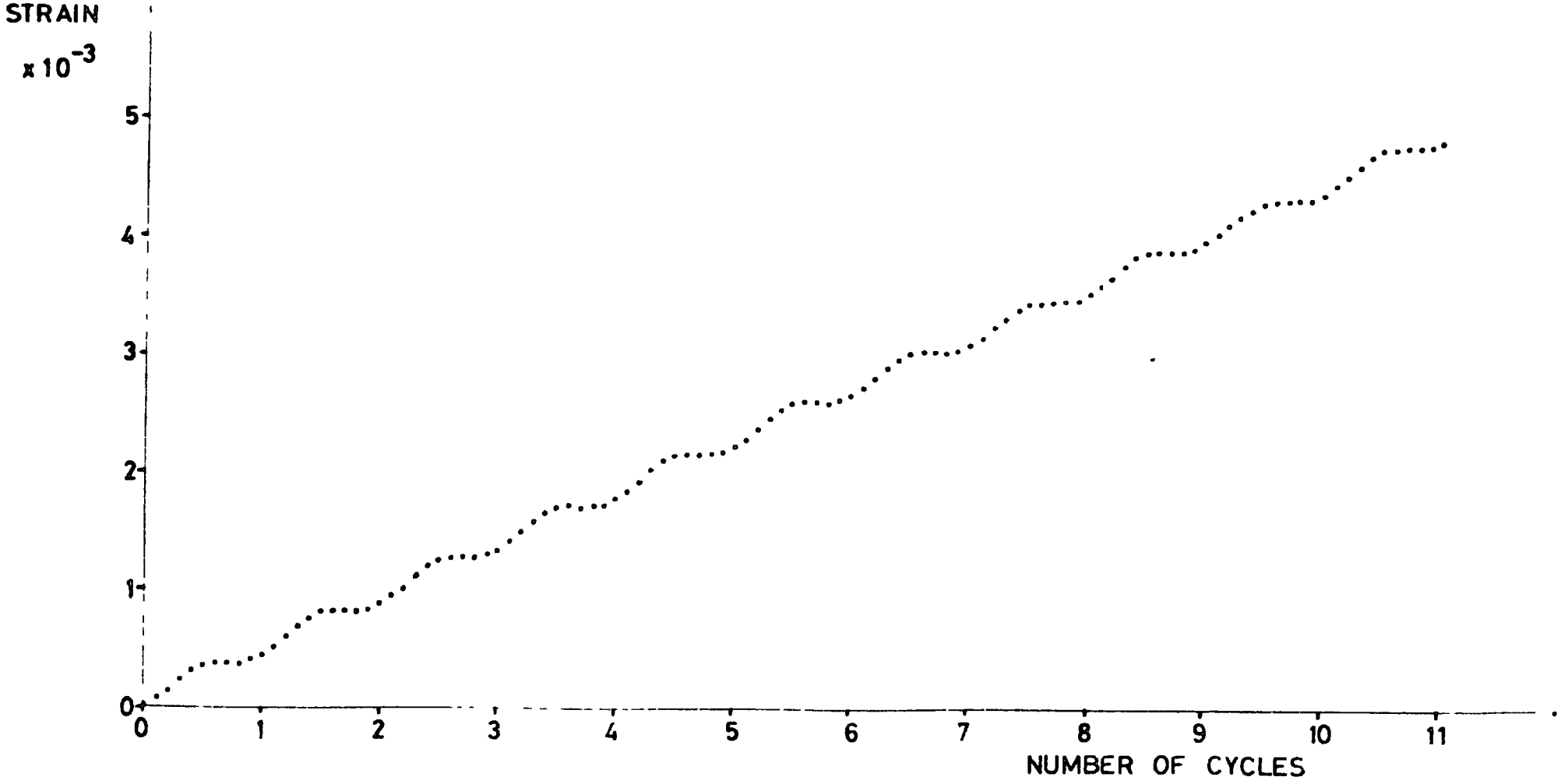

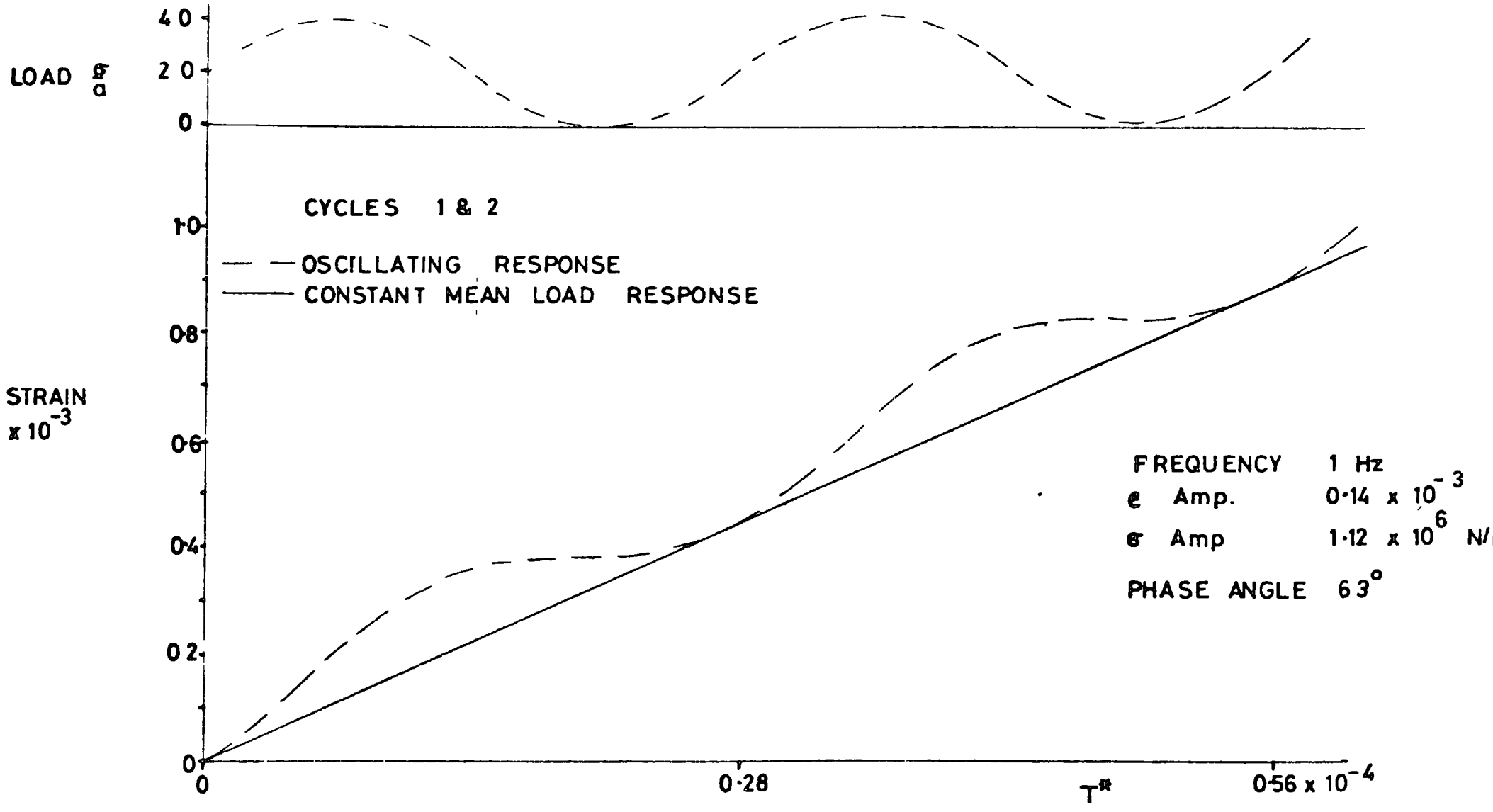

FIG 5 39 COMPUTED FLUID FLOW RESPONSE TO AN OSCILLATING LOAD

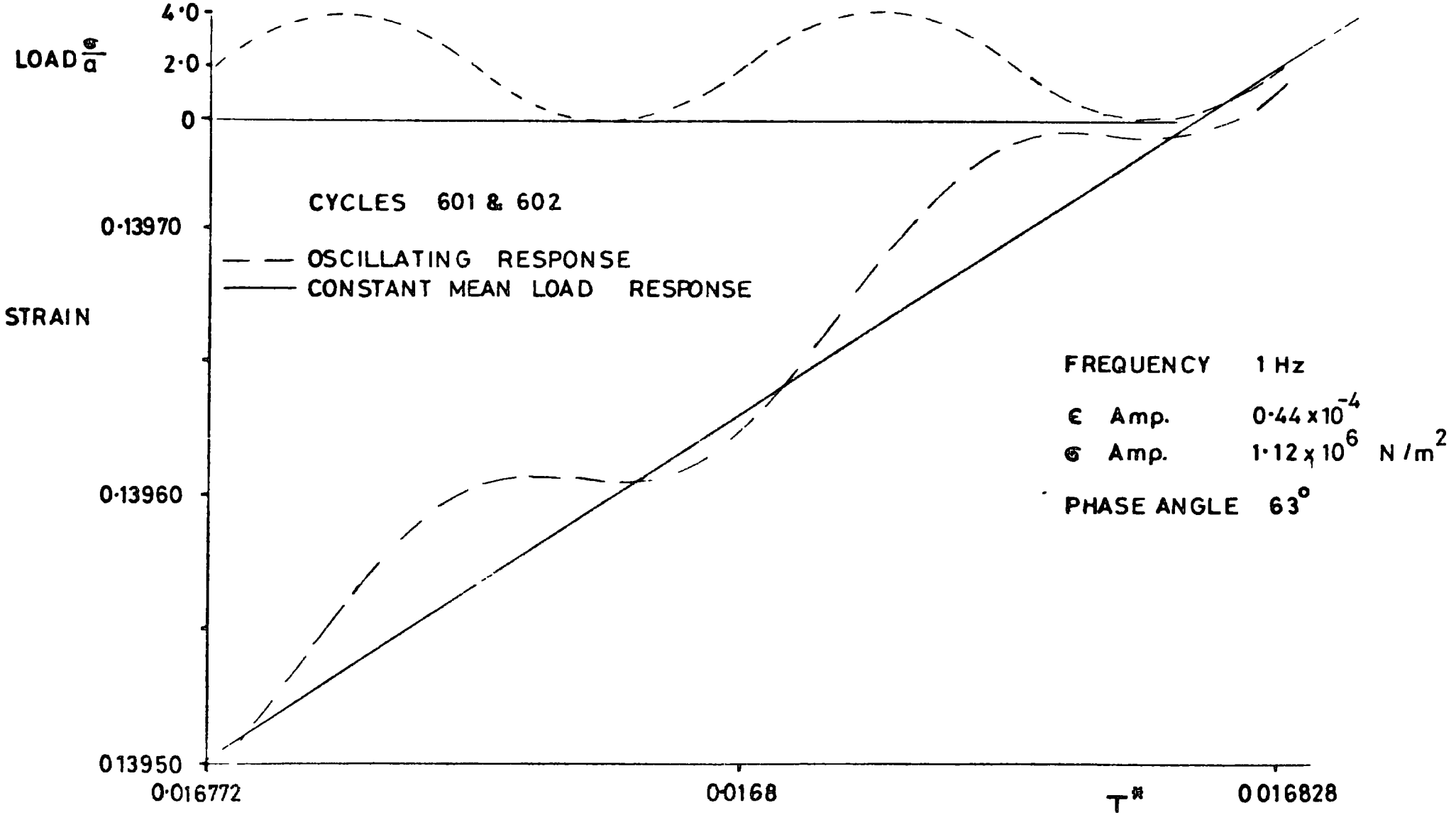

FIG 5·40 COMPUTED FLUID FLOW RESPONSE TO AN OSCILLATING LOAD

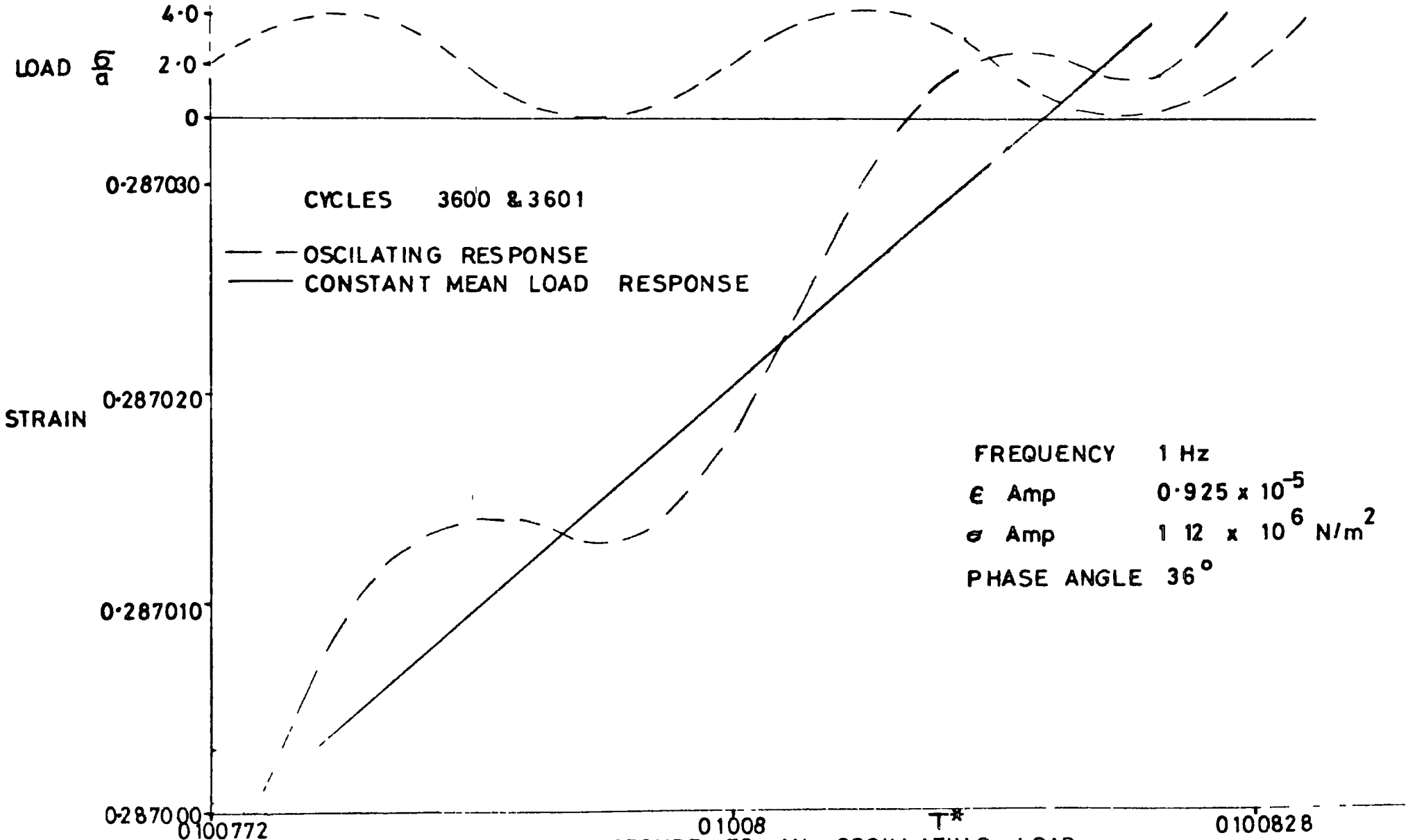

FIG 5 41 COMPUTED FLUID FLOW RESPONSE TO AN OSCILLATING LOAD

FIG 5·42 EFFECT OF LOADING FREQUENCY ON THEORETICAL CARTILAGE STIFFNESS

"FLUID FLOW" ELASTIC MODULUS v CREEP STRAIN

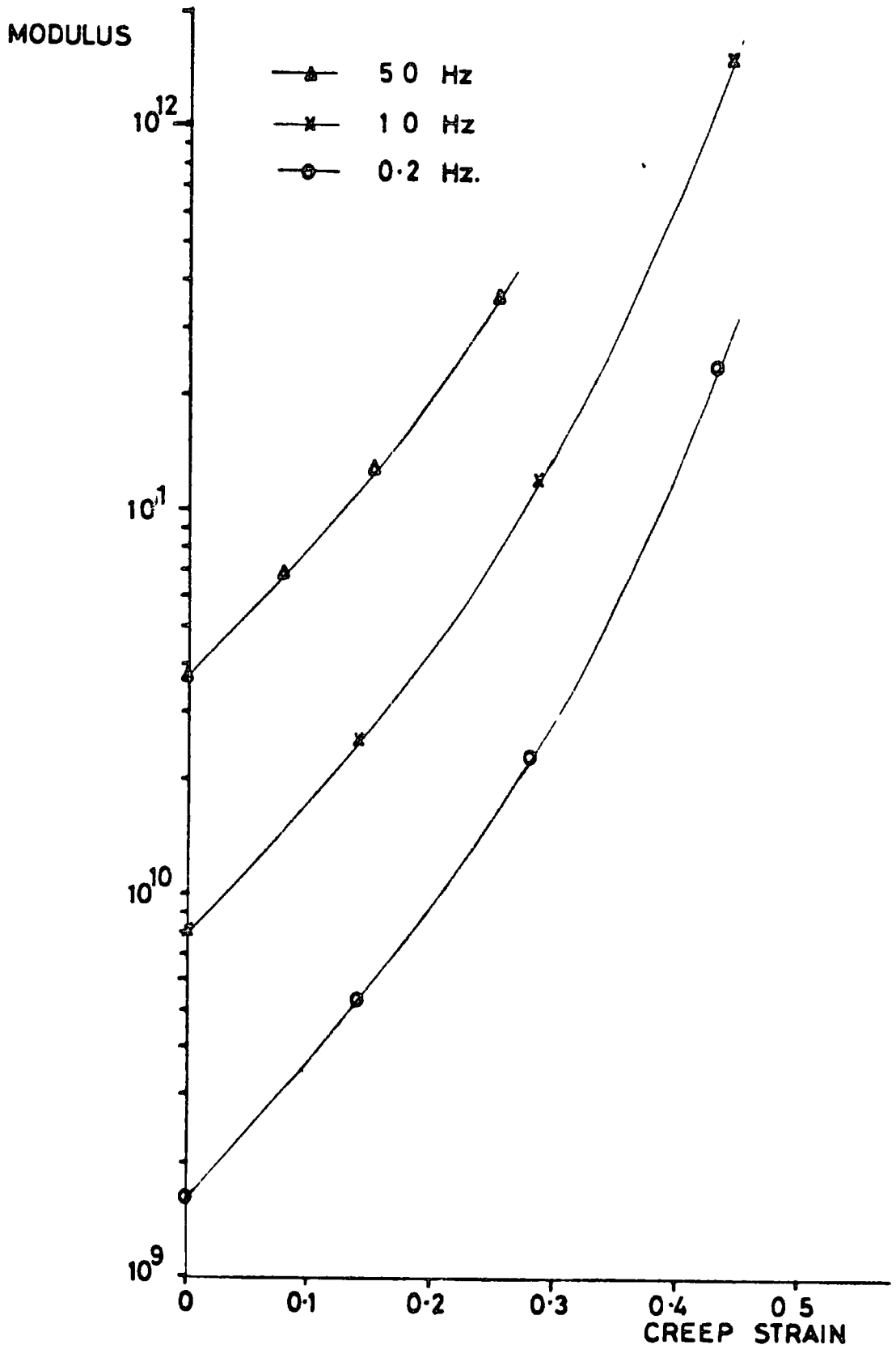

FIG 6·1 ELASTIC MODULI E & E′ v CREEP STRAIN
CONFINED TESTS BOVINE
FREQUENCY 0·83 Hz

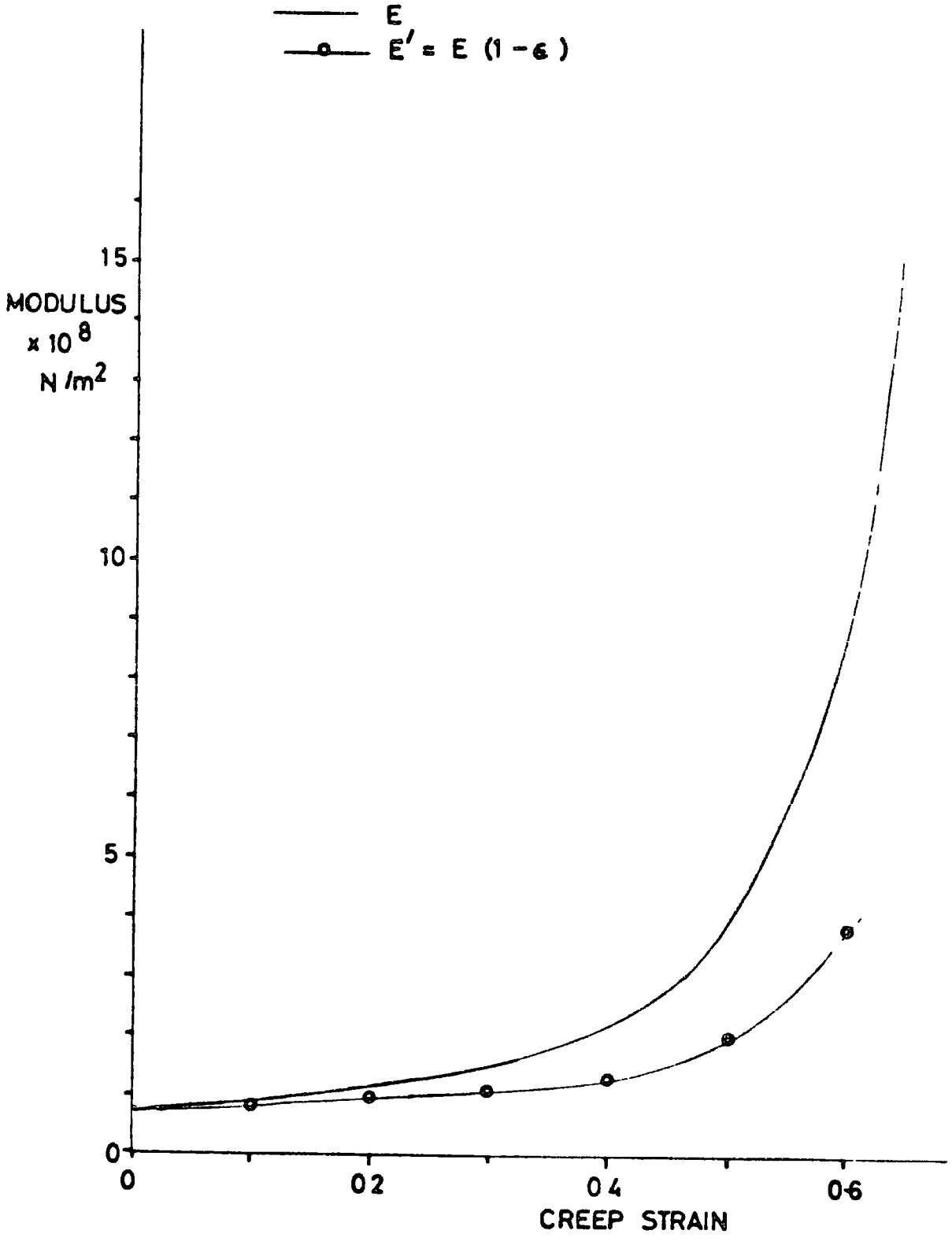

FIG 62 ELASTIC MODULI E & E′ v CREEP STRAIN
CONFINED TESTS HUMAN
FREQUENCY 0·83 Hz

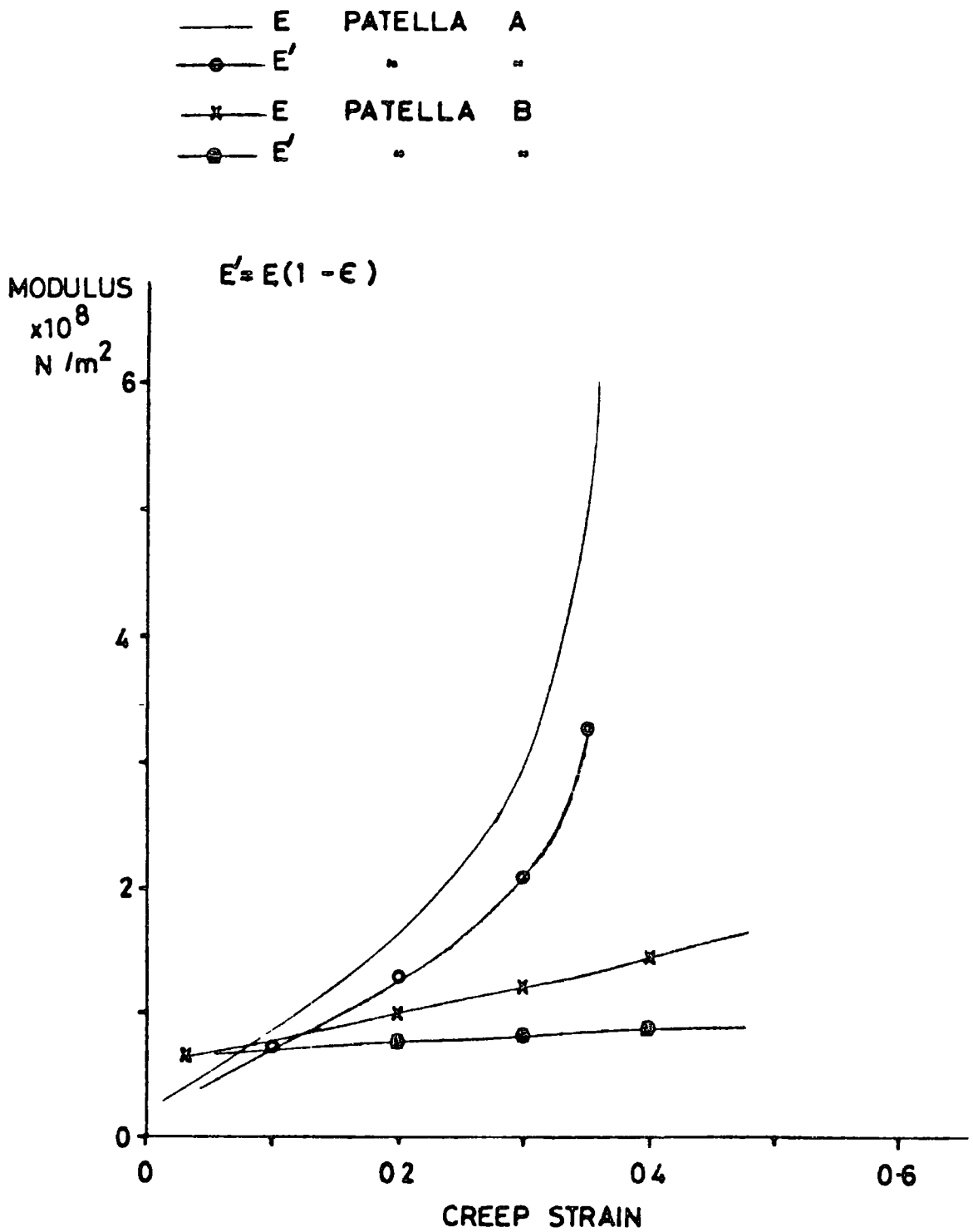

FIG 6·3 ELASTIC MODULI E & E′ v CREEP STRAIN
UNCONFINED TESTS BOVINE CARTILAGE
FREQUENCY 0·83 Hz

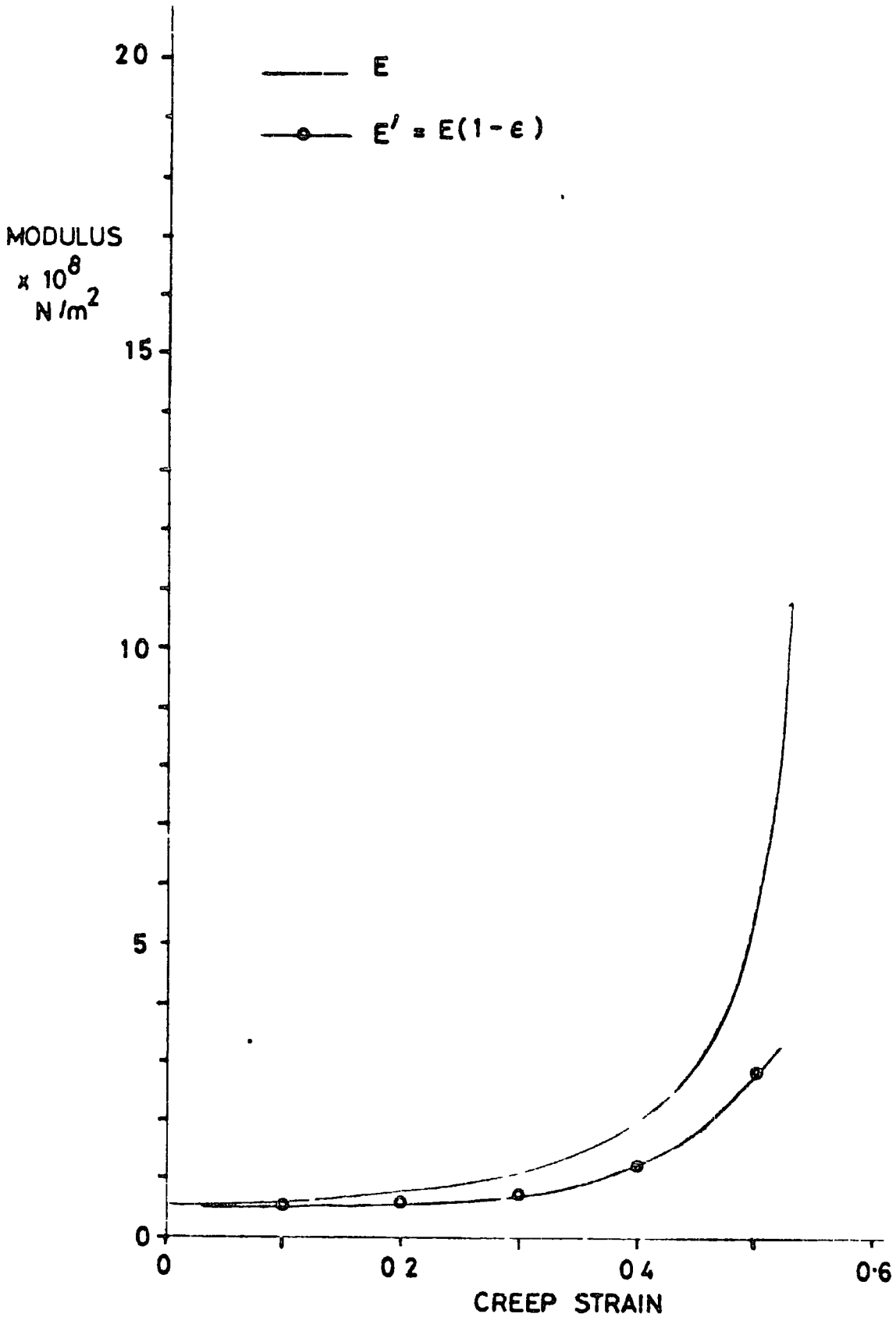

FIG 6·4

A SIMPLE RHEOLOGICAL MODEL OF ARTICULAR CARTILAGE

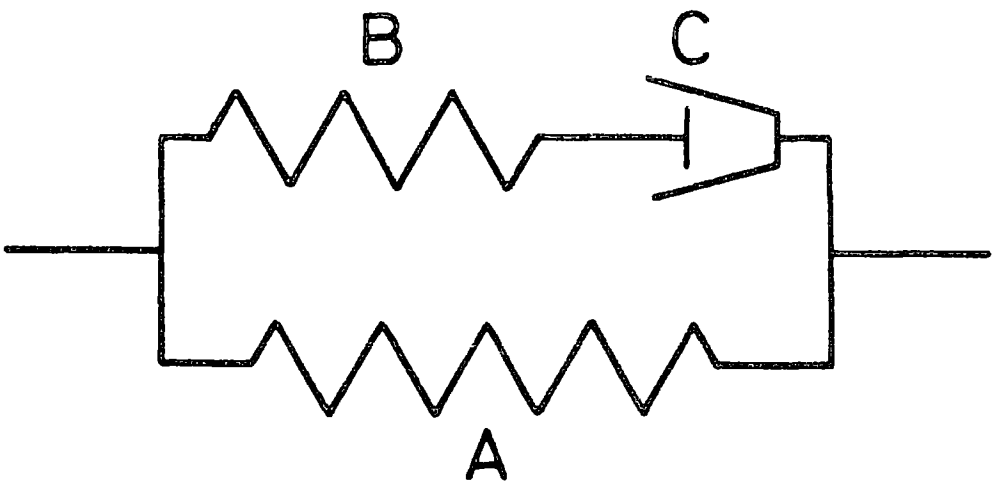

FIG. A1 STRAIN – TIME CHARACTERISTICS OF SUBCHONDRAL BONE
CORRECTED FOR RIG DEFLECTION
APPLIED LOAD $1 \cdot 78 \times 10^6$ N/m^2

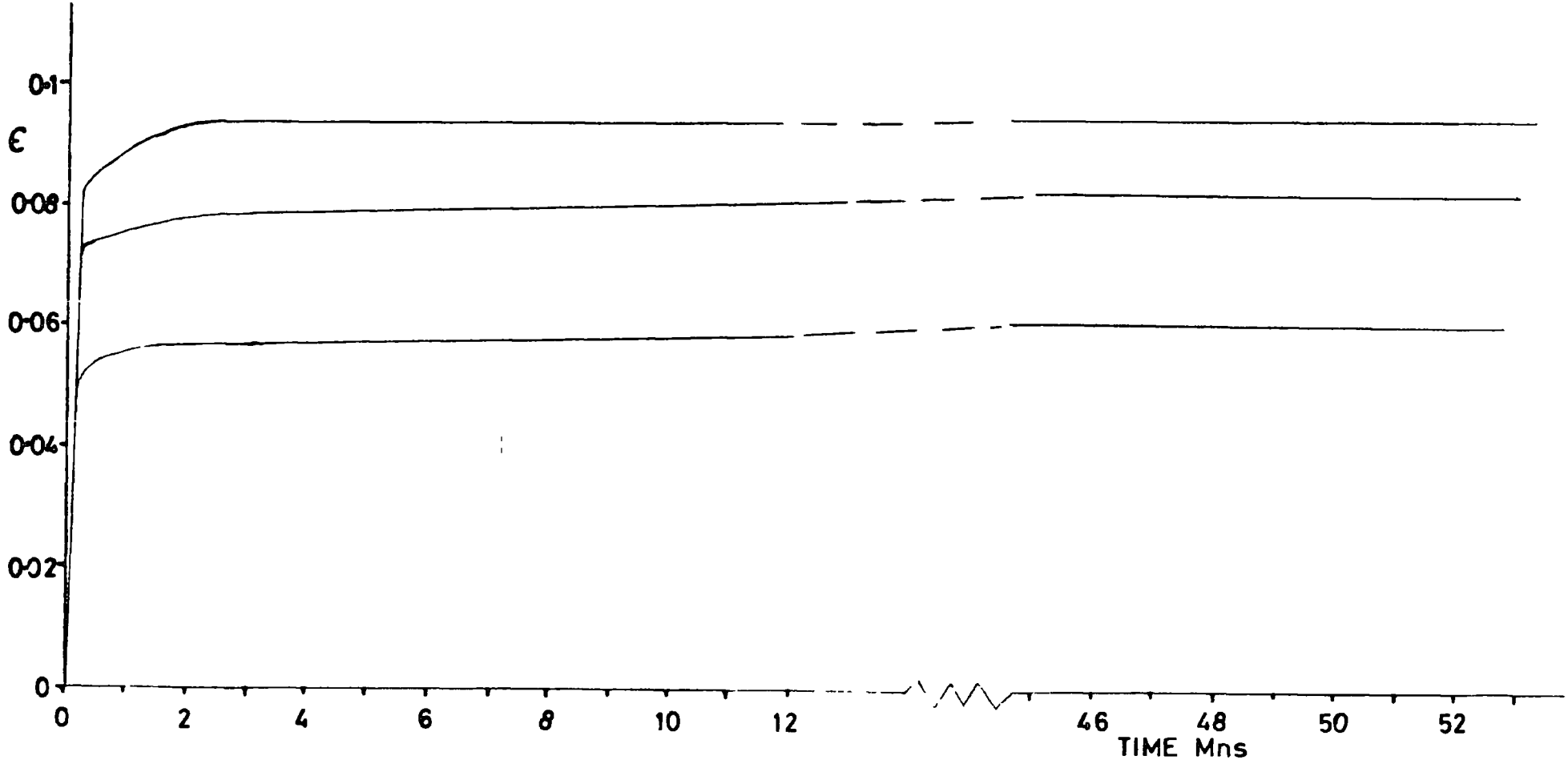

FIG A2 LOAD - DEFLECTION CHARACTERISTICS OF THE RIG AND BONE TOGETHER
INCREMENTAL INCREASES IN LOAD
NO TIME DELAY BETWEEN POINTS